DESIGNED TOPOLOGICAL STATES FROM HYBRID SPIRAL MAGNET-SUPERCONDUCTOR HETEROSTRUCTURES

Christopher James Carroll

A Thesis Submitted for the Degree of PhD
at the
University of St Andrews

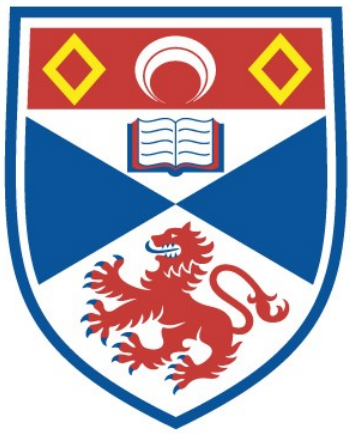

2019

Designed topological states from hybrid spiral magnet-superconductor heterostructures

Christopher James Carroll

University of
St Andrews

This thesis is submitted in partial fulfilment for the degree of

Doctor of Philosophy (PhD)

at the University of St Andrews

September 2018

Candidate's declaration

I, Christopher James Carroll, do hereby certify that this thesis, submitted for the degree of PhD, which is approximately 48,000 words in length, has been written by me, and that it is the record of work carried out by me, or principally by myself in collaboration with others as acknowledged, and that it has not been submitted in any previous application for any degree.

I was admitted as a research student at the University of St Andrews in September 2014.

I received funding from an organisation or institution and have acknowledged the funder(s) in the full text of my thesis.

Date Signature of candidate

Supervisor's declaration

I hereby certify that the candidate has fulfilled the conditions of the Resolution and Regulations appropriate for the degree of PhD in the University of St Andrews and that the candidate is qualified to submit this thesis in application for that degree.

Date Signature of supervisor

Permission for publication

In submitting this thesis to the University of St Andrews we understand that we are giving permission for it to be made available for use in accordance with the regulations of the University Library for the time being in force, subject to any copyright vested in the work not being affected thereby. We also understand, unless exempt by an award of an embargo as requested below, that the title and the abstract will be published, and that a copy of the work may be made and supplied to any bona fide library or research worker, that this thesis will be electronically accessible for personal or research use and that the library has the right to migrate this thesis into new electronic forms as required to ensure continued access to the thesis.

I, Christopher James Carroll, confirm that my thesis does not contain any third-party material that requires copyright clearance.

The following is an agreed request by candidate and supervisor regarding the publication of this thesis:

Printed copy

Embargo on all of print copy for a period of 1 year on the following ground(s):

- Publication would preclude future publication

Supporting statement for printed embargo request

Numerous calculations present in the thesis are also in preparation to be published in journals. Such publication would be precluded without an embargo.

Electronic copy

Embargo on all of electronic copy for a period of 1 year on the following ground(s):

- Publication would preclude future publication

Supporting statement for electronic embargo request

Numerous calculations present in the thesis are also in preparation to be published in journals. Such publication would be precluded without an embargo.

Title and Abstract

- I require an embargo on the abstract only.

Date Signature of candidate

Date Signature of supervisor

Underpinning Research Data or Digital Outputs

Candidate's declaration

I, Christopher James Carroll, hereby certify that no requirements to deposit original research data or digital outputs apply to this thesis and that, where appropriate, secondary data used have been referenced in the full text of my thesis.

Date Signature of candidate

Abstract

In this thesis a Green's function based, analytical formalism is developed to describe dense chains of spiral ordered classical magnetic moments embedded in superconducting substrates. I demonstrate that an understanding of the dimensional mismatch between the substrate and impurity chain is crucial to understand the physics at play. Renormalised gap closures are discovered by exact, analytic solution for a ferromagnetic chain and insights gleaned are used to understand the spiral ordered case to which it can be smoothly tuned.

I investigate the topological characteristics of this model and find an ambiguity in defining effective Hamiltonians due to the dimensional embedding of the chain in the substrate. To aid in resolving this ambiguity I develop formalism which allows one to write down Green's functions for bounded, semi infinite systems in terms of more easily attainable, exact solutions for infinite systems. I derive simple expressions to identify the presence of topological bound states which agrees with purely one dimensional models and changes suggestively when applied to the aforementioned two dimensional model.

I then work to extend the formalism to allow the exact solution of two or three parallel chains, taking into account all possible interactions with the classical magnetic impurities. The solutions are decoupled so that they can be written in terms of the T matrices for a single chain, with additional levels of resummation. I find that the induced sub-gap spectrum for the two chain solution completely replaces those from each individual chain, leading to oscillating, helix like band structures. I use the complicated solution of the three chain solution to inform a potential ansatz to solve the N chain case.

General acknowledgements

With thanks to Bernd Braunecker, without whom this would have been impossible.

Thanks to Tristan Cren, Raquel Queiroz, Pascal Simon, Chris Hooley, Jonathan Keeling, Teemu Ojanen, Maria Laura Staffini and Aline Heyerick for helpful discussions.

Funding

This work was supported by the EPSRC under grant number EP/M506631/1.

Research Data/Digital Outputs access statement

This is a theoretical work and all results are reproducible from the given formulae.

Contents

1 Introduction and motivation

The fact that something could exist, does not mean that it must. As has been found in many cases, the physical universe is under no obligation to use every result we write down. As a particular example, it is still an open question [1] whether any fundamental particle is a Majorana fermion, first predicted in 1937 [2]. Rather than search for such a "native" example, it would be desirable to simply pull on levers controlling the universe such that we can guarantee the emergence of the desired particle. Such is the motivation underpinning our approach to engineering quantum states.

Herein lies the strength we are afforded in condensed matter systems: rather than searching in nature for a system which has the conditions we require, we can combine sub-systems to engineer desired conditions. Though there are numerous approaches to this, we take the view that one should engineer the system such that the internal interplay of interactions is sufficient to give rise to the emergence of the phase and hence excitations *without* the need for tuning of external parameters. Quite aside from the potential simplicity this offers experimentalists, this approach means that the engineered system itself provides a physical scenario where these novel excitations (which are not otherwise known to exist in nature) occur intrinsically. In this way, such systems provide a satisfying answer to the question of where such excitations could occur and why.

A recent focus of this method is to look for parafermionic states of which the Majorana fermion is the simplest example.[1] Unlike in higher dimensions, in two dimensional systems the constraints upon exchange statistics are relaxed such that, rather than only having fermionic or bosonic excitations, it is possible for states which exhibit any arbitrary statistics upon exchange to exist. Such states are referred to as anyons [3–5]. These states can be split into two categories: those with Abelian and those with non-Abelian exchange statistics. Abelian anyons (of which parafermions are a sub-class) are characterised by picking up a phase upon exchange that is not $+1$ (bosonic) or -1 (fermionic) but can be any phase $\mathrm{e}^{i\phi}$. Otherwise, however, their states remain untouched by the exchange. Non-Abelian modes, on the other hand, are characterised by further quantum numbers that are also modified by the exchange process. In this way, through exchange, the states are capable of changing their nature. This modification is different if, for example, the particles are exchanged clockwise or anticlockwise. It is important that one can actually define what clockwise and anticlockwise means, and this is one of the reasons why much of the anyon physics is confined to 2D. As these unusual properties might suggest, non-Abelian states are thus much more complicated to obtain and to stabilise. Our focus on Abelian particles, starting with Majorana fermions is thus clear. We need first to understand how to obtain these before we can think of increasing the complexity.

In this simplest case it has been shown that, through careful combination of physical effects [6, 7], one can find isolated Majorana fermions at the edges of certain models. Similar considerations apply for general parafermions [8]. In many ways, the key observation from these models is that such states are to be expected at the boundary of *topological* phases. In this

[1] though it is worthwhile to note that such particles are then not elementary particles but composites resulting from the interactions present. Such particles are generally distinguished by referring to them instead as Majorana modes or Majorana (bound) states.

way, it is possible for the boundary of the system to exhibit excitations not present in isolation in the bulk.

Beyond these models, a great deal of progress has been made in finding experimentally realisable setups of the same topological phase. Initially focused in quantum spin Hall edge systems [9], the search continued through spin-orbit split semiconducting nanowires in a Zeeman field [10–21] and finally to arrays of magnetic adatoms atop superconducting substrates [22–32]. Such systems are realisable experimentally either in nanowire systems [33–39] or magnetic adatom systems [40–43], including possible observations of Majorana bound states. Very recently observations of their possible nonlocality have been reported [44]. Through this progression we have seen a trend towards finding self tuning phases rather than those that require external tuning.

Though the potential to extend such physical models in the direction of the "clock" models of [8] has been tentatively explored [45–49], in this context it is important to avoid idealised settings. Though it is well known that dimensionality plays a crucial role in determining the nature of topological phases [50, 51] it is not necessarily clear that it is possible to sensibly isolate low dimensional topological systems in the case where their properties are induced from a higher dimensional background. The way to understand two dimensional arrays of non-identical one dimensional structures (which if isolated are potentially topologically non-trivial) is simply not well understood. In this way, over-idealisation may underestimate the further complications in a real world setting, but even more importantly for us, they form a closed world that makes it very difficult to extend and obtain more complicated topological phases.

This is one of the driving features for this work: we want to understand exactly how to embed one dimensional models into the higher dimensional world in which they must realistically reside. In this way we can properly explore a realistic model which is not firmly dimensionally restricted and to exploit the benefits of coupling one and two dimensional systems to design still more exotic states.

Hence, we are able to outline the goals for our formalism: to understand how to construct the topological phases in the bulk of and novel excitations at the boundary of composite systems.

We will study how to take various sub-systems and join them together in such a way that the interplay of their various interactions is fully taken into account. This interplay will allow for a change in the global properties of the composite system to give rise to (topological) properties not present in any individual building block. Such an approach allows us to study the feedback from each system upon the others. We will make heavy use of a Green's function formalism, intrinsically extendible in future work to the inclusion of electron-electron interactions, non-zero temperatures and even out of equilibrium effects using well studied formalism. This "bottom up" approach to studying systems allows us to develop an understanding of the nature of any novel states entirely in terms of the well understood components used to build them. In principle this should aid in elucidating how one should go about designing still more exotic phases built from those studied here. As a principal example: $\mathbb{Z}_3$ parafermions are a potential building block for Fibonacci anyons, a type of non-Abelian anyon which could allow universal quantum computation [52].

We will now outline the content of remaining chapters where this design methodology is applied: we will build an understanding of one dimensional, spiral ordered magnetic adatom

chains embedded in a two dimensional superconductor; study the nature of their boundaries and topological character and finally extend our model to allow for arrays of one dimensional adatom chains embedded in a two dimensional substrate.

In chapter 2 we develop a formalism to describe a one dimensional line of magnetic impurities embedded in a two dimensional superconductor. This analytic approach is focused on the experimentally relevant densely packed chain limit. Our analytic solution provides access to the exact Green's function from which any relevant information can be gathered. This illustrates keenly a major strength of the generality of this formalism rather than requiring specially tailored assumptions as can be required in other methods. This solution is achieved using a T matrix formalism to allow the formation of exponentially localised sub-gap bands from the interplay of two dimensional substrate superconductivity and localised, spiral ordered magnetic impurities. Through a combination of exact solutions and consequent understanding of the physical processes governing their formation we find qualitative differences in the nature of the sub-gap states so formed as compared to those expected without considering the interplay between substrate and induced band structures or equivalently, for more sparse magnetic chains. The location of high symmetry gap closures is found to occur non-analytically in the superconducting gap Δ due to the non equal dimensionality of the substrate and localised magnetic structure.

In chapter 3 we discuss methods by which the model developed in chapter 2 can be topologically classified. We firstly outline the ambiguity in defining effective one dimensional Hamiltonians due to numerous justifiable methods to take into account the second dimension of the substrate. In an entirely localised picture (essentially ignoring the substrate except to allow formation of sub-gap bands in the first place) we find a topological phase diagram similar to that expected from the Kitaev chain toy model but with renormalised interaction strengths due to the dimensional mismatch discussed in chapter 2. In a picture taking into account the leakage of the exponentially localised states we instead find only an approach to a topological phase at the expected interaction strength, without entry into it. Only at comparatively large interaction strength do we find entry into a topological phase.

To disentangle this ambiguity we utilise a method [53–56] to "stitch" Green's functions together so that we may study the boundary at which topological bound states should form. We find a novel condition for the presence of such bound states which depends crucially upon the *zeroes* of the Green's function in the bulk rather than the poles. This condition is found to agree with known conditions for entry into topological phases in entirely one-dimensional models and is found to exhibit a suggestive discontinuity in the two dimensional model developed in chapter 2 at precisely the value expected from an entirely localised picture of the topological classification.

In chapter 4 we construct a formalism which quite generally allows one to find the Green's functions for systems containing N impurities, lines, sheets etc., fully taking into account their interactions with their substrate and also the interactions between them, via the substrate. This is illustrated by calculating the Green's function for two and three spiral ordered magnetic chains embedded in a two dimensional superconductor in such a way that it is possible to disentangle the origins of modifications from the single chain case studied in chapter 2. For the two chain case we are able to observe the exact cancellation of sub-gap structure (and hence poles) due

to the interactions between the chains and simultaneous transferral of spectral weight to other locations.

Through the tools so developed, it is possible to study the boundary of essentially arbitrary networks of impurities stitched together and hence find the potentially exotic excitations intrinsically generated there. This could be achieved entirely within a language which allows for study of dynamical and interaction based effects in such systems.

2 1D spiral ordered magnetic chain in 2D superconductor

As previously introduced, the goal throughout this work is to investigate a particular physical implementation of the Kitaev chain toy model. Here we will briefly outline this model and other approaches taken to realise it physically to justify our approach in more depth.

2.1 Kitaev chain toy model

The Kitaev chain toy model [6, 57] is described by the Hamiltonian:

$$H = \sum_{j=1}^{N} \left(-\mu c_j^\dagger c_j\right) - \sum_{j=1}^{N-1} \left(\left(t c_j^\dagger c_{j+1} + \Delta c_j c_{j+1}\right) + \text{h.c.}\right) \tag{2.1}$$

for a one dimensional chain of spinless (Dirac)[2] fermions described by the operators c_j with a nearest neighbour hopping t, chemical potential μ and p-wave gap Δ which is necessarily nearest neighbour rather than on-site due to the Pauli exclusion principle. In this way the model describes a one dimensional, spinless, p-wave superconductor. This model can illustratively be re-written in terms of two, purely real fields $\gamma_{j,1}$, $\gamma_{j,2}$ defined by:

$$c_j = \frac{1}{2}\left(\gamma_{j,1} + i\gamma_{j,2}\right) \tag{2.2}$$

where the new operators γ obey the relations:

$$\gamma_{j,\alpha} = \gamma_{j,\alpha}^\dagger \qquad \{\gamma_{i,\alpha}, \gamma_{j,\beta}\} = 2\delta_{i,j}\delta_{\alpha,\beta} \tag{2.3}$$

with $\alpha = 1$ or 2 to differentiate the two species. Written in terms of these fields, the Hamiltonian takes the form:

$$H = -\frac{\mu}{2}\sum_{j=1}^{N}\left(1 + i\gamma_{j,1}\gamma_{j,2}\right) - \frac{i}{2}\sum_{j=1}^{N-1}\left((\Delta + t)\gamma_{j,1}\gamma_{j+1,2} + (\Delta - t)\gamma_{j,2}\gamma_{j+1,1}\right). \tag{2.4}$$

We can most clearly demonstrate the existence of distinct topological phases by restricting our focus to the case where $\mu = 0$ whence it is clear that this model is qualitatively different if $|t| = \Delta$. It can be shown that relaxing this restriction does not give rise to any new phases. Focusing for the moment upon the particular case $\Delta = t$, $\mu = 0$ all that remains is:

$$H = -\frac{i}{2}\sum_{j=1}^{N-1}\left((\Delta + t)\gamma_{j,1}\gamma_{j+1,2}\right) \tag{2.5}$$

such that the operators $\gamma_{1,2}$ and $\gamma_{N,1}$ no longer appear in the Hamiltonian at all. As a direct result of this, these states necessarily cost no additional energy to fill, suggesting that once the condition $\Delta = t$ is fulfilled one is left with two states pinned to zero energy.

This result can be interpreted by looking at how the bulk and edge compare for generic Δ,

[2] We explicitly label these excitations as Dirac fermions to distinguish them from Majorana fermions. In this sense, the Majorana fermions are the real and imaginary parts of the Dirac fermions as described in the main text.

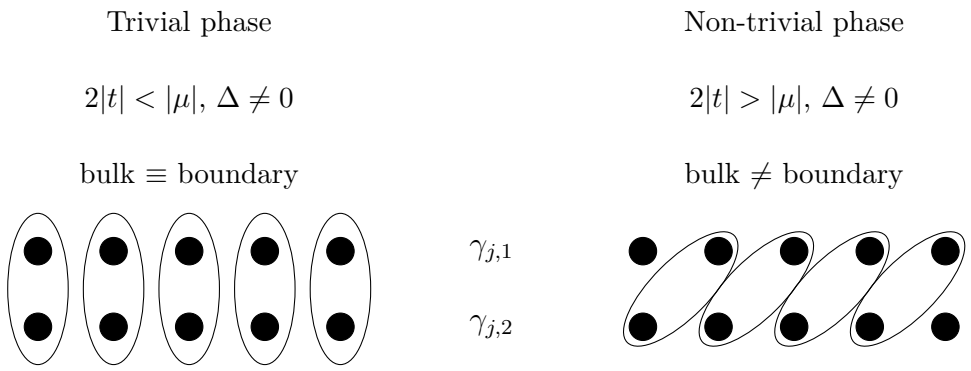

Figure 1: Figure displaying two possible phases in the Kitaev chain toy model. Each row displays each site j's Dirac fermion split into two Majorana fermions $\gamma_{j,1}$,$\gamma_{j,2}$. States pair up differently in trivial and topological phase illustrated by the banding. Note, there exists an additional metallic phase within the non-topological sector if $\Delta = 0$.

t and for the scenario described above as depicted in figure 1. In the former scenario it clearly makes sense to undo the previously applied transform in equation (2.2) so that the Majorana fermions on each site j can be paired up and return to a chain of N Dirac fermions. In cases such as $t = \Delta$ however, one is left with a Hamiltonian such as equation (2.5) where undoing the original transform no longer makes sense due to the absence of two of the original Dirac fermions from the Hamiltonian. One can instead re-write this Hamiltonian by pairing together two Majorana fields on *neighbouring* sites and return once again to a Hamiltonian for a chain of Dirac fermions but with a single, non-local Dirac fermion at the boundary. In this way, the bulk of both situations remains essentially unchanged in either scenario: a chain of Dirac fermions, but at each edge in the latter case has a single, purely real excitation which is completely decoupled from the bulk. In this way, the Kitaev chain toy model illustrates simultaneously the possibility of finding isolated Majorana fermionic excitations and that they occur at the boundaries of *topological* phases where the bulk and boundary are allowed to differ.

2.2 One dimensional realisations of Kitaev toy model

The Kitaev chain toy model is not likely to exist naturally [3]. The combination of factors required are simply not known to exist in any homogeneous system. However, there has been a great deal of effort applied to finding systems which are analogous to the toy model. Such approaches include studies of nanowires with spin orbit interaction as initiated by [10–15, 36–39], on topological insulator-superconductor structures [9], or on Josephson junction arrays [58–60]. Two very similar approaches which are more directly relevant to our approach are those of proximitised nano-wires [16–21] and magnetic chains on substrates [22–31, 61–67] with spiral magnetic order.

The key abstraction that allows these methods to work is that, in order to develop something resembling the Kitaev chain toy model one requires a method to spin filter states and to induce one dimensional, p-wave superconductivity. In this way, all of these approaches re-

[3] With the notable exception of the fact that it is equivalent to a spin chain model with xx, yy and a magnetic field in the z direction via the Jordan-Wigner transform [6]. This is highly non-local however so against the spirit of our aims here.

quire something like a spin-orbit like interaction, a magnetic interaction and superconductivity. Following the realisation that in one dimensional systems spin-orbit interactions are equivalent to a spin-dependent momentum shift [68–70], and hence that one dimensional band structures exhibit a spin dependent Peierls instability [70], the only remaining feature requiring external tuning was the necessity of a Zeeman field. In this way, the approach of constructing magnetic adatom chains, at least in purely one dimensional models, finally provided a system which is *intrinsically* similar to the Kitaev chain toy model, without need for external tuning. What is more, due to the instability sparse chains of magnetic impurities exhibit to the Ruderman-Kittel-Kasuya-Yosida (RKKY) interaction, at least in one dimension, the system is self tuning to the topological phase [16–18]. In this way, all that is required is to bring the temperature below a critical value and the interplay of the various interactions present causes the system to order itself in such a manner that Majorana edge modes form.

Though such models can be considered considerably more physically realistic than the Kitaev chain toy model, it is worth noting that until this point we are still only considering purely one dimensional calculations. Though ordinarily this could be considered as an innocent difference from a physical system, essentially corresponding to an arbitrarily thin line, it is well known that dimensionality plays a crucial role when considering topological phases [50, 51]. Additionally, the RKKY interaction is highly dimension dependent and is known to not be strong enough in two dimensions to stabilise the phase as it would in purely one dimensional systems [71–74] and moreover, that there is no long range order for RKKY type interactions for isotropic interactions in 2D. However, here we will be studying a system where the substrate is 2D but entirely localised, 1D like states will develop. Is this effective one dimensionality enough that the RKKY interaction operates as in 1D and can stabilise the phase without fine tuning? With such considerations in mind it seems worthwhile to properly investigate to what extent the effective, one dimensional, Kitaev chain like model emergences when embedded in higher dimensions (as it necessarily must be in order to be physically realisable).

Additionally, most previous approaches considering magnetic chains on superconducting substrates essentially worked upon the assumption of the chains being relatively sparse [24–29, 31]. In this way, the adatom spacing a_h is much greater than other length scales present: $1/k_F$ where k_F is the electronic Fermi wave-vector and ξ_0, the induced superconducting coherence length.

2.2.1 YSR states

Before considering models constructed from chains of magnetic atoms in superconductors it is worth considering the bound states formed by a single such impurity. Such bound states are known as Yu-Shiba-Rusinov (YSR) states [75–77]. Their existence can be shown using a real space T matrix approach, modelling the magnetic impurity as a local amplitude to cause spin flips between basis elements of a matrix Nambu Green's function $\mathbf{G}$ so that one must solve the so called Dyson equation:

$$\mathbf{G}(\mathbf{r}'', \mathbf{r}') = \mathbf{g}(|\mathbf{r}'' - \mathbf{r}'|) + \mathbf{g}(|\mathbf{r}''|)\mathbf{V}_m\mathbf{G}(0, -\mathbf{r}') \tag{2.6}$$

where $\mathbf{g}$ is a real space, Nambu Green's function for a two dimensional s-wave superconductor and the matrix $\mathbf{V}_m$ describes the spin flip due to local, classical, magnetic moment placed at $\mathbf{r} = 0$. Inclusion of spin flip terms like $\langle c_\uparrow^\dagger c_\downarrow \rangle$ in principle requires use of the full Nambu spinor $\left(c_\uparrow^\dagger, c_\downarrow^\dagger, c_\downarrow, c_\uparrow\right)^T$ [4] rather than the more usually seen subspace $\left(c_\uparrow^\dagger, c_\downarrow\right)^T$ [5]. Using such a basis the matrix $\mathbf{V}_m$ is defined as

$$\mathbf{V}_m = V_m \begin{pmatrix} 0 & 1 & 0 & 0 \\ 1 & 0 & 0 & 0 \\ 0 & 0 & 0 & -1 \\ 0 & 0 & -1 & 0 \end{pmatrix} \tag{2.7}$$

for the magnetic interaction strength V_m. The Dyson equation (2.6) can be solved exactly as in section 2.5 by defining a so called T matrix which describes the changes made between an incoming and outgoing state due to the interactions present in the particular Dyson equation. Such a solution results in writing equation (2.6) in the form

$$\mathbf{G}(\mathbf{r}'', \mathbf{r}') = \mathbf{g}(|\mathbf{r}'' - \mathbf{r}'|) + \mathbf{g}(|\mathbf{r}''|) T \mathbf{g}(|\mathbf{r}'|) \tag{2.8}$$

so that all interaction terms are grouped into the T matrix $\left[\mathbf{V}_m^{-1} - \mathbf{g}(r=0)\right]^{-1}$. As will be discussed in section 2.6, the Lehmann representation [78–81] allows poles of Green's functions to be interpreted as bound states. As there are no sub-gap bound states in a bare s-wave superconductor by Anderson's theorem [82] any bound states in this system can be found in the poles of the T matrix:

$$T = \left[\mathbf{V}_m^{-1} - \mathbf{g}(r=0)\right]^{-1} \tag{2.9}$$

where the 2D, real space Green's function is given by:

$$\mathbf{g}(r=0) = \frac{\pi \rho_0}{\sqrt{\Delta^2 - \omega_+^2}} \left(\omega_+ \sigma_0 + \Delta \sigma_x\right) \tag{2.10}$$

where ρ_0 is the two dimensional density of states, $\omega_+ = \omega + i\eta$ is the frequency with an infinitesimal $\eta > 0$, Δ the bulk superconducting gap and σ_0, σ_x are the unit matrix and x Pauli matrix in Nambu space. By solving for the pole of the T matrix one finds bound states at energies:

$$\omega = \pm \Delta \frac{1 - (\rho_0 \pi V_m)^2}{1 + (\rho_0 \pi V_m)^2} \tag{2.11}$$

where V_m is the magnetic interaction strength (so that we can define a unitless strength $C_m = \rho_0 \pi V_m$). Notably, for any non-zero magnetic interaction this means there are sub-gap bound states, by contrast to the case of scalar impurities where bound states are forbidden by Anderson's theorem [82].

[4] This choice of basis is not unique and for clarity we will use this choice throughout.

[5] One can solve this problem in terms of a cleverly chosen 2 dimensional sub-space by thinking of the magnetic interaction as equivalent to a spin dependent chemical potential shift but we will not proceed in this manner.

As we will be focusing on constructing an array of such states, it is worth considering an additional result where there exists a finite concentration of magnetic impurities as in [76]. In that case, a band develops about the sub-gap points in equation (2.11) with a width (for small impurity concentration c) $W = \Delta\sqrt{8\alpha\sqrt{1-\gamma^2}}$ $\alpha = 1/\Delta(1+(\rho_0\pi V_m)^2)^2 c V_m^2 2\pi\rho_0$ and γ corresponds to the bound state energies in equation (2.11) divided by Δ. This illustrates that sub-gap bands will form starting from the single impurity bound state energy, and build from there to a width with a dependence on the superconducting gap Δ like $W \approx \Delta^{1/2}$ as seen from the dependence of W and α on Δ.

2.3 Return to other approaches

As a result of focusing on comparatively sparse chains, the methods employed in other studies of magnetic adatom chains have been to consider the hybridisation of individual YSR states along the one-dimensional line connecting them. This also rather neatly allows one to consider the system as an essentially one dimensional chain of YSR states in a tight binding like model. Such an approach does however raise the question of how sparse physical chains would be in experiment and whether there is a qualitative difference on reducing the adatom spacing a_h. There has been some exploration of precisely this detail in the literature [83].

To understand the physically relevant sparsity one major consideration is dimensionality. It has been shown that YSR states decay like a power law and thus only very slowly in two dimensional systems [84]. In this way (especially as coherence lengths are $\approx 1\,\text{nm}$ in thin films [84, 85]), they can easily overlap with other states for tens or hundreds or lattice sites [6]. This suggests that, at least in two dimensions, an adatom chain would need to be extremely sparse to be described by a nearest neighbour hopping model. There has been some numerical investigation of the difference made by embedding one dimensional lines into higher dimensional substrates compared to systems without such a dimensional mismatch [62, 65]. In [65] in particular, self consistent calculations were performed and it was found that the system can self organise into spiral ordered, topological phases.

Another feature of experiments to date is that generally, to understand the results in terms of purely one dimensional models one is forced to accept unreasonably large magnetic interaction strengths for adatoms, of the order of a few multiples of E_F. This seems like an unusual requirement and we find scaling relations which may be applied to reduce these estimates to more reasonable values.

It is also worth noting that in experiments one is generally probing the states or response of the substrate in order to note the presence of topological bound states. There have been some indications that the bound states in adatom chain systems in fact reside in the substrate rather than the chain itself [42]. There has been some discussion of encapsulating adatom chains within a capping layer of superconductor to better observe the presence of this phenomenon rather than probing the electronic states of the adatoms [86].

In this way we highlight the key features necessary to fully describe a system comprised of a spiral ordered magnetic chain atop a two dimensional substrate. We will take an approach that

[6] It is noteworthy in experiments on 3D substrates that very little overlap between even *adjacent* magnetic adatoms was detected [43].

takes into account interactions at *all* distances for a dense chain of magnetic impurities and will investigate whether it is possible to extract an effectively one dimensional sub-system from this two dimensional system which is in some way analogous to the Kitaev chain toy model.

2.4 Calculation of full Green's function

In order to construct a continuum model we begin with the Hamiltonian for a 2D, s-wave superconductor in momentum space:

$$H_0 = \sum_{\mathbf{k},\sigma} \epsilon_{\mathbf{k}} c^\dagger_{\mathbf{k},\sigma} c_{\mathbf{k},\sigma} + \sum_{\mathbf{k}} \left(\Delta c_{-\mathbf{k},\downarrow} c_{\mathbf{k},\uparrow} + \text{h.c.} \right), \tag{2.12}$$

where $c_{\mathbf{k},\sigma}$ are electron operators for momentum $\mathbf{k} = (k_x, k_y)$ and spin $\sigma = \uparrow, \downarrow = +, -$, the dispersion $\epsilon_{\mathbf{k}} = (k_x^2 + k_y^2 - k_F^2)/2m$, assumed to have circular symmetry, with effective mass m and Fermi momentum k_F, and the s-wave bulk gap Δ. We set $\hbar = 1$ throughout. In describing the system in this manner we are making the reasonable assumption that the substrate can be described within the effective mass approximation. This is reasonable as, though we must be careful taking such a limit as discussed, the band widths are generally much larger (of order 1 eV) than the superconducting gap. In this way the model is made far simpler than using tight binding, cosine bands, but does not have the invalid assumptions brought about by assuming linear bands. We will further discuss the range of validity of this model and approximations to it in section 2.4.1.

The interaction with a magnetic chain will be added by consideration of a term in the Hamiltonian describing a dense chain of classical moments at $y = 0$:

$$H_m = V_m \int dx\, \mathbf{M}(x) \cdot \mathbf{S}(x, y = 0), \tag{2.13}$$

where (x, y) are the spatial coordinates, V_m is the scattering strength, and $\mathbf{S}(x, y)$ is the electron spin operator. The planar magnetic texture/spiral of the impurities is described by the term $\mathbf{M}(x) = \cos(2k_m x)\hat{\mathbf{e}}_1 + \sin(2k_m x)\hat{\mathbf{e}}_2$ where the period is π/k_m and $\hat{\mathbf{e}}_{1,2}$ are arbitrary orthogonal unit vectors which do not necessarily coincide with our spatial coordinates. This texture is particularly noteworthy due to the fact that, by a spin dependent unitary transformation, a 1D system with such a texture is mathematically identical to the inclusion of spin-orbit coupling [70]. In what follows we will see what effect this same transformation has with a 2D background. The parameters k_m and V_m remain freely tunable in our methodology.

Due to the spiral order in the x direction, this problem is *not* diagonal in k_x. We will proceed by finding a transform to make it so, but such a transform (equation (2.18)) requires the choice of spin quantization axis to be parallel to the real space z axis. In this way we necessarily restrict ourselves to only planar spiral texture, but without this we cannot make the following transformations. With this choice we are thus able to write:

$$\mathbf{S} = \frac{1}{2} c^\dagger_\sigma(\mathbf{x}) \left(\boldsymbol{\sigma}_{\sigma,\sigma'} \right) c_{\sigma'}(\mathbf{x}) \tag{2.14}$$

where $\boldsymbol{\sigma}_{\sigma,\sigma'}$ denotes the corresponding x, y, z Pauli matrix. Hence, the action of the spin ope-

rator may be written in terms of electron spin up/down creation and annihilation operators:

$$S_x(\mathbf{x}) = \frac{1}{2}\left[c^\dagger_\uparrow(\mathbf{x})c_\downarrow(\mathbf{x}) + c^\dagger_\downarrow(\mathbf{x})c_\uparrow(\mathbf{x})\right]$$
$$S_y(\mathbf{x}) = \frac{i}{2}\left[c^\dagger_\uparrow(\mathbf{x})c_\downarrow(\mathbf{x}) - c^\dagger_\downarrow(\mathbf{x})c_\uparrow(\mathbf{x})\right]$$
$$S_z(\mathbf{x}) = \frac{1}{2}\left[c^\dagger_\uparrow(\mathbf{x})c_\uparrow(\mathbf{x}) - c^\dagger_\downarrow(\mathbf{x})c_\downarrow(\mathbf{x})\right]$$

To proceed we must write the interaction term in terms of momentum space electron operators. We can re-write the real space interaction in Fourier modes in the x-direction:

$$H_{int} = \int dx\, V_m \left(e^{i2k_m x}\hat{c}^\dagger_\uparrow(\mathbf{x})\hat{c}_\downarrow(\mathbf{x}) + e^{-i2k_m x}\hat{c}^\dagger_\downarrow(\mathbf{x})\hat{c}_\uparrow(\mathbf{x})\right) \tag{2.15}$$
$$= V_m \int dx \sum_{k_x,k'_x} \Big(e^{i(2k_m+k_x-k'_x)x}\hat{c}^\dagger_{k'_x,\uparrow}\hat{c}_{k_x,\downarrow} + e^{-i(2k_m-k_x+k'_x)x}\hat{c}^\dagger_{k_x,\downarrow}\hat{c}_{k_x,\uparrow}\Big)$$
$$= V_m \sum_{\forall k_x} \left(\hat{c}^\dagger_{k_x+2k_m,\uparrow}\hat{c}_{k_x,\downarrow} + \hat{c}^\dagger_{k_x-2k_m,\downarrow}\hat{c}_{k_x,\uparrow}\right) \tag{2.16}$$
$$= V_m \sum_{\forall k_x} \left(\hat{c}^\dagger_{k_x+k_m,\uparrow}\hat{c}_{k_x-k_m,\downarrow} + \hat{c}^\dagger_{k_x-k_m,\downarrow}\hat{c}_{k_x+k_m,\uparrow}\right) \tag{2.17}$$

where all operators $\hat{c}_\sigma(x)$, $\hat{c}_{k_x,\sigma}$ are understood to be evaluated only at $y = 0$ due to the local nature of the interaction. Henceforth we will omit hats on operators.

This spiral order can be unwound by applying the spin dependent unitary (gauge) transform

$$\tilde{c}_\sigma(x) = e^{-i\sigma k_m x}c_\sigma(x) \tag{2.18}$$

which we will apply in momentum space as

$$\tilde{c}_\sigma(x) = e^{-i\sigma k_m x}c_\sigma(x) \tag{2.19}$$
$$\int dx e^{-ik_x x}\tilde{c}_\sigma(x) = \int dx e^{-i(k_x+\sigma k_m)x}c_\sigma(x) \tag{2.20}$$
$$\tilde{c}_{k_x,\sigma} = c_{k_x+\sigma k_m,\sigma} \tag{2.21}$$

which reduces to a simple momentum shift $k_x \to k_x + \sigma k_m$. Applying this shift to spin flip terms $c^\dagger_{k_x+k_m,\uparrow}c_{k_x-k_m,\downarrow}$ leaves $\tilde{c}^\dagger_{k_x,\uparrow}\tilde{c}_{k_x,\downarrow}$. Other terms transform as:

$$c^\dagger_{k_x,\sigma}c_{k_x,\sigma} \to \tilde{c}^\dagger_{k_x+\sigma k_m,\sigma}\tilde{c}_{k_x+\sigma k_m,\sigma} \tag{2.22}$$
$$c_{-k_x,\downarrow}c_{k_x,\uparrow} \to \tilde{c}_{-(k_x+k_m),\downarrow}\tilde{c}_{k_x+k_m,\uparrow} \tag{2.23}$$

so that we can then relabel momenta and hence transfer the momentum shift entirely into the background bands $\epsilon_{k_x} \to \epsilon_{k_x+\sigma k_m}$.

It is worth noting that one possible operator pair (fortunately not present in our calculation)

does not fit quite as nicely into this formulation:

$$c_{-k_x,\uparrow}c_{k_x,\uparrow} \to \tilde{c}_{-(k_x-k_m),\uparrow}\tilde{c}_{k_x+k_m,\uparrow} \tag{2.24}$$

which, unlike for the kinetic energy and singlet superconducting terms, mixes between $k_x \pm k_m$ sectors in the transformed basis. Though this turns out not to be a problem in our case, it is worthwhile to check that such terms remain zero at time reversal invariant momenta through the calculation. We will see in chapter 3 if this is not the case then the classification by calculating a Pfaffian does not make sense as the resulting transformed Hamiltonian will not be anti-symmetric (it will have non-zero diagonal components).

With this unitary transform applied to all terms, we may now write the Hamiltonian and interaction term in an extended Nambu basis $(\tilde{c}^\dagger_{\mathbf{k},\uparrow}, \tilde{c}^\dagger_{\mathbf{k},\downarrow}, \tilde{c}_{-\mathbf{k},\downarrow}, \tilde{c}_{-\mathbf{k},\uparrow})$. This, non unique, extension is necessary due to the combined presence of both spin-flip terms and spiral order which would otherwise take you out of the conventional Nambu space. To avoid overcounting we restrict summation to $k_x \geq 0$[7]. This basis is defined in the spin shifted basis so that the problem is now diagonal in the x direction. Though possible to approach this calculation with a restriction before applying the above unitary transform, it is far simpler to apply it only at this final stage.

Using the definition of the Green's function in terms of the resolvent, or by direct calculation (see section A.1), the retarded free Green's function for the 2D superconducting substrate takes the form:

$$g(\omega_+, \mathbf{k}) = \sum_\sigma \frac{\tau_0^\sigma \omega_+ + \tau_z^\sigma \epsilon_{\mathbf{k}^\sigma} + \sigma\tau_x^\sigma \Delta}{\omega_+^2 - \epsilon^2_{\mathbf{k}^\sigma} - \Delta^2}, \tag{2.25}$$

where $\omega_+ = \omega + i\eta$ and $\eta > 0$ is an infinitesimal shift so that the function is analytic in the upper half plane of complex ω space; $\mathbf{k}^\pm = (k_x \pm k_m, k_y)$, and $\tau_\alpha^\pm = \tau_\alpha(\sigma_0 \pm \sigma_z)/2$, for τ_α the Pauli matrices in Nambu and σ_α in spin space (with τ_0, σ_0 the unit matrices).

Due to the localised nature of the interaction to $y = 0$ it is natural to go to a mixed (k_x, y) space by calculation of the partial Fourier transform $g(\omega, k_x, y) = \int_{-\infty}^{\infty} dk_y e^{iyk_y} g(\omega, \mathbf{k})$. This can be performed exactly for a quadratic dispersion (see section A.2 for details) and yields:

$$\begin{aligned} g(\omega_+, k_x, y) = &\sum_\sigma \frac{-i\pi\rho}{4k_F\sqrt{\tilde{\omega}_+^2 - \tilde{\Delta}^2}} \\ &\times \left\{\tilde{\omega}_+\xi_\sigma\tau_0^\sigma + \sigma\tilde{\Delta}\xi_\sigma\tau_x^\sigma + \left[(\kappa_\sigma^2 - 1)\xi_\sigma + \chi_\sigma\right]\tau_z^\sigma\right\}, \end{aligned} \tag{2.26}$$

where $\rho = m/\pi$ is the 2D density of states at the Fermi energy, $\tilde{\omega} = \omega/E_F$, $\tilde{\Delta} = \Delta/E_F$, for $E_F = k_F^2/2m$, and we have defined $\kappa_\sigma = (k_x + \sigma k_m)/k_F$, $\xi_\sigma = p_{\sigma,+}^{-1}\mathrm{e}^{i|y|k_F p_{\sigma,+}} + p_{\sigma,-}^{-1}\mathrm{e}^{-i|y|k_F p_{\sigma,-}}$ and $\chi_\sigma = p_{\sigma,+}\mathrm{e}^{i|y|k_F p_{\sigma,+}} + p_{\sigma,-}\mathrm{e}^{-i|y|k_F p_{\sigma,-}}$, with $p_{\sigma,\pm} = \left[1 - \kappa_\sigma^2 \pm (\tilde{\omega}_+^2 - \tilde{\Delta}^2)^{1/2}\right]^{1/2}$.

It should be emphasised that this result is exact and does not require a cutoff and is valid for all parameter regimes where one would expect such a mean field treatment of superconductivity to hold.

[7]This can overcount the state at $k_x = 0$ but given this is only a single state and is important physically we prefer this choice to $k_x > 0$. Practically, as such a state is measure zero in the set of states labelled by k_x this choice must have no impact on observables.

2.4.1 Green's function in long wavelength approximation (LWA)

An approximation of our exact result valid in the long wavelength approximation (LWA) has been reported in the literature. This approximation arises in studies of the limit of sparse chains of magnetic impurities on superconducting substrates (where the separation of magnetic impurities $a_h \gg 1/k_F$) [24–29, 31, 41]. Though the precise methods vary, these methods [24–29, 87–89] often rely heavily upon the result either directly or implicitly.

We will explore in some detail how this approximation can arise from taking what are ordinarily innocent approximations during calculation. The LWA arises in scenarios where one is left with mixed real and momentum space labels, and as a result during calculations which aim to integrate out substrate degrees of freedom. It can occur by assuming, as one is normally safe to do, that the density of states is constant (i.e.: bands are linear in momenta). We will see that this is not valid in precisely the most physically interesting region of momentum space. Interestingly, the same result can be derived by taking the similarly innocuous limit ω/E_F, $\Delta/E_F \ll 1$ (i.e.: assuming a wide bandwidth compared to the gap) from the exact result in equation (2.26). Hence, it is clear that unusual care must be taken here and we will explore precisely how these normally safe approximations are breaking down simply by looking in mixed real and momentum space.

The Green's function in the long wavelength approximation (LWA) can be written:

$$\begin{aligned} g &\approx -\frac{i\pi\rho_0}{\sqrt{\omega_+^2-\Delta^2}}\frac{\cos\left(y\sqrt{k_F^2-k_x^2}\right)}{\sqrt{k_F^2-k_x^2}}(\tau_0\sigma_0\omega_+ + \tau_x\sigma_z\Delta) \\ &= -\frac{i\pi\rho_0}{\sqrt{\omega_+^2-\Delta^2}}\frac{\cos(yp(k_x))}{p(k_x)}(\tau_0\sigma_0\omega_+ + \tau_x\sigma_z\Delta) \end{aligned} \tag{2.27}$$

where ρ_0 is the constant 2D density of states at the Fermi energy for the substrate; k_x is the wave vector along the chain; y transverse distance from the chain in real space; $p = \sqrt{k_F^2 - k_x^2}$; ω_+ is the energy (offset by a small imaginary infinitesimal) and Δ is the substrate, superconducting gap. Though this approximate result should correctly describe the physics for $k_x \ll k_F$ it is completely invalid for $k_x \approx k_F$ or $k_x > k_F$. In this way we can already see the first evidence that something could go wrong: this Green's functions evidently divergences at $k_x = k_F$ because $p(k_x) \to 0$. This result can be thought of as due to assuming a constant density of states at the Fermi energy, restricting to $k_x \ll k_F$ or assuming any bound states which form are disconnected from the continuum or otherwise restricted to be close to $\omega = 0$. To see how these are equivalent we can write the free Green's function (without a spin shift without loss of generality) as:

$$\begin{aligned} g(k_x, y) &= \int dk_y e^{iyk_y}\frac{\omega_+\tau_0 + \epsilon_{\mathbf{k}}\tau_z + \Delta\tau_x}{\omega_+^2 - \Delta^2 - \epsilon_{\mathbf{k}}^2} \\ &= \int d\epsilon \frac{dk_y}{d\epsilon} e^{iyk_y(\epsilon)}\frac{\omega_+\tau_0 + \epsilon\tau_z + \Delta\tau_x}{\omega_+^2 - \Delta^2 - \epsilon^2} \\ &= \int d\epsilon \frac{f(k_x,\epsilon)}{\omega_+^2 - \Delta^2 - \epsilon^2} \end{aligned} \tag{2.28}$$

so that, if the function $f(k_x, \epsilon)$ is analytic, we can solve this integral by enclosing the appropriate

pole in the complex ϵ plane. Hence, for $\omega < \Delta$:

$$g(k_x, y) = \frac{-\pi N(k_x, \omega)}{\sqrt{\Delta^2 - \omega_+^2}} e^{-\frac{|y|k_F}{4\xi_0 p}\sqrt{1-(\omega/\Delta)^2}} \left(\omega_+ \cos(py)\tau_0 + \Delta\tau_x\right). \tag{2.29}$$

It thus remains only to understand the meaning of the function $N(k_x, \omega)$. If we restrict to energies close to the (assumed circular) Fermi surface then the 2D density of states for the substrate can be written as:

$$N(\omega = 0) = \int \frac{d^2k}{(2\pi)^2}\delta(\epsilon_{\mathbf{k}}) = \int \frac{dk}{2\pi} k\delta(\epsilon_k) = \frac{1}{2\pi}\frac{k_F}{\left(\frac{d\epsilon_k}{dk}\right)|_{\epsilon_k=0}} \tag{2.30}$$

which we can relate to the partially integrated 2D density of states, evaluated at the Fermi energy:

$$N(k_x, \omega = 0) = \int \frac{dk_y}{2\pi}\delta(\epsilon_{\mathbf{k}}) = \sum_{k_y=\pm\sqrt{k_F^2-k_x^2}} \frac{1}{2\pi}\frac{1}{\left(\frac{d\epsilon_k}{dk_y}\right)|_{\epsilon_k=0}} \tag{2.31}$$

so that, if we restrict attention to $\omega \ll \Delta$ we can relate

$$N(k_x, \omega = 0) = \frac{2N(\omega = 0)}{p} \tag{2.32}$$

thus, for $\omega \ll \Delta$ $g(k_x, y)$ reduces to equation (2.27). However, in this situation, the normally innocent approximation $\omega \ll \Delta$ leads to equation (2.32) and hence equation (2.27) which both go like $1/\sqrt{k_F^2 - k_x^2}$. In this way, the LWA is formally divergent at $k_x = k_m \pm k_F$ and $k_x = -k_m \pm k_F$. Though perhaps not a problem in general, for the purposes of our calculations these are the points of greatest physical interest. This can be seen by considering the spin up and spin down Fermi surfaces for the system entirely in momentum space shown in the top row of figure 3. We see that, even without applying the spin dependent momentum shift required to take into account spiral ordered interfaces/1D spin orbit interaction (see section 2.4 for more details) one must integrate out the k_y direction in order to find expressions for a wave or Green's function at $y = 0$ where you intend to work out the influence of magnetic impurities. Though it is not problematic to add up contributions for $k_x \ll k_F$, one can see that as $k_x \to k_m + k_F$ the integral must take into account increasingly singular components until, exactly at $k_x = k_m + k_F$, the gradient is strictly infinite and the integral singular.

As shown in the bottom row of figure 3; the superconducting pairing is expected to be strongest in precisely these regions, and for spin dependent momentum shift $k_m = k_F$ in particular one can see that this singular behaviour occurs at the only point where the spin up and down Fermi surfaces make contact (and hence would be expected to have interesting/dominant physics in play) it seems clear that there will be limits where equation (2.27) will either not describe all of the physics present, or will miss the physics present entirely. We will see in our exact calculation that the former case applies for dense chains of ferromagnetically aligned adatoms, the latter to particular helically ordered chains.

It is illustrative to examine the limits in which the LWA is recovered from the exact result

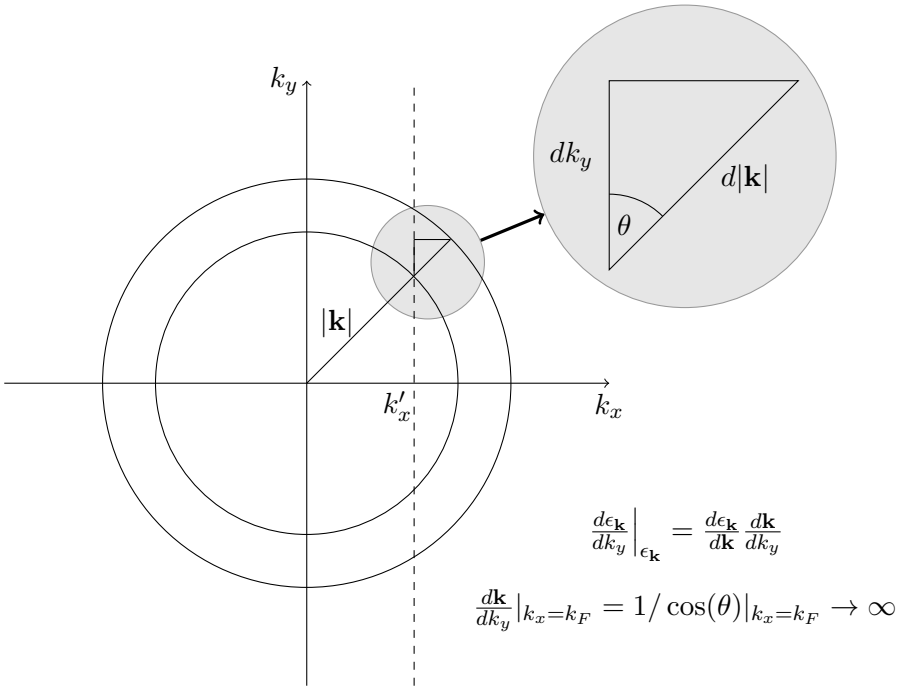

Figure 2: Illustration of the difference between assuming a constant density of states in two dimensions, and hence adding a shell of states of thickness $|\mathbf{k}|$ in a purely radial direction, and integrating along only the k_y direction at fixed k'_x (dashed line) as required in a mixed real and momentum space calculation. Though for small k'_x there is little difference as $d\mathbf{k}$ is essentially parallel to dk_y, as $k'_x \to k_F$ $d\mathbf{k}$ becomes perpendicular to dk_y and the contribution to the integral becomes singular. This is a clear violation of our assumption that the integrand in equation (2.28) be analytic. In this way we demonstrate the subtle difficulty of writing two dimensional wave packets travelling in the x direction in terms of only a y co-ordinate; we end up tracing out/losing all of the interesting information by making unjustified assumptions.

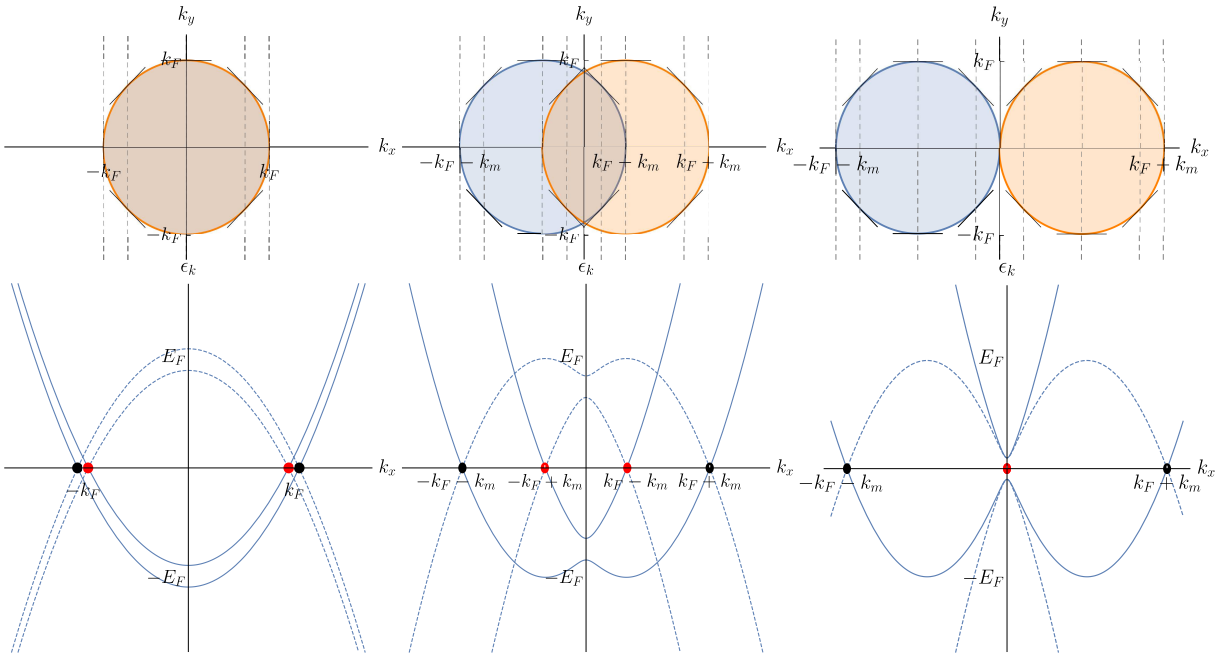

Figure 3: Top: Spin splitting of Fermi surface of a nearly free electron gas under the unitary transform in equation (2.18). Vertical dashed lines indicate direction of integration to calculate semi-Fourier transformed free Green's function. Thick lines display the gradient. Divergence of gradient at $\pm_1 k_F \pm_2 k_m$ indicates the failure of assuming constant density of states/long wavelength approximation. Note in particular top right, $k_m = k_F$ where spin shifted Fermi surfaces touch only at one point, precisely at this point of divergent gradient. Bottom: Band structure for 1D, nearly free electron model in magnetic field with spin dependent Fourier transform for (left to right) $k_m = 0$ (ferromagnet), $k_m = 0.5k_F$, $k_m = k_F$. Dashed curves indicate hole bands. Filled circles are marked in coloured pairs to indicate the locations that would undergo superconducting pairing (opposite momenta, opposite spin). Comparing to above considerations, these locations exactly co-incide with the points where the LWA is expected to break down.

in equation (2.26). Perhaps most notably, the τ_z^σ components must cancel out as there are no such components in the LWA. Thus if we focus on the τ_z^σ components

$$\left[(\kappa_\sigma^2 - 1)\xi_\sigma + \chi_\sigma\right] \tag{2.33}$$

we can see that, with a slightly modified BCS theory assumption that
$\lambda = \frac{k_F}{E_F(1-\kappa_\sigma^2)} \left(\omega^2 - \Delta^2\right)^{1/2} \ll 1$ we are left with:

$$\left[(\kappa_\sigma^2 - 1)\xi_\sigma + \chi_\sigma\right] = 2\cos\left(ip_\sigma y\right)\left(-p_\sigma + p_\sigma\right) + O(\lambda^2) \tag{2.34}$$

where $p_\sigma = \left(1 - \kappa_\sigma^2\right)^{1/2}$. Hence, τ_z terms are zero to first order, but diverge like $1/p_\sigma$ to higher orders. This is a signature of divergence in the LWA discussed previously but here we see that it occurs wherever the condition $\frac{k_F}{E_F(1-\kappa_\sigma^2)} \left(\omega^2 - \Delta^2\right)^{1/2} \ll 1$ is not fulfilled. This naturally reduces to the standard BCS theory expression of $\Delta \ll E_F$ for small momenta, but then tracks the "bandwidth" at each k_x and hence necessarily becomes comparable to Δ at some point. In this way it is fairly clear the failure of the LWA in this limit is arising entirely from having a mixed real and momentum space picture and hence a "spare" momentum label to describe underlying dispersive bands.

It is interesting to note that $p_\sigma^\pm$ very much plays the role of a wave vector in the place of k_y due to the implicit loss of translation symmetry by treating $y = 0$ as a special location. Such a comparison is more valid in regions where

$$k_F p_\sigma^\pm \approx k_y \approx \sqrt{k_F^2 - k_x^2} \tag{2.35}$$

which is precisely the same region as is required to reach the LWA. This suggests an interpretation that the failure of the LWA occurs most obviously for wave packets which are travelling essentially entirely in the x-direction, parallel to where the impurity chain will be implemented. Given that these wave packets essentially travel along the chain and are thus of great physical interest it is troubling that the LWA most clearly fails in this limit.

We may apply the same limit to the τ_x and τ_z components leaving only:

$$g \approx \sum_\sigma \frac{-i\pi\rho_{2D}}{2k_F\sqrt{\omega_+^2 - \Delta^2}} \cos\left(ip_\sigma|y|\right)\left(\tau_0^\sigma\omega_+ + \tau_x^\sigma\Delta\right) \tag{2.36}$$

which differs from equation (2.27) by a factor of two due to the summation over σ. For $k_m = 0$ they are exactly equivalent. This demonstrates that the LWA is valid only for $k_x \pm k_m < k_F$ as expected from our previous discussion.

As this is a subtle and fundamental result for our work we will summarise the link between our exact result and the LWA. Any approach which requires looking at mixed real and momentum space labels causes an implicit failure of ordinarily valid assumptions. It is not possible to assume a constant density of states, nor to focus only at $\omega, \Delta \ll E_F$ as is normally safe for BCS theory. Crucially, this does *not* signal a breakdown of that theory. This result arises essentially from the difference in dimensionality in the mixed real and momentum space Green's function

compared to those entirely in real or momentum space.

Put another way, this exposed divergence tells us that one cannot simply cut out the part of two dimensional wavepackets travelling in the x direction and call that a one dimensional model. A two dimensional system is, due to the connectivity involved, generically more complicated than just a stack of weakly coupled one dimensional systems.

Though limitations of the LWA have been mentioned in the literature [24] we will see that it is rather more serious than simply having an asymptotic range of validity at large distances. In what follows we will show that the LWA completely misses crucial physics compared to the exact result in equation (2.26) precisely because of its restricted range of validity in momentum space.

2.5 Calculation of full Green's function cont'd

With the exact free Green's function attained, we may then write the full Green's function (dropping ω_+ for clarity) in terms of a Dyson equation [78–81]. Though this calculation is standard, we will extend it to discuss multiple chains in chapter 4 so it is illustrative to see how to build from bare interactions as we do here. The Dyson equation [90] for an isolated magnetic impurity at $y = 0$ in terms of a mixed real and momentum space matrix Green's function is given by [91]:

$$G(k_x, y_f, y_i) = g(k_x, y_f - y_i) + g(k_x, y_f)VG(k_x, y_f = 0, y_i) \tag{2.37}$$

which can be solved either formally by solving the supplementary equation:

$$G(k_x, y_f = 0, y_i) = g(k_x, y_i) + g(k_x, 0)VG(k_x, y_f = 0, y_i) \tag{2.38}$$

$$g(k_x, y - y') = (1 - g(k_x, 0)V)\, G(k_x, y_f = 0, y_i = y') \tag{2.39}$$

$$G(k_x, y_f = 0, y_i = y') = (1 - g(k_x, 0)V)^{-1}\, g(k_x, y - y') \tag{2.40}$$

or by a more diagrammatic, recursive, resummation:

$$= g(k_x, y_f - y_i) + g(k_x, y_f)VG(k_x, y_f = 0, y_i) \tag{2.41}$$

$$= g(k_x, y_f - y_i) + g(k_x, y_f)Vg(k_x, y_i) + g(k_x, y_f)Vg(k_x, 0)VG(k_x, y_f = 0, y_i) \tag{2.42}$$

$$= g(k_x, y_f - y_i) + g(k_x, y_f)V\left[1 + g(k_x, 0)V + (g(k_x, 0)V)^2 + \dots\right] g(k_x, y_i) \tag{2.43}$$

resulting in:

$$G(k_x, y_f, y_i) = g(k_x, y_f - y_i) + g(k_x, y_f)\left[V^{-1} - g(k_x, 0)\right]^{-1} g(k_x, y_i) \tag{2.44}$$

$$= g(k_x, y_f - y_i) + g(k_x, y_f)Tg(k_x, y_i) \tag{2.45}$$

from which we can in principle extract any relevant observables.

Note that this method explicitly takes into account arbitrary range interactions along the chain direction. This can be understood best by noting that the Dyson equation for an infinite line of scatterers (supressing the y index as this will be identical to the above calculation) is

given by:

$$G(x_f - x_i) = g(x_f - x_i) + \int dx' g(x_f - x') V G(x' - x_i) \tag{2.46}$$

and has translation invariance in the x direction due to the infinite extent of the impurity chain. We can re-write this equation as:

$$\int dk_x e^{ik_x \delta x} G(k_x) = \int e^{ik_x \delta x} dk_x g(k_x) + \int dx' dk_x dk'_x e^{i(k'_x - k_x)x'} e^{ik_x x_f} e^{-ik'_x x_i} g(k_x) V G(k'_x) \tag{2.47}$$

$$\int dk_x e^{ik_x \delta x} G(k_x) = \int e^{ik_x \delta x} dk_x g(k_x) + \int dk_x e^{ik_x \delta x} g(k_x) V G(k_x) \tag{2.48}$$

$$G(k_x) = g(k_x) + g(k_x) V G(k_x) \tag{2.49}$$

which is the Dyson equation studied above. Hence, in studying this system in mixed real and momentum space we take into account the local nature of the impurities in the y direction and the infinite extent of their interactions in the x direction, as mediated by the substrate.

2.6 Sub gap band structure

One of the key benefits of a Green's function based approach is that once you have the full Green's function for a system, it is usually relatively simple to calculate observables or spectral properties of the system. At the root of a great deal of observables which are readily measurable is the band structure induced by the magnetic impurities. This is at least in part because we know that, for an s-wave gap, one expects there to be no sub-gap states at all, even in the presence disorder due to Anderson's theorem [82]. Hence, there is a relatively clear separation between the effect on observables of the background (above the superconducting gap Δ) and subgap contributions (below Δ) which can often be understood by deep enough analysis of the sub-gap spectrum.

To give some examples: the density of states, readily inferable by transport or scanning tunnelling microscopy (STM), has its greatest peaks at points where bands flatten so that they have maximum curvature. Similarly, spin currents must be carried by available states and an analysis of the gradient of sub-gap bands can give some physical intuition about whether there are net spin currents in particular directions.

In an arguably heavily related theme, topological phase transitions in weakly interacting systems are generally understood to only occur when, on tuning a parameter, states can be made to cross the Fermi surface or zero energy an odd number of times. A frequently seen example of this evidence of nontrivial topology of the mapping from wave functions to the Brillouin zone reduces to the statement that the energy bands cross the Fermi surface an odd number of times. Though it is unclear how well such statements extend to this precise setup [8], it is nonetheless interesting to view the band structure with this lens in mind.

We may extract information on bound states from the full Green's function by realising that

[8] See chapter 3 for a more in depth discussion of the issue of topological characterisation in this system. Accounting for the substrate makes conclusions difficult to attain and ambiguous.

any fermionic retarded Green's function may be written in the Lehmann representation [78–81]

$$g(\omega_+, \mathbf{k}, \mathbf{r}) = \sum_n \frac{\psi_n^*(\mathbf{k}, \mathbf{r})\psi_n(\mathbf{k}, \mathbf{r})}{\omega_+ - E_{\mathbf{k},n}} + \int d\omega' \frac{A(\mathbf{k}, \mathbf{r}, \omega')}{\omega_+ - \omega'} \tag{2.50}$$

where the sum can be understood to refer to n possible families of single particle excitations at energies $E_{\mathbf{k},n}$ and the integral takes into account any continuum/closely spaced excitations present. Here the $\Psi_n(\mathbf{k}, \mathbf{r})$ are the wave functions for state n at wave vector $\mathbf{k}$, position $\mathbf{r}$ and $A(\mathbf{k}, \mathbf{r}, \omega')$ is the spectral density. This representation allows one to see that the poles of g in ω space correspond directly to single particle bound states, so long as they do not exactly coincide with a zero of the wave function in the numerator.

This picture is complicated only slightly by the use of matrix Green's functions in Nambu space as we must search for locations in ω space where elements or sectors of the matrix Green's function diverge like first order poles. Cramer's rule allows a matrix $\mathbf{A}$ to be written as

$$\mathbf{A}^{-1} = \frac{1}{\det \mathbf{A}} \mathrm{adj}(\mathbf{A}) \tag{2.51}$$

where adj$\mathbf{A}$ is the adjugate of $\mathbf{A}$ and can be represented via the Cayley-Hamilton theorem as in terms of traces and powers of $\mathbf{A}$. Hence, the only way for a matrix to be divergent in the manner we are seeking is if $\det \mathbf{A} = 0$.

In many cases, as happens in this calculation, many or all of the elements may share a denominator in the sense of this determinant. In this calculation in particular there can be no bound states in a bare superconductor, hence the poles for the full Green's function G must be entirely from the T matrix:

$$G = g + g\mathbf{T}g \tag{2.52}$$

$$= g + g \frac{1}{\det \mathbf{T}^{-1}} \mathrm{adj}(\mathbf{T}^{-1})\, g \tag{2.53}$$

where adj$(\mathbf{T})$ is a matrix of spectral/wave functions much like those in equation (2.50). In this way, so long as poles do not align with zeros (else you could have a pole with zero spectral weight) in the elements of the matrix $\mathbf{T}$, we may analyse where the matrix $\mathbf{T}^{-1}$ is singular to completely determine the analytic properties of the full Green's function.

It is worth noting that this analysis is still valid despite the loss of translation invariance in the y direction. Though the full Green's function is not diagonal in the y co-ordinate and hence we would in general need to perform an involved operator inversion to properly determine the location of all poles, here we are saved by the fact that, regardless of the y co-ordinate, if $|\omega| < \Delta$ (sub-gap) the bare Green's function has no poles. Hence, the only place they can arise is from the interactions which are entirely wrapped up in the T matrix, which in turn is entirely localised to $y = 0$. In this way, the sub-gap poles in this system at $y \neq 0$ are entirely determined by the behaviour of the system at $y = 0$.

2.6.1 Ferromagnetic chain $k_m = 0$

The case of a linear, magnetic interface may be solved analytically. The resulting T matrix using the exact Green's function derived takes the form (in terms of unitless variables):

$$T_{FM} = \left(\det\left(T^{-1}\right)\right)^{-1} \frac{\pi^3}{fC_m\sqrt{\Delta^2-\omega^2}} \begin{pmatrix} T_{11}(\omega) & T_{12}(\omega) & T_{13}(\omega) & T_{14}(\omega) \\ T_{12}(\omega) & T_{11}(\omega) & -T_{14}(\omega) & -T_{13}(\omega) \\ T_{13}(\omega) & -T_{14}(\omega) & -T_{11}(-\omega) & -T_{12}(-\omega) \\ T_{14}(\omega) & -T_{13}(\omega) & -T_{12}(-\omega) & -T_{11}(-\omega) \end{pmatrix} \tag{2.54}$$

where the four independent elements are:

$$\begin{aligned} T_{11}(\omega) = -\frac{\sqrt{-\tilde{\epsilon}_k+\sqrt{f}}}{\sqrt{f}\sqrt{2}C_m} \Big[& \tilde{\epsilon}_k^3 + \left(\tilde{\Delta}^2-\tilde{\omega}^2\right)\left(\tilde{\omega}+\sqrt{f}\right) \\ & + \tilde{\epsilon}_k^2\left(-C_m^2+\tilde{\omega}+\sqrt{f}\right) + \tilde{\epsilon}_k\left(\tilde{\Delta}^2-\tilde{\omega}^2-C_m^2\sqrt{f}\right) \\ & + C_m^2\left(\tilde{\omega}\left(\tilde{\omega}+\sqrt{f}\right)-\tilde{\Delta}^2\right)\Big] \end{aligned} \tag{2.55}$$

$$\begin{aligned} T_{12}(\omega) = \frac{1}{C_m^2\sqrt{f}\sqrt{\tilde{\Delta}^2-\tilde{\omega}^2}} \Big[& \tilde{\epsilon}_k\sqrt{f}C_m^2\tilde{\omega}^2 + \tilde{\epsilon}_k^2\left(\sqrt{f}\left(\tilde{\Delta}^2-\tilde{\omega}^2\right)-C_m^2\tilde{\Delta}^2\right) \\ & + \left(\tilde{\Delta}^2-\tilde{\omega}^2\right)\left(\sqrt{f}\left(\tilde{\Delta}^2+\left(C_m^2-\tilde{\omega}\right)\tilde{\omega}\right)-C_m^2\tilde{\Delta}^2\right)\Big] \end{aligned} \tag{2.56}$$

$$T_{13}(\omega) = \frac{\tilde{\Delta}}{\sqrt{2}C_m}\sqrt{-\tilde{\epsilon}+\sqrt{f}}\left(C_m^2-\sqrt{f}\right) \tag{2.57}$$

$$T_{14}(\omega) = \frac{\tilde{\epsilon}_k-\sqrt{f}\tilde{\Delta}\tilde{\omega}}{\sqrt{\tilde{\Delta}^2-\tilde{\omega}^2}} \tag{2.58}$$

where $\tilde{\epsilon}_k = k_x^2/k_F^2 - 1$, $\tilde{\omega} = \omega/E_F$, $\tilde{\Delta} = \Delta/E_F$, $f = \tilde{\epsilon}_k + \tilde{\Delta} - \omega^2$ and $C_m = \pi\rho V_m/k_F$ with ρ, the 2D density of states so that all quantities are unitless. The sub-gap poles of the full Green's function are entirely described by solving $\det(T^{-1}) = 0$ for ω so long as such poles never coincide with zeroes of these four functions.

Thus, the condition $\det(T^{-1}) = 0$ which determines the sub-gap bands in this case is:

$$\begin{aligned} \frac{\pi^4}{C_m^4\left(\Delta^2-\omega^2\right)\left(\epsilon_k^2+\Delta^2-\omega^2\right)} \Big(& 2\epsilon_k C_m^2\omega^2 + \epsilon_k^2\left(\Delta^2-\omega^2\right) + C_m^4\left(\Delta^2-\omega^2\right) + \left(\Delta^2-\omega^2\right)^2 \\ & - 2C_m^2\Delta^2\sqrt{\epsilon_k^2+\Delta^2-\omega^2}\Big) = 0. \end{aligned} \tag{2.59}$$

In order to solve this equation, we note that the prefactor can be safely ignored as it never has solutions for $|\omega| < \Delta$, describing the band structure of the background superconductor. It is also worth noting that this factor largely cancels out in the full T matrix in any case.

We can then proceed to extract a polynomial equation in ω by calculating:

$$\left(2\epsilon_k C_m^2\omega^2+\epsilon_k^2\left(\Delta^2-\omega^2\right)+C_m^4\left(\Delta^2-\omega^2\right)+\left(\Delta^2-\omega^2\right)^2-2C_m^2\Delta^2\sqrt{\epsilon_k^2+\Delta^2-\omega^2}\right)$$
$$\times\left(2\epsilon_k C_m^2\omega^2+\epsilon_k^2\left(\Delta^2-\omega^2\right)+C_m^4\left(\Delta^2-\omega^2\right)+\left(\Delta^2-\omega^2\right)^2+2C_m^2\Delta^2\sqrt{\epsilon_k^2+\Delta^2-\omega^2}\right). \tag{2.60}$$

This step does not add any spurious roots as this new factor has no zeroes in ω. We are thus left with an eighth order polynomial in ω:

$$\left(\Delta^2-\omega^2\right)\left(\omega^6+\beta_4\omega^4+\beta_2\omega^2+\beta_0\right)=0 \tag{2.61}$$

where the coefficients β_i are defined by:

$$\beta_4=-\left(2\left(\mathcal{E}-C_m^2\right)^2+3\tilde{\Delta}^2\right) \tag{2.62}$$

$$\beta_2=\left(\mathcal{E}-C_m^2\right)^4+4\left(\mathcal{E}^2-\mathcal{E}C_m^2+C_m^4\right)\tilde{\Delta}^2+3\tilde{\Delta}^4 \tag{2.63}$$

$$\beta_0=-\tilde{\Delta}^2\left(\mathcal{E}^2-C_m^4+\tilde{\Delta}^2\right)^2 \tag{2.64}$$

with $\mathcal{E}=(k_x/k_F)^2-1$ (the free electron dispersion at $k_y=0$). Clearly, the pre-factor could have been removed earlier, but is more obvious after this 'doubling' procedure, avoiding the need to deal with factors of ω nested inside roots.

This squared, cubic equation can then be solved using the general solution to the cubic equation[9] resulting in a single sub-gap ($\omega<E_k$ rather than $\omega<\Delta$ due to the k_x dependence of the 'effective' gap as one can see in figure 4) band described by $i=0$ in:

$$\tilde{\omega}=\pm\sqrt{-\left(\beta_4+\xi^i\gamma+\delta_0/\left(\xi^i\gamma\right)\right)/3}, \tag{2.65}$$

where $\gamma=[(\delta_1+\sqrt{\delta_1^2-4\delta_0^3})/2]^{1/3}$, $\delta_0=\beta_4^2-3\beta_2$, $\delta_1=2\beta_4^3-9\beta_4\beta_2+27\beta_0$, [10] and $\xi^i=\frac{1}{2^i}\left(\sqrt{3}i-1\right)^i$ for $i=0,1,2$ are the cube roots of unity.

This solution arises as one of a triplet of solutions to a particle-hole symmetric, cubic polynomial in ω of which this is the only part which is ever sub-gap. The black curves in figure 5 display how this band evolves over a range of magnetic impurity strengths C_m from small values in a), through a gap closure at $k_x=k_F$ when $C_m=\tilde{\Delta}^{1/2}$ which is unexpected from the point of view of hybridised Shiba bands as we will discuss, until beyond a second gap closure at $k_x=0$ when $C_m=\left(1+\tilde{\Delta}^2\right)^{1/4}$. Though plotted only for $k_x>0$, naturally these bands are symmetric with respect to $\pm k_x$ so that this exact solution suggests there are *always* an even number of crossings at $\omega=0$ due to the protection of the higher momentum gap closure. Though far from definitive in suggesting the ferromagnet cannot undergo a topological phase transition as

[9] There is some freedom in how to group together the three possible solutions to this cubic equation. We have made the choice such that one solution is purely real for all k_x and thus smoothly connects to $\omega=\Delta$ as $V_m\to 0$. Another potentially useful choice splits purely into states $\omega>0$ and $\omega<0$ but requires use of the general solution to the quartic equation.

[10] γ, δ_0 and δ_1 play a role in classifying whether all roots are real, in conjugate pairs etc. The changing classification with k_x can be seen in figure 4.

is generally understood to be the case, it is reassuring that this feature seems to emerge here. By comparison, the bands derived from the LWA appear gapless in the pathological sense that the Shiba chain bands show that the superconducting gap is always closed near k_F, regardless of how weak the strength of magnetic impurity scatterers. A gap is only formed at comparatively large magnetic interaction strength. The former case seems more physically realistic than the latter.

Interestingly, it is possible to break the structures present in this band down into two, roughly separate, physical mechanisms. For structure near $k_x = 0$ we may, rather than using the exact result derived in section 2.4 instead use the long wavelength approximation (LWA) highlighted there. This approximation is known to be invalid as $k_x \to k_F$ but does result in the subgap bands:

$$\omega = \pm\Delta \frac{(1 - k_x^2/k_F^2) - C_m^2}{(1 - k_x^2/k_F^2) + C_m^2}, \tag{2.66}$$

which is identical to the YSR energy for a single impurity in equation (2.11) at $k_x = 0$ so that the band structure from overlapping YSR states forms a band around this single impurity energy level, similar to the phenomenon seen by Shiba in [76] for randomly distributed impurities. As the quantity $1 - k_x^2/k_F^2 = -\epsilon_{k_x,k_y=0}/E_F$ it seems that each independent k_x acts as if it were an isolated YSR state but with a wave vector dependent band width, reducing from E_F for $k_x = 0$ to the clearly problematic 0 at $k_x = k_F$.

These bands are plotted in dashed red in figure 5 to compare to the exact result in black. Based on this correspondence, we understand the structure near $k_x = 0$ in the exact bands to physically originate from the hybridisation of individual YSR states. Such a band is central to the theoretical models in the limits of sparse chains of magnetic moments.

However, as one can see in figure 5 rather clearly, in this dense limit this is not the complete picture. The failure of the LWA near and beyond $k_x = k_F$ means that there must be some other mechanism for the additional structure, including a novel gap closure, to occur. If, instead of looking at a 1D chain of ferromagnetically aligned impurities embedded in a 2D superconductor, we look at the bands present for a 1D chain embedded in a 1D superconductor (hence just a 1D superconductor with a global magnetic field) by diagonalising the Hamiltonian:

$$H = \begin{pmatrix} c_{k_x,\uparrow}^\dagger & c_{k_x,\downarrow}^\dagger & c_{-k_x,\downarrow} & c_{-k_x,\uparrow} \end{pmatrix} \begin{pmatrix} \epsilon_{k_x}^+ & V_m & \Delta & 0 \\ V_m & \epsilon_{k_x}^- & 0 & -\Delta \\ \Delta & 0 & -\epsilon_{-k_x}^+ & -V_m \\ 0 & -\Delta & -V_m & -\epsilon_{-k_x}^- \end{pmatrix} \begin{pmatrix} c_{k_x,\uparrow} \\ c_{k_x,\downarrow} \\ c_{-k_x,\downarrow}^\dagger \\ c_{-k_x,\uparrow}^\dagger \end{pmatrix} \tag{2.67}$$

where $\epsilon_{k_x}^\pm = E_F \left((k_x/k_F \pm k_m/k_F)^2 - 1 \right)$ one can find simple expressions for the V_m required to close the gap:

$$V_m = \pm_1 \sqrt{\Delta^2 + E_F^2 \left(\left(k_x^2/k_F^2 - 1\right)^2 - 2\left(1 + k_x^2/k_F^2\right) k_m^2/k_F^2 + k_m^4/k_F^4 \right) - 4i\Delta k_x k_m/k_F^2} \tag{2.68}$$

which contains the results tabulated in table 1 as limits[11]. In particular, the intuitive result

[11]Note that this also displays neatly that there can only be gap closures if at least one of $k_x = 0$, $k_m = 0$ or $\Delta = 0$ to remove the imaginary part of the argument.

	2D model	1D model
$k_m = 0$, $k_x = k_F$	$C_m = \tilde{\Delta}^{1/2}$	$\check{V}_m/E_F = \tilde{\Delta}$
$k_m = 0$, $k_x = 0$	$C_m = [1 + \tilde{\Delta}^2]^{1/4}$	$\check{V}_m/E_F = [1 + \tilde{\Delta}^2]^{1/2}$
$k_m \neq 0$, $k_x = 0$	$C_m = [(1 - k_m^2/k_F^2)^2 + \tilde{\Delta}^2]^{1/4}$	$\check{V}_m/E_F = [(1 - k_m^2/k_F^2)^2 + \tilde{\Delta}^2]^{1/2}$
$k_m = k_F$, $k_x = 0$	$C_m = \tilde{\Delta}^{1/2}$	$\check{V}_m/E_F = \tilde{\Delta}$

Table 1: Comparison of possible gap closures in 2D model and 1D model. Here $C_m = \pi\rho V_m/k_F$, such that $k_F V_m$ and $\check{V}_m$ have units of energy illustrating the slight difference in units and prefactors depending on dimensionality. In the 1D model these are the only possible gap closures; either Δ, k_x or k_m must be 0 to obtain a gap closure.

that the superconducting gap will close when $V_m = \tilde{\Delta}$ clearly does hold in a *purely* 1D model. This would be attributed to Zeeman shifting of underlying bulk bands and that this closure occurs where $k_x = k_F$ as this is the part of the Boguluibov bands closest to zero energy. This is precisely what one does see, with an additional closing point at $k_x = 0$ when $V_m = E_F(1+\Delta^2)^{1/2}$ which simplified in the limit of $\Delta/E_F \ll 1$ to $V_m \approx E_F$, a condition which can be understood as having shifted underlying bands far enough that they exceeded the bandwidth. It is worth emphasising that this interpretation makes no mention of YSR states.

In our 2D model we see gap closures occurring at precisely the same k_x values but at renormalised V_m. It seems reasonable to thus interpret the gap closure present in our continuum calculation but explicitly absent for models built only from hybridisation of YSR states as due to the closure of bulk electronic bands by a Zeeman like effect but which closes the gap much more slowly because the magnetic field exists only locally rather than globally as one would normally expect when discussing the Zeeman effect. We summarise the comparison between gap closures present in 1D versus 2D models in table 1. Though the only change appears to be a simple change of power, this makes the gap closure in the 2D model at $k_x = k_F$ nonanalytic in Δ and hence inaccessible in a nonperturbative fashion.

One can also understand that this extra gap closure arises from the normal state without recourse to analogous 1D models. If, rather than restricting to sub-gap features, one looks for poles for $\omega > \Delta$ as plotted in figure 4 one can see that the feature near $k_x = k_F$ is smoothly connected to what appear to just be the underlying Bogoluibov bands for the background superconductor when V_m is small. This smooth connection does continue to higher V_m, but we only plot the exact poles/the real parts of bound states with the understanding that this band has some finite lifetime associated with it for $k_x < k_F$. Interestingly, the band structure for $\omega > \Delta$, $k_x > k_F$ continues to resemble what one would expect from just looking at Zeeman shifted electronic bands and, in what is perhaps an unsurprising conclusion from a physical point of view, once the superconducting gap is closed by this local magnetic field, it stays closed as you increase the field.

As a third point, much in the same vein, one can look at what the band structure would look like if $\Delta \to 0$ whereupon the bands induced by the magnetic scatterers become $\omega = \pm(k_x^2 - k_F^2 - C_m^2 k_F^2)/2m$ which converges to the cross like extra closing point in the exact band structure in the limit of large V_m as one would expect from this analysis. Crucially, to reiterate, this Zeeman like behaviour occurs only once the superconducting gap has been closed, at a dimensionally renormalised value of V_m ($\Delta^{1/2}$ rather than Δ as in the conventional Zeeman

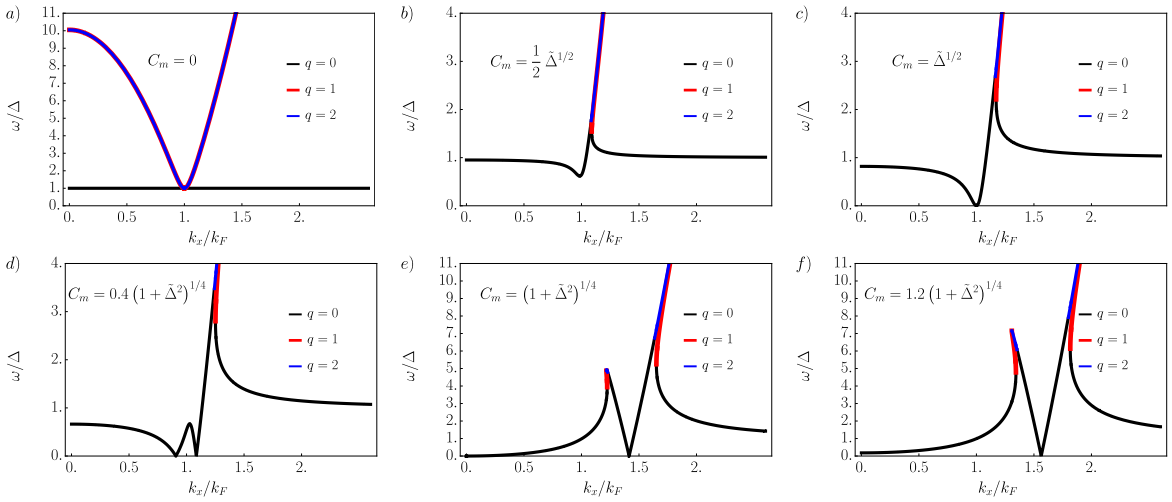

Figure 4: Exact subgap bands for ferromagnetic interface showing only real solutions. Complex branches split off at the end points of the lines of different q. We have chosen $\tilde{\Delta} = 0.1$ here but changing this makes no qualitative difference.

effect) and that the structure persists for arbitrary $V_m > (E_F\Delta)^{1/2}$, increasingly resembling what one would expect if there was no superconductivity present at all.

Based on the threefold arguments presented, we think of this additional gap closure as having its origin in the interactions between the magnetic scatterers and the *normal state* rather than superconducting bands. This is of interest, not least because it is clear that in the exact solution this band hybridises with the Shiba bands present for $k_x \approx 0$ so that the physics in this system requires an understanding of both mechanisms.

2.6.2 Origin of renormalised closures

Perhaps the most clear way to see why the critical C_m scales like $\Delta^{1/2}$ rather than Δ is to look at the argument of the exponential factors in the full Green's function:

$$yk_F\left(1-(k_x/k_F+\sigma k_m/k_F)^2+i/E_F\left(\Delta^2-\omega^2\right)^{1/2}\right)^{1/2} \tag{2.69}$$

where we have explicitly written out all of the unitful factors (i.e.: y has units of length, Δ of energy etc.). If we evaluate this at $k_x = 0$, $k_m = k_F$ (or $k_x = k_F$, $k_m = 0$) at the gap centre then all that is left is:

$$yk_F\left(i\Delta/E_F\right)^{1/2}. \tag{2.70}$$

Note that this not only highlights the origin of the renormalised index of Δ but also the factor of k_F which may otherwise seem mysterious in the gap closing conditions as noted in table 1. One can also see explicitly how this quantity is to be compared to V_m by evaluating the T

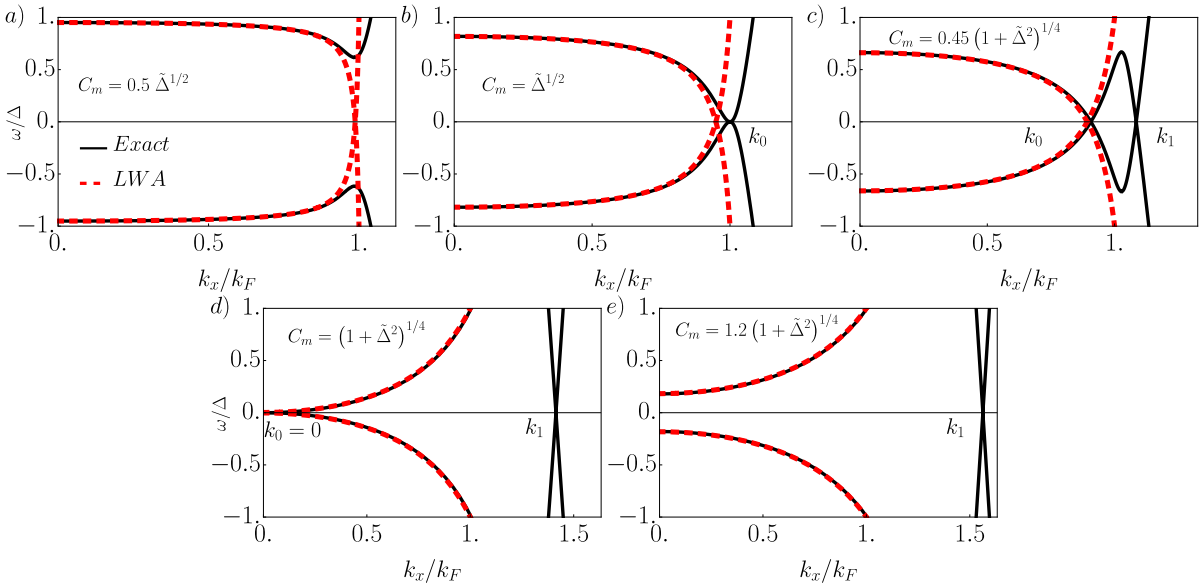

Figure 5: Sub-gap bands obtained from the exact Green's function (thick, black) and the LWA (dashed, red) for $k_m = 0$, for increasing C_m from (a) to (e). The LWA predicts a gap closure near $k_x = k_F$ for arbitrarily small C_m which moves to $k_x = 0$ with increasing C_m until $C_m = 1$ after which a gap opens. In contrast, the exact result correctly has a gap at small C_m, which closes at $C_m = \tilde{\Delta}^{1/2}$ but splits for larger C_m into *two* gap closing points $k_{0,1}$. While the k_0 gap moves to $k_x = 0$ and reopens at $C_m = (1+\tilde{\Delta}^2)^{1/4}$, the k_1 gap stays closed above k_F for any $C_m > \tilde{\Delta}^{1/2}$.

matrix in these same limits:

$$\mathbf{T}(\omega = 0, k_x = k_F, k_m = 0) = \left[\frac{\rho_0 \pi}{k_F \sqrt{2}\tilde{\Delta}} \begin{pmatrix} 1 & 0 & 1 & 0 \\ 0 & 1 & 0 & -1 \\ 1 & 0 & -1 & 0 \\ 0 & -1 & 0 & -1 \end{pmatrix} + \frac{1}{V_m} \begin{pmatrix} 0 & 1 & 0 & 0 \\ 1 & 0 & 0 & 0 \\ 0 & 0 & 0 & -1 \\ 0 & 0 & -1 & 0 \end{pmatrix} \right]^{-1} \tag{2.71}$$

where the $\sqrt{2}$ arises only to account for the first matrix having two elements per row. Finding the poles of this expression, or just direct comparison of elements, thus leads to the expression:

$$\frac{\rho\pi}{k_F} V_m = C_m = \tilde{\Delta}^{1/2} \tag{2.72}$$

as seen in table 1. Put succinctly, the renormalised quantities arise due to the dimensional mismatch accounted for by the exact, partial Fourier transform.

2.6.3 Spiral ordered chain $k_m \neq 0$

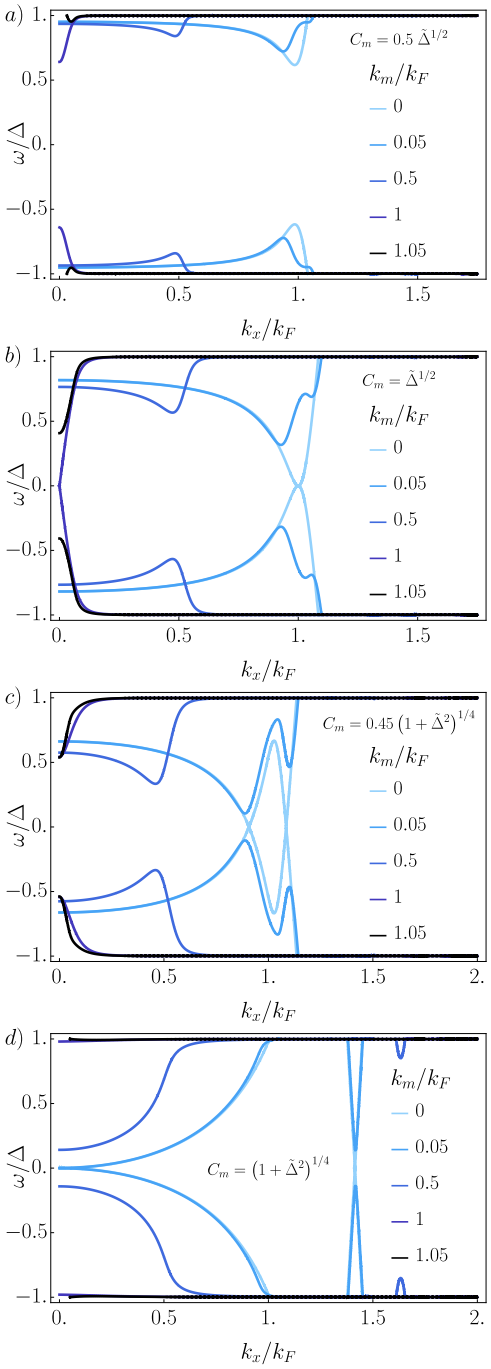

Figure 6: Exact sub-gap band dispersions from continuum model (in gauge transformed basis) at various C_m, tuning k_m from 0 to $1.05k_F$ as the curves darken. $\tilde{\Delta} = 0.1$ here but the shown behaviour is independent of the value of Δ.

Building from the understanding provided by the exact solution for a ferromagnetic chain we can trace the origins of the band structures in the more complicated spiral ($k_m \neq 0$) case. As one is able to solve $\det T^{-1} = 0$ for any k_m implicitly we can then understand the feature of the case with $k_m \neq 0$ by pairing our understanding of the physical origins of feature in the analytically understood ferromagnetic chain, with the smooth evolution of the spiral chain as k_m is increased from 0. The simplest form we have found so far for $\det T^{-1} = 0$ is:

$$\begin{aligned}&(\tilde{\Delta}^2 - \tilde{\omega}^2)\left(S^+S^- + C_m^4\right) - \\ &C_m^2\sqrt{(\mathcal{E}^- - S^-)(\mathcal{E}^+ - S^+)}\times \\ &\left[(\mathcal{E}^- + S^-)(\mathcal{E}^+ + S^+) + \tilde{\Delta}^2 + \tilde{\omega}^2\right] = 0,\end{aligned} \tag{2.73}$$

where $\mathcal{E}^\pm = (k_x \pm k_m)^2/k_F^2 - 1$, $S^\pm = \sqrt{\mathcal{E}_\pm^2 + \tilde{\Delta}^2 - \tilde{\omega}^2}$. One can utilise the same technique as for the ferromagnetic solution to de-nest the ω dependence from the square roots but equation (2.73) corresponds to a polynomial of far too high an order in ω, without any evident symmetry or roots that can be readily cancelled out that can be used to reduce it to a simpler form as for $k_m = 0$.

Recall that for the case of a ferromagnetic line impurity we learned to understand the sub-gap bands as a hybridisied mixture of a band of Shiba states near $k_x = 0$ (present in the LWA) and a band arising from consideration of the background superconductor being influenced by the local magnetic field near $k_x = k_F$ (absent in the LWA). Building from our understanding of the bands in the case of a ferromagnetic line impurity we can understand the effect of a small k_m by comparing the two lightest curves in figure 6. Recalling that the spiral order in a purely 1D model is identical to a spin orbit interaction, we can think of looking at the effect of such a small

k_m as allowing us to see which momenta are protected by addition of such a 'local' spin orbit interaction. Focusing in particular upon figures 6 (b-d) where $C_m \geq \tilde{\Delta}^{1/2}$ (so that the gap at $k_x = k_F$ is closed if this were a ferromagnetic interface) we see that the gap closure originating from the bulk, underlying bands is re-opened, in an asymmetric fashion with respect to k_F. This occurs because the point $k_x = k_F$ is not symmetry protected under the action of this new kind of operation, resulting in a lifted degeneracy and opening of a mini-gap. In figures 6 (b) and (c) one can most clearly see that the resulting minima from this mini-gap opening behave asymmetrically with respect to k_F. The band minimum which shifts to higher momentum moves to higher energy far more quickly, moving above the bulk gap energy Δ at rather small values of k_m, likely due to the background bands also exhibiting this behaviour. The band minimum moving to lower wave vector however, always stays sub-gap. The re-opening of this gap allows for the possibility of an odd number of zero energy crossings to occur as seen in figure 6 (d) where, near $k_x = 0$ the curves for $k_m = 0$ and $k_m = 0.05k_F$ are almost identical, but at $k_x = k_F$ the former is gapless whilst the latter is gapped. Hence, an odd number of crossings cannot happen in the case of a ferromagnetic chain but even a tiny k_m can make this possible. If, on looping through the Brillouin zone, bands cross the Fermi energy an odd number of times, one would expect entry to a topological phase. The features near $k_x = 0$ [12], those reproducible using the LWA and are largely unchanged by the addition of a small k_m, suggesting that at least from a symmetry point of view Shiba physics is largely unaffected by the inclusion of this spin orbit like interaction.

To understand the effects of larger k_m we can smoothly tune k_m smoothly towards and even beyond k_F. In particular, if we focus on the darker bands in figure 6 (b), the remaining sub gap band minimum formed from the splitting of the higher momentum gap closure at $k_x = k_F$ migrates to higher, but sub gap energies, then begins to move towards zero again on passing $k_m = k_F/2$. Crucially, the band structure near $k_x = 0$ remains essentially unchanged from the prediction of the LWA [13], and hence from a theory built of just hybridised Shiba states, until $k_m \approx k_F$, at which point the LWA bands rejoin the continuum, whilst the now spin dependent, wave vector shifted underlying electronic bands can become Dirac like at $k_x = 0$ (as see in figures 7 (b), (f), (j) and (n) where k_m is tuned from 0 to $1.25k_F$ for $C_m = \tilde{\Delta}^{1/2}$). This seems to imply a crossover from the band structure being largely governed by Shiba physics to being governed by the modified background superconductor. Such an effect is entirely absent in the LWA. As we are able to smoothly trace all features from the exactly solved ferromagnetic case, it is clear that the sub-gap structure for the more complex spiral ordered case can be described in precisely the same terms.

Hence, it seems that, if $k_m \geq k_F$, or even $k_m \approx k_F$, the proper description of these sub gap bands is in terms of the underlying bulk electronic band structure, not requiring reference to Shiba states at all. This has been noted in models of sparse chains of magnetic impurities, identifying this point as relating to Bragg reflections [92]. In particular, though expected to be the most interesting region due to singular overlap of spin shifted Fermi surfaces, there are *no* sub gap states in the LWA.

[12] Recall that we always work in the shifted basis with $k_x \to k_x + \sigma k_m$ to restore translation invariance for non-zero k_m in the x direction. This allows us to talk about bands meaningfully.

[13] Note for example that the curves near $k_x = 0$ in figure 6 (b) for $k_m = 0$ and $k_m = 0.5k_F$ are very similar.

These results seem to suggest a qualitative change between dense and sparse chains which has seen some interest in the literature [83, 93].

One can, in fact, write down a closed form expression for the V_m required to close the gap in terms of all other system parameters. This can be achieved because V_m appears only four times in the 4×4 matrix structure, so when calculating $\det T^{-1}$ it can appear at most to powers of 4. Such polynomial equations can always be solved in closed form. Though difficult to prove in the full 2D theory, reference to purely 1D theories suggests that the only places where the gap can first close are at $k_x = 0$ or k_F for any V_m [14].

One particularly noteworthy case of this exact solution is that we can write the V_m required to close the gap at $\omega = k_x = 0$ exactly in a very simple manner. This solution exists as this case is mathematically exactly the same as solving the *ferromagnetic* chain for any k_x, which as we have noted we can write in closed form! In this way, we can write an exact form for what the single state at k_x looks like, offering necessary corrections to the single impurity Shiba model which would otherwise be used to track this point.

Moreover, one can show that for *any* k_m it is possible to close the gap at $k_x = 0$. The closures always appear to be Dirac like as one can see from examples in figure 7 (d, h, k, p) and occur at precisely:

$$C_m = \left(\left(1 - k_m^2 / k_F^2 \right)^2 + \Delta^2 / E_F^2 \right)^{1/4}, \tag{2.74}$$

a result derived from the general solution for V_m (and hence C_m, its dimensionless cousin) in terms of all other system parameters.

[14] The former occurs as it is protected by time reversal symmetry (in addition to the inversion and particle-hole symmetries that are present generically) whereas the latter has no obvious symmetry associated with it. The closure at $k_x = k_F$ seems to occur because this is the lowest energy point on the background superconducting bands (for $k_m = 0$) so that a Zeeman shift will first close the gap at that wave-vector.

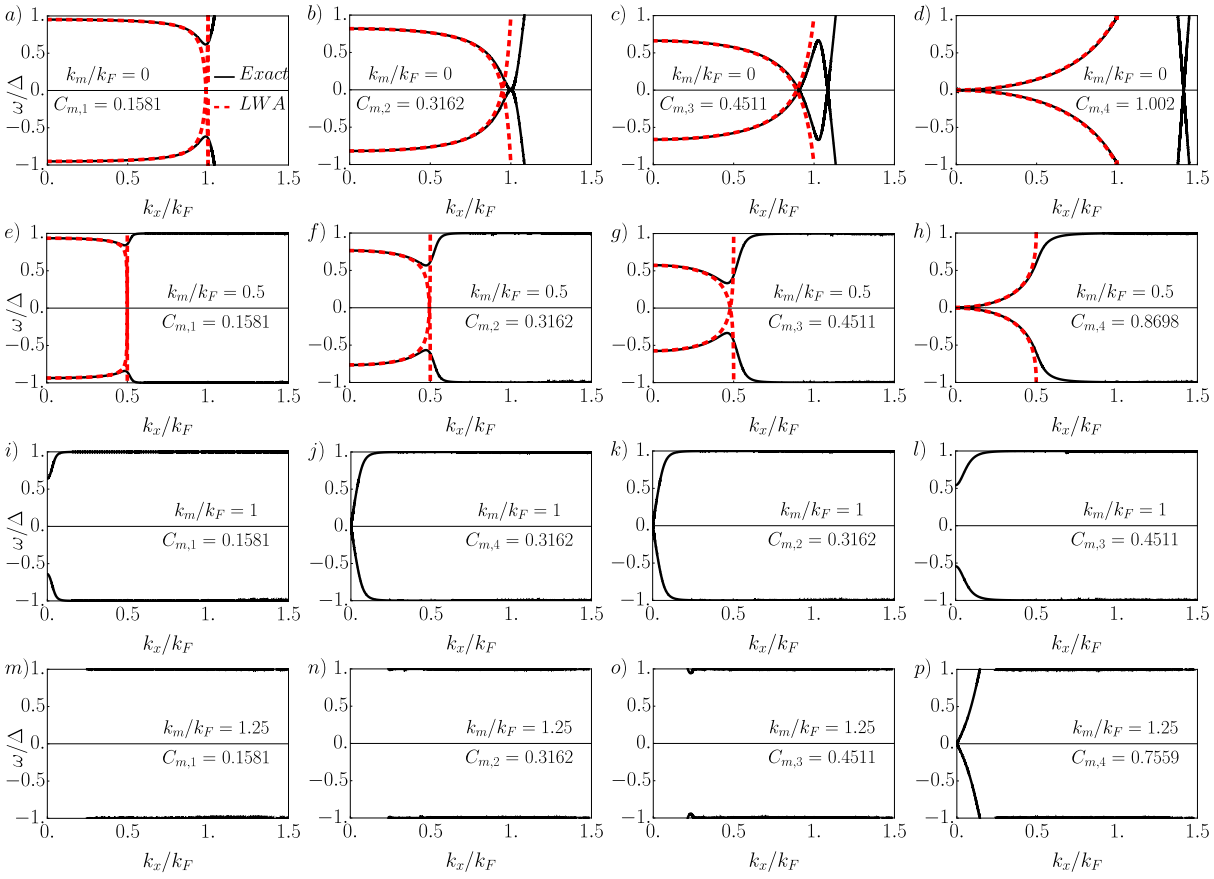

Figure 7: Comparison between the exact and LWA results of the sub-gap bands, extending the comparison at $k_m = 0$ to $k_m \neq 0$. Plots (a)–(d) reproduce Fig. 2. Different columns correspond to interaction strengths $C_{m,1} = \frac{1}{2}\tilde{\Delta}^{1/2}$, $C_{m,2} = \tilde{\Delta}^{1/2}$, $C_{m,3} = 0.45\left(1+\tilde{\Delta}^2\right)^{1/4}$ and $C_{m,4} = \left[(1-(k_m/k_F)^2)^2 + \tilde{\Delta}^2\right]^{1/4}$ ordered such that C_m increases from left to right, and in different rows we increase the value of k_m from top to bottom. LWA solutions exist only in the shrinking region of $k_x \leq k_F - k_m$, and notably for $k_m \geq k_F$ [plots (i)–(p)] the LWA does not predict any sub-gap bands, in contrast to the exact calculation. In particular, Dirac like closing points exist at $k_x = 0$ for all k_m at interaction strength $C_{m,4}$ [plots (d),(h),(k),(p)]. Note that plots (j),(k) are identical as $C_{m,2} = C_{m,4}$ if $k_m = k_F$ and that plots (k),(l) are ordered differently to other rows because $C_{m,3} > C_{m,4}$ (there can be no intermediate value because $C_{m,2} = C_{m,4}$). We have chosen $\tilde{\Delta} = 0.1$ here but changing this makes no qualitative difference.

2.7 Comparison to numerics

Given the apparent unusual nature of the dependence of sub-gap states on system parameters, we would like to take some time to ensure they are present in complementary models. That these other models are built from different assumptions would thus help rule out the possibility that our results are artefacts of the methods applied. In particular, the reader may find it concerning that the results seem to heavily rely upon *not* taking the weak coupling BCS limit of a small gap compared to the bandwidth so here we construct numerics that explicitly calculate the gap in a self consistent manner which should explicitly not violate this assumption.

In this section we will hence describe the numerical approach used, show that the gap closures outlined in table 1 and more generally all qualitative features of sub-gap bands are reproduced with either a fixed (non-self consistent) or fully self consistent gap. The correspondence between the results from numerical and continuum approaches are almost indistinguishable in the appropriate limits. We also explore how the folded band structure resulting from moving away from the dense chain limit (expected to correspond to the continuum approach) can still be understood in terms of the continuum model.

2.7.1 Outline of numerical model

We construct a single band, tight binding model on a 2D square lattice described by:

$$H = \sum_{\langle i,j\rangle,\sigma} (-t-\mu) c^\dagger_{i,\sigma} c_{j,\sigma} + \sum_i \left[\Delta_i c_{i,\downarrow} c_{i,\uparrow} + \text{h.c.}\right], \tag{2.75}$$

where $\langle i,j\rangle$ label nearest neighbour lattice sites with hopping integral t and chemical potential μ, and $\sigma = \uparrow, \downarrow$ are the spin projections. For the chemical potential μ to lie within the bandwidth it must be such that $\mu \in \{-4t, 4t\}$. Naturally, one should also take care to avoid choices which lead to atypical behaviour such as half filled bands where pathological forward and backscattering events can occur which could hide the physics we are interested in. Similar concerns govern avoidance of the band edges where physical behaviour naturally changes abruptly.

Though we could allow for arbitrary pairing in the spatially varying gap parameters Δ_i we have made the choice to allow only on-site singlet pairing. This has the benefit of keeping the model as simple as possible whilst still containing the ingredients we wish to simulate. The further addition of triplet pairing does not make a significant difference and is dwarfed by that generated by magnetic scattering in any case. The gap function is calculated at mean field level and given by:

$$\Delta_i = -V_p \langle 0 | c^\dagger_{i,\uparrow} c^\dagger_{i,\downarrow} | 0 \rangle, \tag{2.76}$$

where $|0\rangle$ is the BCS ground state and V_p the interaction potential strength.

The interaction with the chain of magnetic impurities is given by the Hamiltonian

$$H_m = V_m \sum_{i=(i_x,0)} \mathbf{M}_i \cdot \mathbf{S}_i, \tag{2.77}$$

where V_m is the magnetic interaction strength, $\mathbf{M}_i$ are unit vectors that are either ferromag-

netically aligned or twisted into a spiral, and $\mathbf{S}_i = \sum_{\sigma,\sigma',n} \boldsymbol{\sigma}_{\sigma,\sigma'} c^\dagger_{i,n,\sigma} c_{i,n,\sigma'}$ is the electron spin operator, with $\boldsymbol{\sigma} = (\sigma_x, \sigma_y, \sigma_z)$ the vector of Pauli matrices. We use a 2D square lattice of dimensions $N_x \times N_y$ with periodic boundary conditions in both directions (unless otherwise stated). For spiral ordered $\mathbf{M}_i$ we proceed similarly to in the continuum calculation and choose the spin axis so that the $\mathbf{M}_i$ rotate in the spin (x, y) plane. Though this restricts our attention to planar spirals rather than including possible canted phases we are left with a translation invariant, effectively ferromagnetic system under the transformation $k_x \to k_x + \sigma k_m$ where σ refers to spin up/down sectors. Application of periodic boundary conditions after this transformation leads to the standard quantisation of k_x so that the system smoothly connects to the infinite system as $N_x \to \infty$ and avoids the case distinctions required if boundary conditions were applied before the transformation.

The magnetic impurities are placed at the centre of the system ($i_y = 0$), explicitly breaking the translation symmetry in the y direction. The system size is made large enough (around $N_y = 70$) to suppress finite size effects in the sub-gap band structure (visible as oscillations within the structure). Due to the block diagonalisation in the x direction we can choose significantly larger N_x (e.g.: $N_x = 450$) such that quickly varying details in momentum resolved spectral functions are resolvable.

Self consistent solutions are obtained by fixed point iteration. From initially chosen, uniform values of Δ_i we diagonalise the Hamiltonian and compute each Δ_i from the resulting eigenstates using equation (2.76). The chemical potential is similarly recalculated iteratively. This process is repeated until a relative error of around 10^{-4} is obtained; typically after around $10 - 20$ iterations. In this way the self consistent solution should reflect the stable, superconducting ground state regardless of initially chosen chemical potential or Δ_i. In the presence of non-zero magnetic interaction V_m such solutions suppress the Δ_i in the vicinity of the magnetic impurities as might be expected due to pair breaking.

To aid in investigating what effect this spatial suppression of Δ_i in the self consistent solution has compared to the continuum model we also use a non-self consistent solution. This is achieved by imposing uniform Δ_i throughout the system corresponding to the value taken by the Δ_i in the self consistent solution far from the interface (or equivalently when $V_m = 0$ so that the solution is naturally uniform). The Hamiltonian is then diagonalised only a single time rather than iteratively.

Hence, we are now armed with a continuum model which in principle takes into account all possible feedback with the substrate superconductor, a self consistent numerical model which finds the stable configuration of superconducting gap and doping; and a non-self consistent version of the same numerical model. Crucially, all three models can essentially be set to the same bulk gap Δ_0 so that we can directly compare results. This care is required as we have noted gap closures can occur non-analytically in Δ_0 so that one cannot simply compare results of systems with different Δ_0 by normalising energies to Δ_0 as would normally be safe.

2.7.2 Comparison without self consistent gap

In figures 10 (a) - (d) we plot the eigenvalues of the Hamiltonian at each k_x and hence the sub-gap energy bands from the numerical model with the chemical potential $\mu = -3.6t$ chosen

so that we are exploring the limit $k_F \ll \pi/a$ expected to correspond to the exact continuum model. Comparison with figure 6 shows the remarkable degree similarity that the numerics display to the exact result.

In order to make the correspondence between continuum and numerical model one can identify that the bulk bands in the absence of magnetic scatterers or superconductivity in the two dimensional square lattice will be:

$$\epsilon_{\mathbf{k}} = -2t\left[\cos(k_x a) + \cos(k_y a)\right] - \mu \tag{2.78}$$

which can be compared to the quadratic bands in the continuum model by expanding for $|\mathbf{k}| \ll \pi/a$ so that

$$\begin{aligned} \epsilon_{\mathbf{k}} &\approx a^2 t\left(k_x^2 + k_y^2\right) - (\mu + 4t) \\ &\equiv \frac{\hbar^2}{2m^*}\left(k_x^2 + k_y^2\right) - E_F \end{aligned} \tag{2.79}$$

which allows us to estimate what is essentially the bandwidth E_F and effective mass m^* of this tight binding like model. One can identify k_F by locating points in the Brillouin zone where the cosine dispersion crosses zero energy (at $k_y = 0$ [15]) for a given chemical potential $\mu < 0$ so that $k_F a = \arccos(-(\mu + 2t)/2t)$ most clearly seen in figure 8 where the 'bubble' feature expected from the continuum model tracks this value for changing chemical potential. It is noteworthy that the periodic nature of the cosine bands in the numerical approach also necessarily identifies $k^\star = \pi - k_F$ as an important scale as seen in the summary of possible gap closures in table 2.

In particular, figure 10 (b) displays the same smooth evolution of a quadratic gap closure at k_F as for a ferromagnetic chain, through until there is a Dirac like gap closure at $k_x = 0$ when $k_m = k_F$ (chosen to correspond to the point where the quadratic gap closure appeared). This behaviour occurs at precisely $\hat{V}_m = (4t\Delta)^{1/2}$ regardless of the chemical potential (so long as one stays within the bandwidth). This formula is in direct correspondence based on our above comparison to the quadratic bands with the derived formula in the continuum model: $V_m = (E_F\Delta)^{1/2}$.

In figure 8 we plot the sub-gap states calculated in a non-self consistent manner at a fixed V_m for a range of chemical potentials. In this way one can see the evolution of the band structure as the lattice spacing is modified from small (top, left) when $\mu = -3.8t \approx -4t$ to comparatively large (bottom, right) where $\mu = -0.1t$. The features observed in the continuum model are recognisable for a wide range of the plots and hence for a wide range of magnetic adatom chain separations a_h as necessarily the numerical model has both the underlying lattice and magnetic chain with the same atomic spacing. Between $\mu = -0.3t$ and $-0.2t$ this picture quickly changes. Though in the continuum model the band structure at large wave-vector returns to the continuum (and continues to increase, tending towards the form of the underlying quadratic bands) here we begin to see the influence of the underlying cosine bands re-entering the gap. Unlike for a quadratic approximation cosine bands do not monotonically increase with large k_x and for sufficiently small μ the 'band width' near the Brillouin zone edge which the

[15] Notably one might expect a range of values to be important zero crossings as k_y is varied due to the additional dimensionality of the underlying band structure. Only this single value seems to come up noticeably however.

	Continuum model	Numerical model
$k_m = 0$, $k_x = k_F$	$C_m = \tilde{\Delta}^{1/2}$	$\hat{V}_m = \sqrt{4t\Delta}$
$k_m = 0$, $k_x = 0$	$C_m = (1+\tilde{\Delta}^2)^{1/4}$	$\sqrt{4t\Delta} < \hat{V}_m < 2t(1+(\tilde{\Delta}/2t)^2)^{1/4}$
$k_m = 0$, $k_x = k_F^\star$	n/a	$\hat{V}_m = 2t(1+(\tilde{\Delta}/2t)^2)^{1/4}$
$k_m \neq 0$, $k_x = 0$	$C_m = ((1-k_m^2/k_F^2)^2+\tilde{\Delta}^2)^{1/4}$	$(4t\Delta)^{1/2} < \hat{V}_m < 2t\left(\left(1-\frac{k_m^2}{k_F^2}\right)^2+\left(\frac{\Delta}{2t}\right)^2\right)^{1/4}$
$k_m = k_F$, $k_x = 0$	$C_m = \tilde{\Delta}^{1/2}$	$\hat{V}_m = (4t\Delta)^{1/2}$
$k_m = k_F^\star$, $k_x = \pi/a$	n/a	$\hat{V}_m = (4t\Delta)^{1/2}$

Table 2: Comparison of possible gap closures in 2D continuum model and 2D numerics, with $C_m = \pi\rho V_m/k_F = k_F V_m/2E_F$. Notice that $\hat{V}_m$ and $k_F V_m$ have units of energy. In the numerical model $k_F = \frac{1}{a}[\arccos(-(\mu+2t)/2t)]$ for $\mu < 0$. Note that the periodicity with respect to the Brillouin zone edge in the numerics identifies a second important scale $k^\star = \pi - k_F$ where gap closures impossible in the continuum model can occur. Though they cannot occur within the continuum model, the magnetic interaction strength at which they occur can be predicted exactly from interaction strengths for closures which *are* possible in the continuum model.

sub-gap structure will tend towards becomes small enough that it essentially enters the gap once modified by V_m. One can see that this occurs as k_F (the point the 'bubble' is built around) becomes comparable to the Brillouin zone edge at π/a. As a result, there seem to be two rather well separated regimes: small a_h (dense chains) where the sub-gap band structure is smoothly connected to the continuum bands and large a_h where the sub-gap band structure is completely disconnected and can be studied quite independently. This behaviour change, especially in light of the sudden possibility of different numbers and locations of gap closures through the transition, is likely to have topological consequences. We compare the gap closures in the continuum model and numerics in table 2. The expressions shown do describe the dependence of the gap closures on the bulk superconducting gap Δ in all cases, however, understanding the effect of the chemical potential μ on the prefactor in expressions for generic k_m at $k_x = 0$ is a difficult and unsolved problem beyond the limits given. By contrast, the gap closure at $k_x = k_F$ is completely unaffected by the chemical potential (so long as it remains within the bandwidth) and follows the dependence shown exactly.

2.7.3 Comparison with self consistent gap

In figure 10(e-h) we display the self consistently obtained sub-gap energy bands obtained from the numerics for $\mu = -3.6t$ so that $k_F \ll \pi/a$ (compare to figure 6 for the exact, continuum model).

Compared to figure 10(a-d) which are non-self consistent but have the same bulk gap, there is a remarkable degree of agreement for V_m chosen to display the same sub gap features. This choice is far from arbitrary and all of the results in table 2 describe the gap closures even once self consistency is taken into account, once parameters are correctly renormalised. This renormalisation takes into account the local change to the density of states, which effectively changes the strength of the magnetic interaction as seen in the unitless quantity $C_m = \pi\rho_0 V_m$ and seems to be the majority of the effect self consistency has here. Most of the difficulty in providing nice formulae for these closures comes down to the difficulty of extracting what

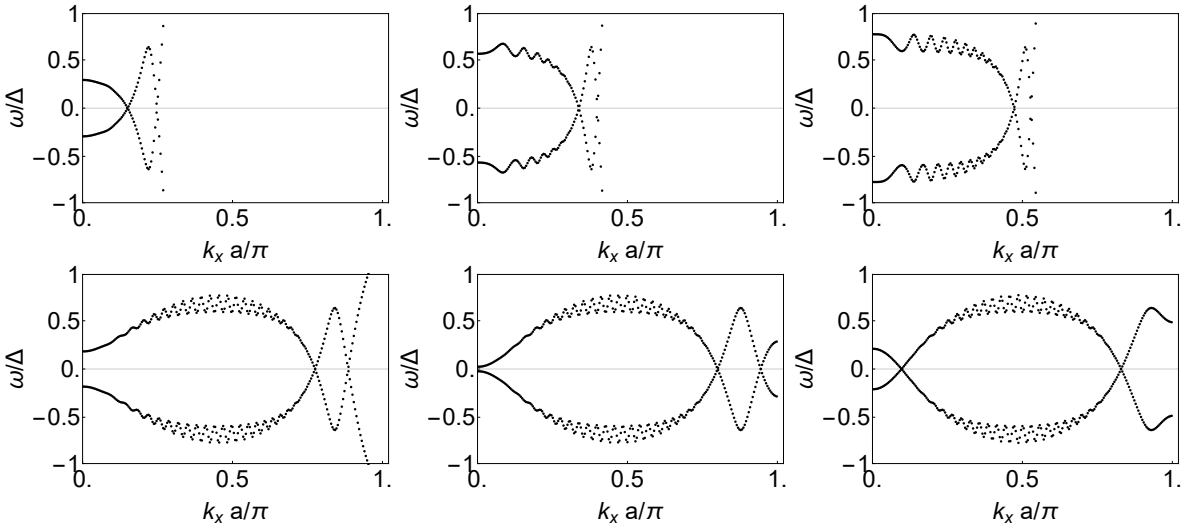

Figure 8: Eigenvalues of non self consistent Hamiltonian at each k_x, from numerical model for a range of different chemical potentials ((top, left to right): $\mu = -3.6t$, $-2.8t$, $-2t$, (bottom, left to right): $\mu = -0.3t$, $-0.2t$, $-0.1t$) for the same V_m. Tuning chemical potential in this way effectively probes increasing lattice spacing a_h so that we see the range of validity for our continuum approach and how it should be modified as the finite Brillouin zone and underlying cosine dispersion become increasingly important. Note that the bubble feature formed from the higher momentum gap closure around k_F (as k_F increases with tuned μ) remains essentially unchanged for $\mu \lessapprox -0.3t$ along with the rest of the band structure which undergoes no drastic changes. Between (bottom, left) and (bottom, middle) there is an abrupt change compared to the continuum model as the large momentum, roughly linear structure re enters the gap. This cannot occur in the continuum model as a quadratic dispersion has only one turning point, compared to two within the Brillouin zone for a cosine band. In this sense the cosine band has two 'bandwidths', one of which remains finite on constructing a continuum model and one which is sent to infinite energy. Here we see the effect of this becoming important, leading to an abrupt change in the possible gap closures at both $k_x = 0$ and $k_x = \pi/a$. Additionally, in this regime, the sub gap band structure can meaningfully be said to be disconnected from the continuum states. This suggests there is an abrupt crossover between dense and sparse chains.

value the chemical potential takes after self consistent solution as we are allowing it to change to maintain the same *doping* level. There is a notable exception to this difficulty as the gap closure at $\hat{V}_m = (4t\Delta)^{1/2}$ is completely unchanged by the chemical potential so long as it is within the bandwidth so this result also holds exactly in the self consistent case.

Crucially, all of our results are displayed with the same *bulk gap* as in the non-self consistent case. As we have seen in the continuum model, this is the important quantity to be understood and its local suppression by the magnetic adatom chain under self consistent solution does not significantly change matters except to modify the local density of states slightly. This viewpoint makes some intuitive physical sense as starting with a fixed substrate superconductor and modifying local states slightly on putting in adatoms is what is happening physically when one actually builds such a system. Clearly, the bulk gap will not be noticeably changed by only local impurities.

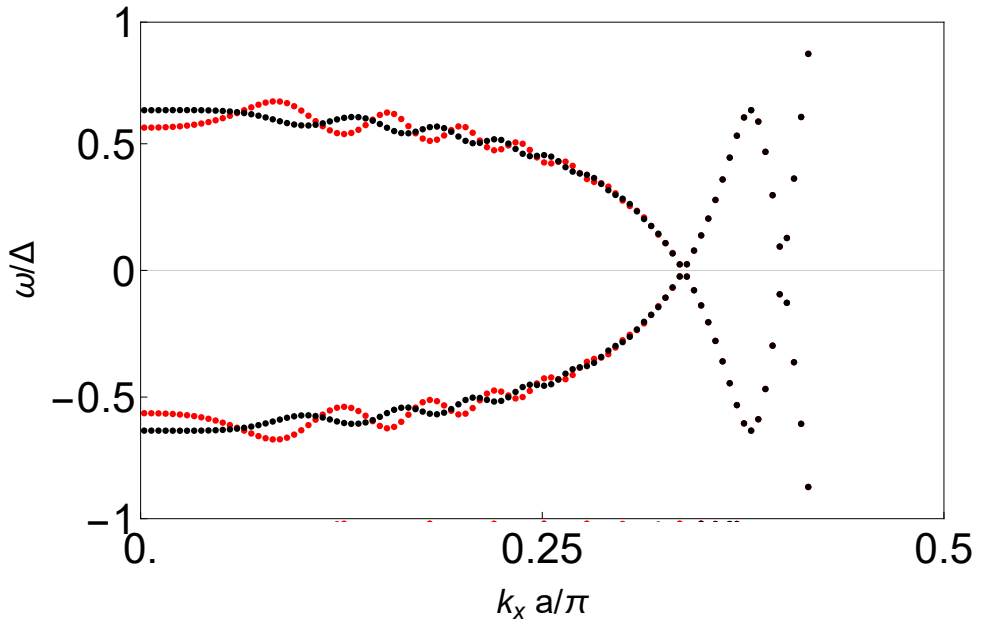

Figure 9: Eigenvalues of non self consistent Hamiltonian at each k_x, from numerical model comparing (red): hard wall (or 'open') to (black): periodic boundary conditions. The same system size $N_y = 70$, $N_x = 450$ was used in both cases at a chemical potential of $\mu = -2.8t$. Both cases show finite size oscillations differing by a π phase shift, possibly due to the difference between a hard wall (open boundary) and scattering from an effective second magnetic chain (periodic boundary). The amplitude of periodic boundary condition oscillations appears larger. Comparing periodic boundary conditions to the analytic model in chapter 4 we do not see the double helix like band structure present there in these numerics. This difference may be due to the difference between a second magnetic chain being present in the system as in chapter 4 and only a single chain seeing a reflection of itself due to boundary conditions.

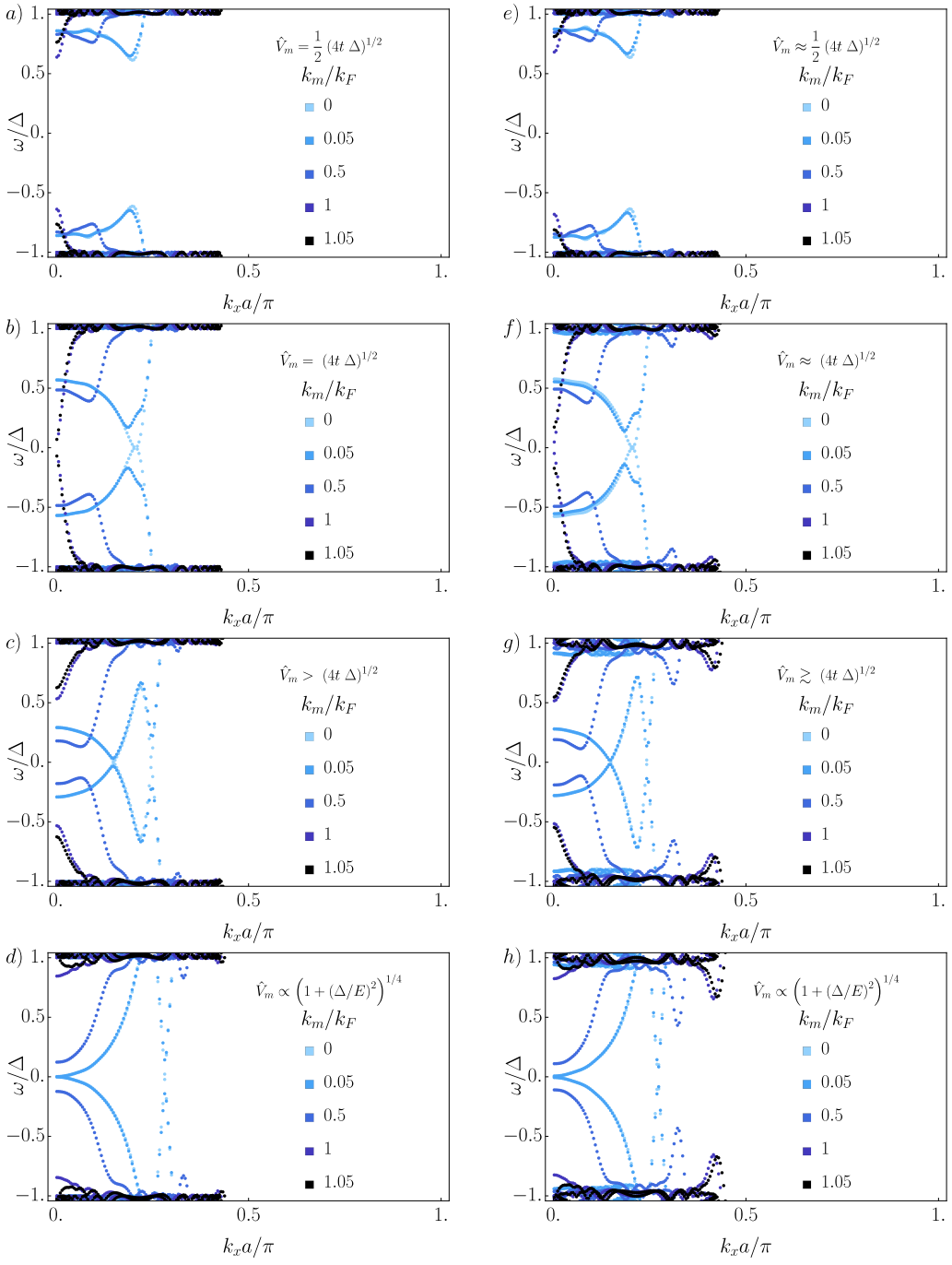

Figure 10: Non-selfconsistent [left, (a)–(d)] and fully self-consistent numerical solution [right, (e)–(h)] for scattering strengths $\hat{V}_m$ and $C_m = \pi\rho V_m/k_F$ as indicated in plots. $\hat{V}_m$ and $V_m k_F$ have units of energy. Scattering strengths are chosen such that plots in a row correspond to similar magnetic interaction strengths $\hat{V}_m$ and k_m tunes from 0 to $1.05k_F$ as the curves darken (compare to analytic solution in figure 6). We note an excellent agreement between the numeric and analytic results. The main difference arises from a modified density of states in the dimensionless variables $\tilde{\Delta}$ and C_m. While the analytic result of $C_m = \tilde{\Delta}^{1/2}$ matches $\hat{V}_m = (4t\Delta)^{1/2}$ in the numerics, the modified density of states causes a correspondence of $C_m = (1+\tilde{\Delta}^2)^{1/4}$ with $\hat{V}_m \propto [1+(\Delta/E)^2]^{1/4}$ with E and the proportionality factor resulting from the hopping t and chemical potential μ. The scaling dependence on Δ, however, is fully reproduced. We show the full Brillouin zone to demonstrate that there are no further sub-gap features. The parameters used are: $\Delta = 0.1$, $t = 1$, $a = 1$, $N_y = 70$, $N_x = 450$ and $\mu = -3.6t$. In the right column we self-consistently adjusted the pairing potential V_p to obtain the selected Δ far away from the magnetic scatterers, and identify k_F by comparison with the gap closure at k_F in figure 6 (b) or by direct calculation as in the main text.

3 Topological classification

As per the complete classification of topological phases by Altland and Zirnbauer (AZ) [50, 51] and, due to the original intention of this being an implementation of the one dimensional Kitaev chain toy model, one might expect this system to be classified by a $\mathbb{Z}_2$ topological index[16].

For a purely 1D model, this is exactly the case and has been well studied [22, 24, 26, 28].

However, in this section we note that the unusual presence of a local magnetic field in the form of localised magnetic moments occupies a strange seat with regards to the topological classification. Ordinarily, for a two-dimensional (2D) system where one expects a one-dimensional topologically non-trivial sub-system the approach would be to either: calculate the appropriate one-dimensional index for an effective 1D model that appropriately describes the sub-system; or calculate the relevant two-dimensional, weak topological index of the full 2D model. These approaches should be equivalent due to the repeating structure of the AZ topological classification in different dimensions.

Both approaches will be attempted, and we highlight that the loss of translational symmetry in one spatial direction, and resultant loss of the good momentum quantum number in that direction, make calculation of the topological index with confidence rather challenging. Though it seems likely the AZ classification should hold in this system in some form, we find that dimensionality seems to play an interesting role. By tuning the bulk superconducting gap Δ one can make the 'localised bands' smoothly less one-dimensional as the wave-functions spread away from the interface, but still always be able to go out to find a large enough distance from the magnetic spiral where the system must return to being the trivial background. This seems to be a case where, due to the local nature of the magnetic field and one-dimensional spin orbit interaction from the spiral ordering, the system would be expected to be topologically non-trivial in a region "close" to the interactions but which is smoothly connected to a trivial superconductor. As one would not expect topologically distinct regions to be connected in this way, we must develop an understanding of whether this is the case and how this seeming inconsistency is reconciles. Conventionally, for a one-dimensional weak topological index in a system with translational symmetry, the interpretation is that the system has entered into a phase deformable onto one comprising a ladder of weakly interacting topologically non-trivial one-dimensional chains. A good example of this analysis, relevant to our purposes has been carried out on a model of 2D p-wave superconductivity by Nagaosa [95] where it was seen that tuning parameters can leave the system in these weak topological phases akin to ladders of Kitaev chain toy models in either the x or y direction, or a strong topological phase which does not have such an interpretation. In this case, it is clear that the Hamiltonian readily breaks down into weakly coupled, *identical* copies of the Kitaev chain toy model in the weak phases. In this case we have essentially only one such chain, embedded within an otherwise trivial background. How is this interpretation to be modified when the interactions which drive the topological transition are inherently local and one-dimensional, completely breaking translational symmetry? If our model had either a 0 or 1D boundary cutting the impurity chain, what would we expect to observe, given this interpretation?

[16]There has been some discussion of the additional possibility of a $\mathbb{Z}$ index [94] though this would not have the same strong protection to local disorder.

There is a worrying ambiguity in how to calculate an effective one-dimensional model in this system. Though the simplest method of just focusing at the interface and calculating the resolvent of the Green's function produces very elegant formulae (looking somewhat like a renormalised picture of what one would see in a purely 1D implementation), this method would seem to completely ignore the fact that the induced bands are not localised entirely at the interface. Unlike in a purely 1D model, here all bound states formed by interactions near the interface are constructed from 2D wave packets and are not restricted to stay near the interface. As seen in the previous chapter, it can be a surprisingly subtle matter to describe a system which is somehow local in one co-ordinate, and delocalised in the other.

How are we to filter out from what are ostensibly 2D states which ones are essentially one dimensional? Using our previous analysis of the induced band structure it should be possible to see which states smoothly evolve into 2D, continuum states and which are the new, localised (if not entirely 1D) states. If one instead tries to take the spread of the wave-function into account in this sort of way by tracing over the perpendicular spatial co-ordinate there are large regions of phase space where the topological phase diagram appears quite different to that expected from comparison to a purely 1D model. Such regions can be made smoothly smaller by taking into account less and less of the background. It remains unclear how to interpret this ambiguity.

A rather more definitive signature of entry into a topological phase would be the sudden and persistent presence of bound states at an interface with a trivial system. In light of the ambiguity more standard tools seem to give, we also develop Green's formalism based on [53, 54] to add boundaries to our system. The formalism is able to reproduce expected results from purely one-dimensional systems and shows a discontinuous change in behaviour in the fully 2D treatment.

In a similar direction, there has been progress in the literature on calculating topological indices purely from Green's functions [96–98] which potentially helps bypass the issues with ambiguity in finding effective Hamiltonians as we see in this model. Such methods have the potential to be generalisable to include interactions, by contrast to the methods of Altland and Zirnbauer [50, 51]. Interestingly, the additional structure that allows this extension is to consider not just the poles of the Green's function (and thus bound states) but also the *zeroes*, which have a less obvious interpretation but necessarily involve nodes of the wave-functions. Such an interpretation allows one to understand how, on continuously moving away from the interface, the band structure present at the interface itself should be 'cancelled' or otherwise smoothly disappear once you are sufficiently far away. As the presence or absence of states is described by the presence or absence of poles in the Green's function and the only obvious way to cancel a pole is with a zero, it would seem that, quite unusually, the nodes, or zeroes of the Green's functions are hugely important in this system [17].

[17] We note the considerable recent interest in the role played by zeroes generated in strongly interacting Green's functions [99–115]. Surfaces of such zeroes ("Luttinger surfaces", c.f. Fermi surfaces for poles) allow for additional sign changes in the Green's function and hence must be taken into account when considering Luttinger sum rules [101]. The proper understanding of these zeroes, arising from divergent self-energy, has been suggested as a mechanism underlying the existence of the psueudogap in the 2D Hubbard model and, relatedly, to correct interpretation of ARPES (angle resolved photoemission spectroscopy) data of Fermi arcs [99–101, 106–109, 111–115]. As noted in [103, 104] QCD potentially provides another example of a theory requiring understanding of both poles and zeroes rather than only the former, in this case to understand the asymptotic freedom of Quarks.

We will see this become relevant in this section both when developing conditions for entry into the topological phase based on Green's functions and when calculating an effective 1D Hamiltonian that takes into account the substrate. It seems preferable to be able to utilise Green's function methods if they are able to offer greater physical insight into what happens on entering a topological phase. This is especially desirable due to the difficulty in physically interpreting more usual methods where the indices emerge from properties of the mapping between the spaces of Brillouin zone and wave functions in the system.

In topological systems, local structure is normally present only to provide an impurity on which bound states can occur in an otherwise translationally invariant system. Here, the system is topologically trivial, but the presence of the line impurity is itself expected to induce the system into a weak, 2-dimensional topological phase. There has been some investigation very recently into this phenomenon as in [116]. There, a 'Shiba glass' is described which explicitly breaks translation invariance in all directions and the topological classification was thus achievable by direct calculation of the Chern number in *real* space [117]. This seems like a class of systems which merit further investigation.

We will proceed by describing the variety of methods used to clarify our understanding of the nature of the topological phases present in this system but firstly make a detour to put the system into a more appropriate co-ordinate basis for thinking about the variety of one dimensional effective Hamiltonians possible.

3.0.1 Topological classification of purely 1D implementation

We reproduce the key elements of a purely 1D classification to allow for later comparison to our attempts to classify the fully 2D model. The classification can be seen by looking at the band structure found from finding the zero eigenvalues of the 1D Hamiltonian:

$$H_k = T\tau_z + B\sigma_z + \Delta\sigma_x + S\sigma_y\tau_z \tag{3.1}$$

where $T = (-2t\cos(ka) - \mu)$, $S = \alpha_R \sin(ka)$, B is a magnetic field, the τ Pauli matrices operate on particle-hole (Nambu space) and the σ on spin. This is a model of a 1D, spin orbit coupled (or equivalently spiral ordered) superconductor in a magnetic field and thus analogous to the Kitaev chain toy model for large enough magnetic field B. The condition for eigenvalues of this Hamiltonian to be zero (so that there are bound states at zero energy) is given by:

$$\sqrt{B^2 + \Delta^2 + T^2 \pm 2\sqrt{(B^2 + S^2)\,(\Delta^2 + T^2)}} = 0. \tag{3.2}$$

The AZ classification tells us to focus on time reversal invariant momenta of which there are two: $k = 0$ and $k = \pi/a$. At $k = 0$ one has $T \to -2t - \mu$ and $S \to 0$ so that the above condition simplifies to $B^2 = \pm\left((2t + \mu)^2 + \Delta^2\right)$ and at $k = \pi/a$, $T \to 2t - \mu$ and $S \to 0$ so that $B^2 = \pm\left((2t - \mu)^2 + \Delta^2\right)$. These two curves describe the boundaries of the topological phase diagram for the Kitaev chain toy model plotted in figure 1.

Note that in what follows we will be studying a continuum model (in the case that the chemical potential $\mu < 0$ as discussed in section 2.7.3) so the upper curve will necessarily

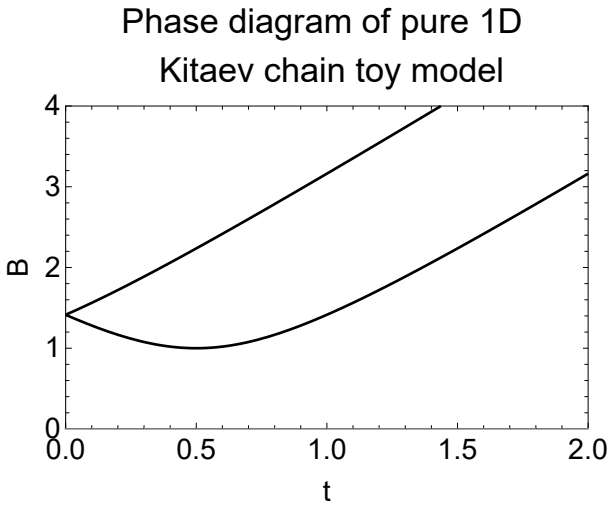

Figure 11: Phase diagram for 1D model analogous to the Kitaev chain toy model. Note that the upper curve is absent in continuum models as it arises from consideration of the edge of the Brillouin zone which is at infinity. The region between the two curves is the topologically non-trivial region. In what follows the role of t, a kinetic energy, will essentially be played by k_m, a spin dependent kick to the kinetic energy.

always be absent as the edge of the Brillouin zone is pushed to infinity.

3.1 Wigner function

The Green's function for a system with a single, line impurity, though it lacks translation invariance in the direction perpendicular to the impurity, can be written in a slightly different set of co-ordinates:

$$G(y_i = y, y_f = y^{'}) = g(|y - y^{'}|) + g(|y^{'} - 0|)Tg(|0 - y|) \tag{3.3}$$

$$= g(|\delta y|) + g(|2\bar{y} - \delta y|)Tg(|2\bar{y} + \delta y|) \tag{3.4}$$

$$= G(\delta y, \bar{y}) \tag{3.5}$$

where all other co-ordinates have been suppressed and $\delta y = y - y^{'}$ is the so called "difference" co-ordinate and $\bar{y} = \frac{1}{2}(y + y^{'})$ is the centre of mass co-ordinate. This is advantageous largely as it allows one to see in which limits one expects to recover a translation invariant system and allows us some sort of classification of the ambiguity in calculating the topological invariant in this system.

Though in what follows we will provide the justification for a variety of methods for calculating 1D effective Hamiltonians from a 2D Green's function we begin by simply enumerating the possibilities. We will refer to these methods in turn as (I) $\delta y = \bar{y} = 0$ (II) $\delta y = 0$, integrate over $\bar{y}$ (III) $\bar{y} = 0$, integrate over δy and (IV) integrate over both δy and $\bar{y}$ [18].

[18] We do not explore case (IV) deeply as we are not aware of a strong argument for why it would provide a good description of the topological classification.

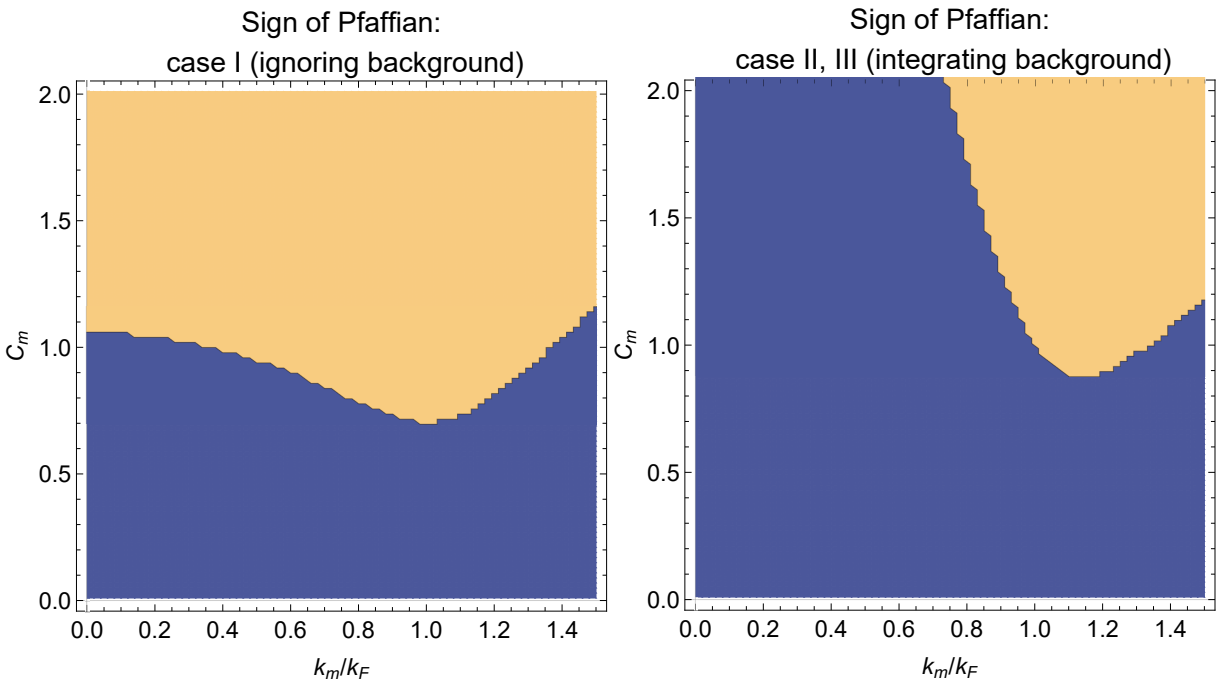

Figure 12: Topological phase diagrams for $\tilde{\Delta} = 0.5$ based on consideration of (left): condition I (entirely local, ignoring the long distance tails of sub-gap bands) which bears strong resemblance to pure 1D models as in figure 11. Changing $\tilde{\Delta}$ makes no qualitative difference. (right): condition II or equivalently III integrating out the background analytically. In both cases, the sign of the Pfaffian is calculated from the resulting 1D Hamiltonian after applying the necessary transform to anti-symmetrise it. Though the two approaches are similar for large k_m there is clearly a difference when one takes into account the expontentially decaying tails of the sub-gap states. Reducing $\tilde{\Delta}$ increases the value of the $k_m = 0$ intercept of the phase boundary.

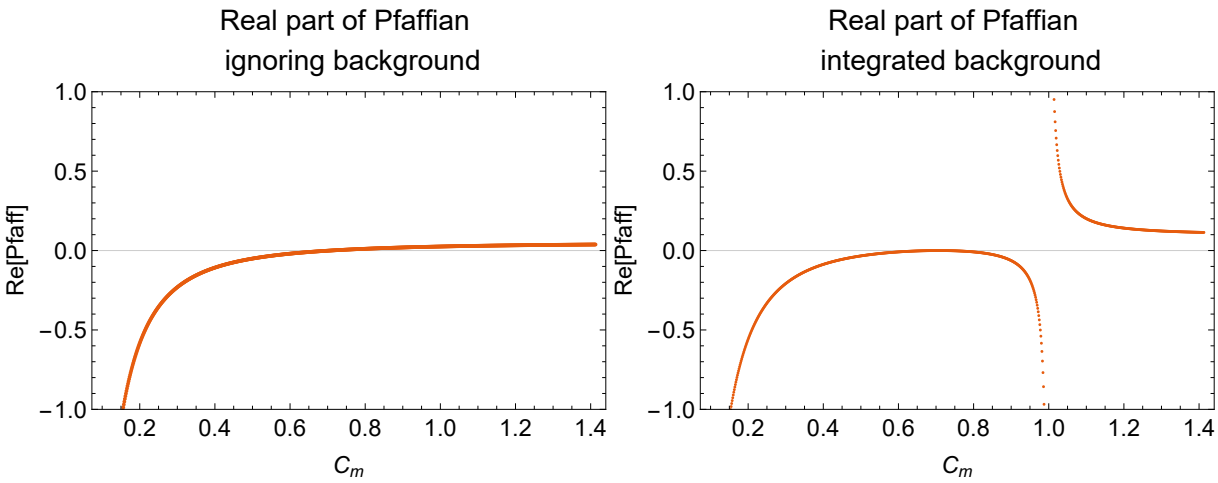

Figure 13: Comparison of the Pfaffian calculating from 1D Hamiltonians for $k_m = k_F$ and $\tilde{\Delta} = 0.5$ from (left): entirely local and (right): on integrating over the background analytically. At small and large V_m both approaches seem to agree well but in the intermediate region integration over the background displays striking differences. At precisely the point where the transition occurs in the purely local picture ($C_m = \tilde{\Delta}^{1/2}$) the curve exactly touches the axis (thus momentarily fulfilling the condition to enter the topological phase) before rebounding back into the trivial phase. More striking still, there is a pole near $C_m = 1$ after which the system suddenly transitions to the non-trivial condition. By reducing the distance one integrates out to, one can smoothly transition from one curve to the other, the pole disappearing as it meets a zero. It is unclear what a pole in the Hamiltonian could refer to, but by relating to a Green's function via the resolvent this could refer to a zero of a Green's function as in work by [96, 97].

3.1.1 Condition I: $\delta y = \bar{y} = 0$

$\delta y = \bar{y} = 0$ corresponds precisely to the scenario described in section 3.1.1 where the classification reduces to locating when the subgap bands cross $\omega = k_x = 0$. This phase diagram bears a striking resemblance to that of a purely 1D implementation of the Kitaev chain toy model but with two key differences. Firstly, the second boundary line which represents exit from the topological phase at large V_m in the Kitaev chain toy model is absent as this comes from consideration of the gap closure at the Brillouin zone edge. As this point has been pushed to infinity in our continuum model, the exit from the topological phase has likewise been pushed to $V_m \to \infty$ so cannot be seen. Secondly, the precise values for the phase boundaries are not those one might expect from the purely one-dimensional models analogous to the Kitaev chain toy model (see the phase diagram in figure 11 for comparison). In such 1D models the entrance into the phase occurs when magnetism is able to close the gap ($V_m = \Delta$). By contrast, in the fully 2D model described in section 2 this closure instead occurs at $V_m k_F = E_F \left(\left(1 - k_m^2/k_F^2\right)^2 + \Delta^2/E_F^2 \right)^{1/4}$ [19] which reduces to $V_m k_F = (E_F \Delta)^{1/2}$ when $k_m = k_F$. This renormalisation of physical quantities is entirely due to the dimensional mismatch of the 2D substrate and the 1D line of impurities (also noted recently in [118]). This accounts for the intuition that acting only locally with a magnetic field it is more difficult to effect a change to a global background (for small Δ, $\Delta^{1/2} > \Delta$).

[19] Note that the units of V_m are different due to the different dimensionalities of the models. As written all equations have units of energy.

In some sense we expect this phase diagram, or one very much like it, must hold at least in a limit where the wave functions are very localised around the interface as this is pretty undeniably the correct phase diagram for a truly 1D system (where there is none of this ambiguity due to the loss of translation symmetry and generation of a potentially topological phase from local rather than global fields). The fact that we are able to tune the degree of localisation using the coherence length of the background superconductor is in this sense a helpful feature.

We begin by justifying this approach to calculation of the topological index. Following Kitaev [6] one may, for any translation invariant, one-dimensional Hamiltonian on a lattice with short range interactions identify the potential presence of Majorana bound states even in the absence of chain ends by calculating the so called Majorana number $\mathcal{M}$:

$$\mathcal{M} = \text{sgn}\left[\ \text{Pf}\ \left[B(k_x = 0)\right]\ \text{Pf}\ \left[B(k_x = \pi/a)\right]\right] \tag{3.6}$$

where $B(k_x)$ is the one-dimensional effective Hamiltonian H_{1D} transformed into the Majorana basis (which comprises a unitary transform we will make explicit later in this section for our choice of basis). The points $k_x = 0, \pi/a$, where a is the lattice constant, are singled out as they are the points in a one-dimensional Brillouin zone which remain invariant under time-reversal symmetry, however, only the former of these are present in our continuum model due to the limit $a \to 0$ being taken (and thus $k_x \to \infty$) in equation (3.6). Hence, we may write

$$\mathcal{M} = \text{sgn}\Big[\ \text{Pf}\ \Big[H^{1D}_{\text{eff}}(k_x = 0)U\Big]\ \text{Pf}\ \Big[H^{1D}_{\text{eff}}(k_x \to \infty)U\Big]\Big] \tag{3.7}$$

where U is the unitary matrix responsible for transforming to the Majorana basis. Here we may write the Hamiltonian in terms of the full Green's function $G(\omega, k_x, y_i, y_f)$ which describes the combined superconductor, spiral ordered chain system as calculated in section 2.4 via the resolvent. Herein we encounter an ambiguity in how to properly construct a 1D Hamiltonian from a 2D Green's function. In this section we will take the view that, from the topological point of view, all that is necessary for a transition to occur is that there be superconductivity present and there be a closure of the bulk gap at time-reversal symmetric momenta.

Due to the fact that the line of magnetic impurities is the only location where interactions occur, it should also be the only location such closures can occur in the system. In addition, the background superconductor will remain trivial in the topological sense so that we may focus on the *change* in Majorana number due to the presence of interactions. This assumption seems reasonable as one would not expect a local interaction to be capable of driving the 2-dimensional bulk into a non-trivial topological phase. The argument for this is essentially two-fold. Firstly, the effect of adding in magnetic impurities to a superconductor is only to add a small number (in the thermodynamic limit) of localised states and to renormalise the band structures present. Hence, as there are no mechanisms to fundamentally alter the wave functions at arbitrarily large distances it seems clear that the effect of the impurities must be localised and hence cannot change the entire 2D substrate. Secondly, one could consider how the substrate screens[20] out the magnetic impurities by the appearance of spin polarised sub-gap states. In a gapless system

[20] As the magnetic moments are classical they cannot strictly be screened out. However, the response of the system will still be to act in opposition to their presence so the heuristics of this argument are still valid.

one would expect a screening response due to current flow causing a local change to the density of states. This is not possible in this case due to the gap, so the system instead responds, as the impurities are magnetic, by breaking Cooper pairs and hence forming spin polarised sub-gap states. This process can be thought of as a way of creating a local, spin dependent change to the density of states in an attempt to screen out the presence of localised magnetic moments.

In light of these arguments for the localisability of any effect the magnetic impurities must have, it seems reasonable to write:

$$H'_{\text{eff},y=0} = -\Big[G(\omega = 0, k_x, y_i = y_f = 0) - g(\omega = 0, k_x, y_i = y_f = 0)\Big]^{-1}. \tag{3.8}$$

Such a definition allows us to proceed rather further with our analysis in terms of gap closures as this amounts to searching for zero eigenvalues (as there must be a zero between any sign change) in the Hamiltonian or, equivalently, poles of the Green's function. Hence, we may proceed by analysing the structure of the poles of the full Green's function or equivalently:

$$\text{Pf}\Big[(g(\omega = 0, k_x, y_i = y_f = 0)Tg(\omega = 0, k_x, y_i = y_f = 0))^{-1}\Big] = 0. \tag{3.9}$$

As the background superconductor described by the bare Green's function g has no poles below the gap Δ this equation is equivalent to:

$$\text{Pf}\Big[T^{-1}\Big] = 0 \tag{3.10}$$

which can more easily be analysed by simply equivalently calculating $\det T^{-1} = 0$ as $(\text{Pf}(T^{-1}))^2 = \det(T^{-1})$. Though this method will more easily allow us to locate the phase boundaries, the identification of the topological classification of a phase requires knowledge of sign(Pf) rather than just the determinant. In this way we can seemingly reduce the calculation of the boundary of the topological phase diagram to an analysis of the zero energy states of the sub gap bands as in section 2.6. Hence, this analysis would suggest that the change in Majorana number from the trivial background, and hence the line on which a topological phase transition will occur, is given by

$$k_F V_m = E_F \left(\left(1 - k_m^2/k_F^2\right)^2 + \Delta^2/E_F^2\right)^{1/4} \tag{3.11}$$

as seen in the previous chapter and summarised in table 1.

By comparison with the topological phase diagram for a purely 1D implementation of the Kitaev chain toy model in figure 11 the upper curve is notably absent in our continuum model. This occurs because the upper curve arises from consideration of the time reversal invariant momentum at the edge of the Brillouin zone, which has been sent to infinity in the continuum model. As a result, for any k_m, in order for there to be zero energy states at this momentum one would need $V_m \to \infty$ so that the upper curve becomes unplottable. This tells us that we can neglect this point at infinity as topologically trivial and consider only the point at $k_x = 0$. One can also directly calculate the Pfaffian at this point by expanding the Green's function about the point $k_x \to \infty$ and seeing that it is always trivial.

It seems particularly noteworthy that, if one takes the usual BCS limit of this equation one is left with $V_m = \left(\kappa_m^2 - 1\right)^{1/2}$ which suggests rather unphysically that a spiral with $k_m = k_F$

does not require any magnetism to undergo a topological phase transition. This is to be taken as further evidence that this seemingly innocent limit is dangerous in this system as discussed in section 2.4.

3.1.2 Condition II: $\delta y = 0$, integrate over $\bar{y}$

Calculation of the topological index in this system would, in a system with translation symmetry, require one to identify the effect of time reversal invariance on the Hamiltonian, identify momenta at which this invariance is exact, and analyse the system only at those points. This analysis reduced to how co-ordinates (whether in real space, momentum space etc.) are transformed under time reversal symmetry. In a continuum system this is often simplified as some time reversal invariant momenta (e.g.: the edge of the Brillouin zone $k_x = \pi/a$) are irrelevant as the lattice spacing $a \to 0$. In this way, one would look at the action of time reversal on k_x as: $k_x \to -k_x$ hence, for points to be invariant it must be the case that $k_x = -k_x$ which is only fulfilled for $k_x = 0$. In real space, one might think initially, as is conventionally seen with this type of analysis, that co-ordinates are unchanged by time reversal. However, for 2-point functions one has both a beginning and end point hence under time reversal: $y_i \to y_f$ and $y_f \to y_i$. Hence, in real space, one should make the identification $y_i = y_f$ to fulfill time reversal symmetry. In terms of sum and difference co-ordinates, this translates to: $\delta y = 0$, $\bar{y} = y_i = y_f$ so that this analysis seems to suggest integrating over all $\bar{y}$.

The index resulting from condition II is identical (up to constant factors) to the one derived from III as will be discussed in section 3.1.4.

3.1.3 Condition III: $\bar{y} = 0$, integrate over δy

Due to the loss of translation invariance in the y direction, the Green's function is not diagonal in this co-ordinate. As a result, in order to calculate an effective 1D Hamiltonian which takes into account this co-ordinate one must invert an integral operator. As a result, regardless of the approach taken, at some point we will need to integrate the full Green's function over all y.

There is a great deal of similarity between the conditions $\int d\delta y$, $\bar{y} = 0$ and $\int d\bar{y}$, $\delta y = 0$ as can be seen just by inspection of the Green's function:

$$\begin{aligned}
\int d\bar{y}\; G(\delta y = 0, \bar{y}) &= \int d\bar{y}\; g(\delta y = 0) + \int d\bar{y}\; g(|2\bar{y}|) T g(|2\bar{y}|) \\
\int d\delta y\; G(\delta y, \bar{y} = 0) &= \int d\delta y\; g(\delta y) + \int d\delta y\; g(|-\delta y|) T g(|\delta y|) \\
&= g(k_y = 0) + \int d\delta y\; g(|-\delta y|) T g(|\delta y|)
\end{aligned} \tag{3.12}$$

where in particular we note that, excepting the manner in which the 2D background enters, these expressions are identical up to a constant factor. Certainly, in the vicinity of the topological phase transition (i.e. near the critical V_m) the difference due to the background 2D superconductor should make a minimal difference compared to the effect of the pole in the T matrix. In all of these methods we focus on $\omega = 0$ to analyse the topological transition hence, in the limit that small ϵ in the retarded Green's function is taken to zero we expect there to be no imaginary part, no poles and thus both expressions $\int d\bar{y}\; g(\delta y = 0)$ and $g(k_y = 0)$ should

just give a small, real offset to the Green's function and hence, a small correction to the topological phase diagram. It is worth noting that the former of these expressions would be strictly divergent due to the lack of $\bar{y}$ dependence in the free Green's function.

Another more pragmatic argument as to why this difference in background terms matters little is that we are interested in the change in topological characteristics from the trivial background. Hence, regardless of what this background term does we should be able to safely disregard it and study only the gTg part of the full Green's function. This is, in many ways the same argument that focusing near the poles of T will naturally drown out any other features due to the presence of the background superconductor.

Reassuringly, method II and III come out equivalent (without the background term) as, from different viewpoints, one can see that they are both valid ways to take into account time reversal invariance. Integration over $\bar{y}$ would mean summing up all points where $y_i = y_f = y$ which is the identification required to locate time reversal invariant points in real space. By contrast, on integration over δy one can note that the background term reduces to just $g(k_x = 0, k_y = 0)$ as δy is the co-ordinate one expects to be left with on restoration of translation symmetry at large $\bar{y}$. As a result, though there is not translation symmetry in this system, integration over all δy is something like picking out $k_{\delta y} = 0$ which, in the limit of large $\bar{y}$ or $V_m \to 0$ should reduce to just $k_y = 0$, the time reversal invariant momentum.

Such a method of extracting a 1D Hamiltonian can also be thought of from a field theoretic point of view: tracing out the effect of the superconducting fields on a chosen line. This approach leads to similar integrals as required to calculate the exact Green's function in the limit of dense chains as in the previous chapter, and in the literature only the sparse chain limit or long wavelength approximation (LWA) has been explored [11].

There are a number of justifications one can make for calculation of an effective one-dimensional Hamiltonian by integrating out the transverse co-ordinate. Firstly, we note that the dependence on the y co-ordinate in the full Green's function is such that it provides amplitudes to get to and from the interface. Hence, though the interaction is entirely localised to the interface, we see a long distance response to its presence carried by the oscillations in the Green's function as one moves away from the interface. It is not immediately clear what consequences this spreading out of states (which if entirely one-dimensional are known to trigger a topological phase transition) could have at least in part because we are looking in real space rather than momentum space where topological properties are more clear. As a result, we could quite justifiably integrate out this co-ordinate in order to trace out the long distance oscillations or any other effects that the decaying tails of the wave-functions could have. In this sense we are thinking of the long distance tails as something like the 'leakage' from the localised states at the interface. As one can naturally tune the degree of localisation via the coherence length in the background superconductor, this allows us to see how higher dimensional substrates could be qualitatively different.

Another way that this integration can be justified is by comparing to how we would calculate the weak 2-dimensional indices in a translationally invariant system. In such a system, one would set one of the momenta k_y to a time reversal invariant point (such as $k_y = 0$) in the full, 2-dimensional Hamiltonian. This will leave a Hamiltonian describing a one-dimensional "strip" in

momentum space in the original 2-dimensional system. If this strip undergoes a one-dimensional topological phase transition then the system has a non-zero weak 2-dimensional index. Though k_y is not a good quantum number here, we can still calculate the Fourier transform with respect to the co-ordinate δy with the expectation that, for large $\bar{y}$ $k_{\delta y} \to k_y$:

$$\begin{aligned}
&\int d\delta y e^{i\delta y k_{\delta y}} G(k_x, \delta y, \bar{y})|_{k_{\delta y}=0} \\
&= \int d\delta y e^{i\delta y k_{\delta y}} g(k_x, \delta y)|_{k_y=0} \\
&+ \int d\delta y e^{i\delta y k_{\delta y}} g(k_x, 2\bar{y} - \delta y) T g(k_x, 2\bar{y} + \delta y)|_{k_y=0}
\end{aligned} \tag{3.13}$$

where, for the free Green's function, taking this transform must undo the partial Fourier transform calculated in section 2.4. Hence, though we cannot simply pick out a single k_y in the gTg part of the full Green's function, we are left with:

$$\tilde{G}(k_x, \bar{y}) = g(k_x, k_y = 0) + \int d\delta y g(k_x, 2\bar{y} - \delta y) T g(k_x, 2\bar{y} + \delta y) \tag{3.14}$$

where it is worth noting that a true Fourier transform would have involved replacing all factors of $g(k_x, y)$ by $g(k_x, k_y)$ which would make the consequences of the loss of translation invariance to momentum space apparent in the form of an integral over all internal momenta. In this sense, the above equation is not a 'true' Fourier transform as the above function is *not* $G(k_x, k_y)$ but will, in the limit of $\bar{y} \gg 1/k_F$ or $V_m \to 0$ smoothly transform into it.

In this sense, the above equation describes $G(k_x, \bar{y}, k_{\delta y} = 0)$ so that we can identify the point $\delta y = 0$ which, in the limit as $k_{\delta y} \to k_y$, would be the 2D time reversal invariant point in momentum space. Hence, this method seems to be the clearest way to see how to perform a calculation of the weak 2D index in this system in a manner that smoothly transforms into a calculation of the weak 2D index of a trivial 2D superconductor. This method also highlights that the standard picture of building up an array of identical systems with a non-trivial index in a lower dimension as corresponding to weak 2D indices does not exactly correspond here. As we have seen, this picture only really seems to apply for $\bar{y} \gg 1/k_F$ or equivalently, distances very far from the interface. This neatly raises the possibility: can we interpret the phase present here as an array of one dimensional systems which smoothly vary from trivial to topological? The consequence of this would be that one could look at a boundary to the system and would see a region which has Majorana like bound states and, beyond a certain distance, no such states.

Of course, one could argue that such a scenario is essentially impossible to disentangle from suggesting there is a single Majorana bound state precisely on the chain and that the long range effects suggested above are merely the background superconductor allowing for leakage (much as we do see in the leakage of the states formed by the interaction on the chain). Such possibilities will be explored in the following sections where we explicitly add ends to our currently infinite chains to investigate the nature of the topological states that form there.

3.1.4 Comparison of cases

The integral required for cases II or III over either δy or $\bar{y}$ can be performed analytically [21] resulting in topological phase diagrams plotted in figure 12 (right). The features of this phase diagram appear similar to those for case I ($y_i = y_f = 0$) in figure 12 (left) but distorted to different critical V_m values. However, this is deceptive as there appear to be not just zeros in the Pfaffian but poles too. This can be seen below where we actually do reproduce the zero of the Pfaffian at the value predicted by the entirely local theory but, instead of entering into the topological phase beyond this value, the system seems to remain trivial until it runs through the pole. It is unclear what interpretation can be assigned to the pole of the Pfaffian, if any. It may be an artefact of inverting a non-invertible matrix. If there is an interpretation to be made for this pole in the Pfaffian, and hence the 1D effective Hamiltonian, it could probably best be made in terms of zeros in the Green's function which can, according to Gurarie [96, 97], be created in pole-zero pairs in interacting systems and can have effects on the topological characterisation of systems.

Looking at figure 13, it seems as though the phase diagrams would agree if the section of the curve between the exact zero and the sign change due to the pole were inverted. Hence, we attempted to understand the nature of the contributions to the Pfaffian from nonzero $\bar{y}$ (in the case $\delta y = 0$) by splitting the full Green's function into local and non-local parts in the Pfaffian:

$$\mathrm{Pf}\left[BH^{1\mathrm{D}}\right] = -\mathrm{Pf}\left[B\left(G(\delta y = \bar{y} = 0) + \sum_{\bar{y}\neq 0} G(\delta y = 0, \bar{y})\right)^{-1}\right] \tag{3.15}$$

where B is the matrix transform to the Hamiltonian to transform it to the Majorana basis. The full Green's function split in this way can be written:

$$\left[G(\delta = \bar{y} = 0) + \sum_{\bar{y}\neq 0} G(\delta y = 0, \bar{y})\right] = \left[g(k_y = 0) + g(\bar{y} = 0)Tg(\bar{y} = 0) + \sum_{\bar{y}\neq 0} g(\bar{y})Tg(\bar{y})\right] \tag{3.16}$$

whence it is clear that unless the $\sum_{\bar{y}\neq 0}$ term is zero, there is some difference between looking entirely locally, and integrating over the background. Near to the critical V_m which would signal the entry to a topological phase when considering only the local contribution the poles in T will mean that the background has little impact and only terms multiplying T which are strictly non-zero should contribute. The sub-gap, free Green's function will look like a damped oscillator and hence should have strict zeros only as $\bar{y} \to \infty$.

In an effort to understand these contributions indirectly, one can study the spectra formed from the eigenvalues of the effective Hamiltonian $H^{1\mathrm{D}}(k_x, \bar{y})$. This would correspond to the 1D Hamiltonian if the entire system were just the single strip at the particular, chosen $\bar{y}$. One should then be able to freely tune $\bar{y}$ and see how the band structure deforms from the induced structure at $\bar{y} = 0$ to the Boguliubov bands as $\bar{y} \to \infty$. Unfortunately, one cannot simply

[21] This is possible as the only y dependence enters the gTg terms from the free Green's functions and hence only takes the form of exponential factors. One can thus decouple this product into a small number of independent integrals and perform them exactly. The derivation is not very enlightening so is omitted.

analyse the Pfaffian of each of these to see how they contribute as one cannot split the above fraction into contributions each at a different $\bar{y}$. The essential observation of this analysis is that, using $\bar{y}$ as a tuning parameter, one can always find a large enough $\bar{y}$ that can unwind the band structure back to the trivial background *unless* $V_m = V_m^{\text{crit}}$ at which point the state at $k_x = 0$ is stuck at zero energy for even very large $\bar{y}$. This seems to corroborate the above feature of the phase diagram that, even when $V_m > V_m^{\text{crit}}$ the system is trivial topologically as we can, using a smoothly tuneable system parameter, bring the bands back to trivial bands. A possible future direction would be to analyse the band structure itself as a surface either directly or via a Hopf mapping to ascertain when a transition has occurred.

3.2 Introducing chain ends-changing boundary conditions

As illustrated above, there is an ambiguity in defining 1D effective Hamiltonians and hence topological indices in this system. Instead of attempting to calculate a topological index we can instead attempt to investigate whether any new bound states form at the system edge when stitched onto a topologically trivial background. This method also has the advantage that it does not rely upon classifications of topological states valid for weak interactions. If we are looking only at zeros and poles of the Green's functions then even for strongly interacting systems we should in principle be able to understand the nature of any transitions which occur [96, 97]. Such a method may thus provide a picture of topological phase transitions with more physical insight than the more standard approach involving mappings from the Brillouin zone to the band structure. This calculation largely follows [53–56] but we include here full derivations to illustrate the method and define our notation.

Quite aside from these considerations, construction of a method which allows one to take exact solutions to Green's functions in infinite systems and stitch them together into composite systems would seem relevant in a huge variety of physical systems. Here we will outline an approach for stitching together two subsystems which are one or two dimensional, but the method is easily generalisable to other situations. We will use matrix Green's functions to allow for the simple inclusion of superconducting or other additional degrees of freedom using the Nambu formalism.

To be concrete, we aim to find the composite Green's function $G(\mathbf{x}, \mathbf{x}')$ for the system outlined in figure 14 where the spiral ordered magnetic chain at $y = 0$ ends at $x = 0$. This system can be partitioned by splitting the 2D plane into regions A, defined by $x < 0$, and region B, defined by $x > 0$. In this way the chain is entirely contained within region A.If either region A or B were infinite, we would know the Green's functions from our previous calculations as G_A or G_B respectively. Our goal here, following García-Moliner and Rubio [53–56], is to stitch together the known Green's functions for infinite systems G_A and G_B at the, artificial, boundary $x = 0$ to calculate the composite Green's function $G(\mathbf{x}, \mathbf{x}')$. In this manner we will have effectively modified the boundary conditions on the Green's function G_A valid for an infinite system to be something like a semi infinite system instead. The equation of motion for the compound system can be written:

$$\left(\omega - (\overrightarrow{H}_0 + V_m\theta(-x))\right)\mathbf{G}(\mathbf{x}, \mathbf{x}') = \delta(\mathbf{x} - \mathbf{x}') \tag{3.17}$$

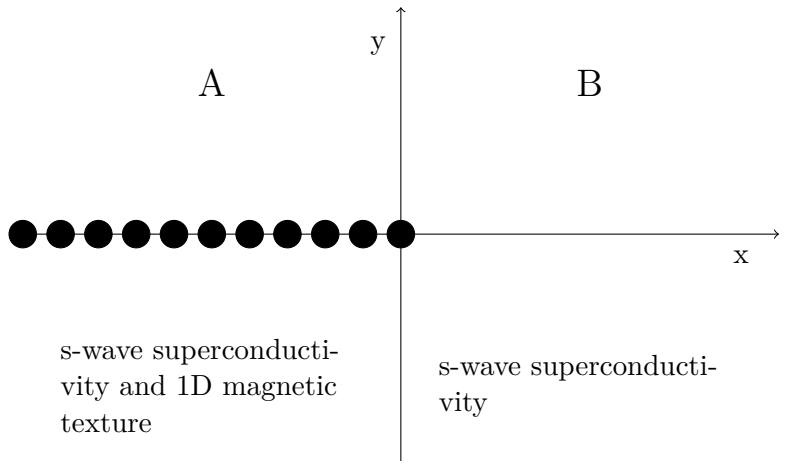

Figure 14: Diagram of system containing a semi-infinite, spiral ordered magnetic chain along $y = 0$, ending at $x = 0$ embedded in a 2D s-wave superconductor. The system is partitioned into regions A where $x < 0$ and B where $x > 0$. Hence, if either region A or B were instead infinite they would have Green's functions G_A describing an infinite spiral ordered chain in a superconductor and G_B describing the background superconductor alone.

where operators $\overrightarrow{O}$, $\overleftarrow{O}$ are understood to act to the right and left respectively. This notation is required due to the inclusion of matrix structure in the Green's function that restricts the ordering of operators. The magnetic interaction is understood to act only in region A by the function $\theta(-x)$ where the x should be understood as either $\mathbf{x} \in A$ or $\mathbf{x}' \in A$.

The framing of this calculation is that we would like to solve this equation of motion using only the known solutions to the equations of motion for infinite systems A (as though B were not present at all):

$$\mathbf{G}_A(\mathbf{x}'', \mathbf{x}) \left(\omega - (\overleftarrow{H}_0 + V_m)\right) = \delta(\mathbf{x}'' - \mathbf{x}) \tag{3.18}$$

and system B (as though A, and hence the magnetic interaction, were not present):

$$\mathbf{G}_B(\mathbf{x}'', \mathbf{x}) \left(\omega - \overleftarrow{H}_0\right) = \delta(\mathbf{x}'' - \mathbf{x}). \tag{3.19}$$

In order to find the full Green's function for the compound system we will need to approach the interface between them from both directions in an extremely careful manner.

Restricting to $\mathbf{x}, \mathbf{x}' \in A$, multiplying equation (3.18) from the right by $\mathbf{G}(\mathbf{x}, \mathbf{x}')$ and multiplying equation (3.17) from the left by $\mathbf{G}_A(\mathbf{x}'', \mathbf{x})$ one can cancel out all but the effect of the background Hamiltonian by taking the difference of the resulting equations:

$$\int_{\mathbf{x}\in A} d\mathbf{x} \left(\mathbf{G}_A(\mathbf{x}'', \mathbf{x}) \left[\cancel{\omega} - \overrightarrow{H}_0(\mathbf{x}) - \cancel{V_m(\mathbf{x})}\right] \mathbf{G}(\mathbf{x}, \mathbf{x}')\right. \tag{3.20}$$

$$\left. - \mathbf{G}_A(\mathbf{x}'', \mathbf{x}) \left[\cancel{\omega} - \overleftarrow{H}_0(\mathbf{x}) - \cancel{V_m(\mathbf{x})}\right] \mathbf{G}(\mathbf{x}, \mathbf{x}')\right) \tag{3.21}$$

$$= \mathbf{G}_A(\mathbf{x}'', \mathbf{x}') - \mathbf{G}(\mathbf{x}'', \mathbf{x}') \tag{3.22}$$

where we have explicitly noted that the chain of magnetic impurities could have some additional texture, but would still be cancelled in the same fashion as a ferromagnetic array of impurities.

Focusing on the ∇^2 terms present in the free Hamiltonian, we can rewrite as a complete

derivative and hence reduce our problem to integrating only along the boundary connecting regions A and B. The careful choice of which direction operators act is necessary due to the fact that G_A and G_B should only ever take arguments from regions A and B respectively. There is no discontinuity in those systems when extended beyond these regions, hence doing so would defeat our purpose here. We approach the calculation in this way so that only terms like ∇ rather than ∇^2 are present as the equation of motion makes it clear ∇^2, and thus the kinetic terms in general, have a discontinuity which makes calculation difficult.

With this, we are able to write, for $x', x'' \in A$:

$$\begin{aligned}\mathbf{G}(\mathbf{x}'', \mathbf{x}') = \mathbf{G}_A(\mathbf{x}'', \mathbf{x}') \\ - \frac{1}{2m} \int dy \, [\mathbf{G}_A(x'', x = 0; y'', y) \, \partial_x \mathbf{G}(x = 0, x'; y, y') \\ - (\partial_x \mathbf{G}_A(x'', x = 0; y'', y)) \mathbf{G}(x = 0, x'; y, y')]\end{aligned} \tag{3.23}$$

To form the second equation required to find the full Green's function in the compound region we return again to the equations of motion, this time with $x' \in A$ but now restricting $x'' \in B$ and no restriction required on y'', y'. In this way we will have equations for the full Green's function to start and end at any location in A, and now also to start at any location in A, but end in B. Through their careful combination we are thus able to cross from region A into region B.

The equations of motion under these conditions are then:

$$\left(\omega - \overrightarrow{H}_0\right) \mathbf{G}(\mathbf{x}, \mathbf{x}') = \mathbf{0} \tag{3.24}$$

$$\mathbf{G}_B(\mathbf{x}'', \mathbf{x}) \left(\omega - \overleftarrow{H}_{\mathbf{0}}\right) = \delta(\mathbf{x}'' - \mathbf{x}) \tag{3.25}$$

where crucially in the equation of motion for the compound region there is no inhomogenous part (delta function) because x' and x are always in different sub-systems and hence cannot be at the same location as one another. This is not the case for the equation for G_B as there $x'', x \in B$. We can thus combine these into one equation for G where $x' \in A$ and $x'' \in B$ as:

$$\begin{aligned}\mathbf{G}(\mathbf{x}'', \mathbf{x}') = \frac{1}{2m} \int dy \, [\mathbf{G}_B(x'', x = 0; y'', y) \, \partial_x \mathbf{G}(x = 0, x'; y, y') \\ - (\partial_x \mathbf{G}_B(x'', x = 0; y'', y)) \mathbf{G}(x = 0, x'; y, y')]\end{aligned} \tag{3.26}$$

where the difference in overall sign is due to the different orientation of the boundary region with respect to regions A and B.

Proceeding formally, we can rearrange equations (3.23) and (3.26) for G by evaluating at $x'' = 0^-$, and $x'' = 0^+$ a point slightly to the *left*/*right* of the boundary respectively. Following

García-Moliner and Rubio [53–56] we introduce the short hand notation:

$$\begin{aligned}
\mathcal{G}_A(y'', y) &= G_A(x'' = 0^-, x = 0; y'', y) \\
\mathcal{G}_B(y'', y) &= G_B(x'' = 0^+, x = 0; y'', y) \\
\backslash\mathcal{G}_A(y'', y) &= \partial_x G_A(x = 0, x = 0^-; y'', y) \\
\mathcal{G}'_A(y'', y) &= \partial_x G_A(x = 0^-, x = 0; y'', y)
\end{aligned} \tag{3.27}$$

which encapsulates the careful need to take limits approaching the boundary in a certain order. For clarity: variables at precisely 0 are to be taken first, followed by the directional limits $0^{\pm}$. This must be done in precisely this way to avoid sign issues from crossing the boundary between regions A and B.

For this particular example, where the background is identical and modified only by the additional presence of the magnetic adatom chain, it is not so necessary to be this careful when taking limits in the compound region Green's function G as we expect there to not be a discontinuity at the boundary.

With this notation we can rewrite and rearrange equation (3.23) as:

$$\begin{aligned}
\mathcal{G} &= G_A - \frac{1}{2m}\left[\mathcal{G}_A \backslash \mathcal{G} - \mathcal{G}'_A \mathcal{G}\right] \\
\mathcal{G} &= \left[1 + \frac{1}{2m}\mathcal{G}'_A\right]^{-1} \left(G_A - \frac{1}{2m}\mathcal{G}_A \backslash \mathcal{G}\right)
\end{aligned} \tag{3.28}$$

and equation (3.26) as:

$$\begin{aligned}
\mathcal{G} &= \frac{1}{2m}\left[\mathcal{G}_B \backslash \mathcal{G} - \mathcal{G}'_B \mathcal{G}\right] \\
\mathcal{G} &= \left[1 - \frac{1}{2m}\mathcal{G}'_B\right]^{-1} \frac{1}{2m}\mathcal{G}_B \backslash \mathcal{G}.
\end{aligned} \tag{3.29}$$

Assuming continuity at the boundary in the compound region, which is to say that the order $x'' \to 0^{\pm}$ does not matter in the compound region, one can hence solve for $\backslash\mathcal{G}$ in terms of only terms depending on G_A and G_B:

$$\frac{1}{2m}\backslash\mathcal{G} = \left[\left[1 - \frac{1}{2m}\mathcal{G}'_A\right]^{-1}\mathcal{G}_A + \left[1 + \frac{1}{2m}\mathcal{G}'_B\right]^{-1}\mathcal{G}_B\right]^{-1}\left[1 - \frac{1}{2m}\mathcal{G}'_A\right]^{-1} G_A. \tag{3.30}$$

In order to avoid inverting as many infinite matrices as possible, this equation can be recast into a slightly different form by making note of the relation $\mathcal{G}_B \backslash \mathcal{G}_B = \mathcal{G}'_B \mathcal{G}_B$ such that

$$\frac{1}{2m}\backslash\mathcal{G} = \left[1 + \frac{1}{2m}\backslash\mathcal{G}_B\right]\left[\mathcal{G}_A\left[1 + \frac{1}{2m}\backslash\mathcal{G}_B\right] + \left[1 - \frac{1}{2m}\mathcal{G}'_A\right]\mathcal{G}_B\right]^{-1} G_A \tag{3.31}$$

The relation $\mathcal{G}_B \backslash \mathcal{G}_B = \mathcal{G}'_B \mathcal{G}_B$ can be derived most clearly by returning to the equations of motion. We note that, we made the arbitrary choice in writing down the equations of motion that we would consider $\mathbf{x}'', \mathbf{x}' \in A$ for the first equation of motion (3.23) and $\mathbf{x}'' \in B$, $\mathbf{x}' \in A$ for the second equation (3.26) which results in the asymmetry between the equations. If instead

we had chosen $\mathbf{x}'', \mathbf{x}' \in B$ we would get:

$$\mathcal{G} = \mathcal{G}_B + \frac{1}{2m}\left[\mathcal{G}_B \backprime \mathcal{G} - \mathcal{G}'_B \mathcal{G}\right].$$

If we consider that this result must, in the limit $V_m \to 0$ just return to the known solution G_B *everywhere* (because regions A and B are identical apart from the magnetic chain in A) then it must be true that, at the interface we can take $\mathcal{G} \to \mathcal{G}_B$ so that

$$\mathcal{G}_B = \mathcal{G}_B + \frac{1}{2m}\left[\mathcal{G}_B \backprime \mathcal{G}_B - \mathcal{G}'_B \mathcal{G}_B\right] \tag{3.32}$$

which we can re-arrange to get $\mathcal{G}_B \backprime \mathcal{G}_B = \mathcal{G}'_B \mathcal{G}_B$.

At this point we are equipped with equations for both $\backprime\mathcal{G}$ and $\mathcal{G}$ in terms of only G_A and G_B and their derivatives so all that remains is to substitute back into equations (3.23) and (3.26) to find the Green's function in the composite region. Here we have focused only on the composite Green's function in region A and at the boundary but it is fairly straightforward to follow the same method to find the composite region Green's function in region B also.

Hence, for $x', x'' \in A$ we have:

$$\begin{aligned}\mathbf{G}(\mathbf{x}'', \mathbf{x}') = \mathbf{G}_A(\mathbf{x}'', \mathbf{x}') - \mathbf{G}_A(\mathbf{x}'', \mathbf{x}_S)\mathcal{D}_B\left[\mathcal{G}_A\mathcal{D}_B + \mathcal{D}_A\mathcal{G}_B\right]^{-1}\mathbf{G}_A(\mathbf{x}_S, \mathbf{x}') \\ + \mathbf{G}'_A(\mathbf{x}'', \mathbf{x}_S)\mathcal{D}_A^{-1}\left(1 - \mathcal{G}_A\mathcal{D}_B\left[\mathcal{G}_A\mathcal{D}_B + \mathcal{D}_A\mathcal{G}_B\right]^{-1}\right)\mathbf{G}_A(\mathbf{x}_S, \mathbf{x}')\end{aligned} \tag{3.33}$$

where $\mathbf{x}_S = (x = 0, y)$; the integral along y has been suppressed and:

$$\mathcal{D}_A = \left[1 - \frac{1}{2m}\mathcal{G}'_A\right] \qquad \mathcal{D}_B = \left[1 + \frac{1}{2m}\backprime\mathcal{G}_B\right]. \tag{3.34}$$

The form of the composite Green's function makes it clear that the condition for novel bound states at the boundary is for either $\mathcal{D}_B$ to be singular or that

$$\left[\mathcal{G}_A\mathcal{D}_B + \mathcal{D}_A\mathcal{G}_B\right]^{-1} \tag{3.35}$$

is singular. As is implicit in the notation the $\mathcal{G}_{A,B}$ and $\mathcal{D}_{A,B}$ are matrices in all remaining degrees of freedom at the interface $x = 0$. These degrees of freedom refer not only to the Nambu and spin indices but also, for this two-dimensional problem, the position indices y along the interface. Due to the presence of this continuous parameter, matrix inversion, or even deciding whether the matrix is singular, is in general an involved process.

However, for an entirely one-dimensional problem there is no such continuous parameter y and we are left with only a finite matrix. To gain some familiarity with this condition, we will investigate such a system initially.

3.3 Stitching 1D chain onto 1D superconductor

As a simple test of this formalism, we apply it to an entirely one dimensional system. In this way we avoid the need to take an operator inverse in some manner as the boundary is a zero dimensional point: the location where the two systems meet. Hence, the condition for

bound states to exist reduces down to just taking a regular matrix determinant and solving the equation:

$$\det\left[\mathcal{G}_A(\mathbf{1}+\frac{1}{2m}\backprime\mathcal{G}_B)+(\mathbf{1}-\frac{1}{2m}\mathcal{G}'_A)\mathcal{G}_B\right]=0 \tag{3.36}$$

where here $\mathcal{G}_A=\mathbf{G}_A(x''=0,x'=0^-)$, $\mathcal{G}_B=\mathbf{G}_B(x''=0,x'=0^+)$ and primes indicate whether derivatives are taken with respect to the first or second x co-ordinate, as in the archetypical 2 dimensional example in the previous section (see equations (3.27)). As previously, the correct ordering to take co-ordinates to zero in derivative terms is, for example: $\mathcal{G}'=\partial_x\mathbf{G}_A(x''=0^+,x=0)$ so that the derivative is taken, *that* co-ordinate sent to the boundary, then the Green's functions for regions A or B are taken to 0^- or 0^+ respectively. In this sub-section Green's functions $\mathbf{G}_A$ and $\mathbf{G}_B$ are naturally understood to refer to the Green's functions in the now *one*-dimensional sub-systems if there was no boundary.

As we are intending to study topological phases, and hence states which should exist regardless of the nature of the trivial phase to which they are attached, it should be the case that the states which are identified from this equation are essentially the same regardless of the form of the topologically trivial region B. The simplest case one could consider is hence stitching our potentially topological phase onto the vacuum, where $g_B=0$ but $\backprime g_B^+$ may be non-zero.

3.3.1 Stitching onto the vacuum

Though very useful for simplifying equations, the particular manner in which we will stitch region A onto a vacuum does require some justification. Regardless of method, without worrying about quantum mechanical fluctuations, the vacuum is here used to refer to region B being essentially impenetrable i.e. there being no probability of finding states there occupied. In this way we are looking to justify a limit where $\mathcal{G}_B=0$.

Crucially, this condition must be taken *after* the stitching formalism has been applied, otherwise we simply return to the additional difficulty in stitching Green's functions together compared to wave functions due to the additional spatial co-ordinate (hence the great deal of attention required throughout the derivation to take the limits of the two Green's function co-ordinates to the same point on the interface, but from its different *sides*).

Once the stitching has been applied, we can be sure that, regardless of what parameters we change, all parameters which should stay smooth through the boundary will do so. In order to approach a vacuum in region B therefore, we will take the gap $\Delta\to\infty$ there. This is acceptable despite the calculation being constructed to have a uniform background superconductor as the formalism will readily take into account any smooth connection required. It is also worth noting that, as one can see in the equations of motion, only the kinetic energy parts are discontinuous so this is completely safe to do.

As a simple illustration one can take the gap dependence of the Green's function in an entirely 1D region B from which it is clear the entire matrix tends to 0 at worst like $\Delta^{-1/2}$ as $\Delta\to\infty$.

Though the gradient terms $\backprime g_B^+$ do *not* go to zero in this limit (instead approaching a constant), all factors of D_B will drop out regardless. As a result we can proceed to safely take the

limit $\mathcal{G}_B \approx 0$ and simplify down to the condition:

$$\det \bar{D}_B \det \mathcal{G}_A = 0. \tag{3.37}$$

for there to be bound states at $x = 0$. Though always worth checking, $\bar{D}_B$ does not generally have additional poles (and as we will see cancels out from the expression for the full Green's function in this limit), our attention will be focused on the behaviour of $\det \mathcal{G}_A$ in what follows.

Though pleasingly simple, it is noteworthy to compare this condition to the condition for bound states to occur on the chain within region A. In that case, new bound states could be identified by searching for poles in G_A which occur whenever $\det\left\{G_A^{-1}\right\} = 0$ regardless of x coordinates due to translation invariance. However, here we find a condition which depends upon $\mathbf{G}_A$ rather than $\mathbf{G}_A^{-1}$ and hence probes the *zeroes* of the Green's function (which is itself pinned to the boundary) rather than the poles of the Green's function in region A. This suggests a link to work by [96, 97] on interpretation of topological invariants in terms of poles and zeroes of Green's functions.

This condition can be written in terms of momentum space Green's functions by just writing in integrals explicitly. However, care should be taken when returning to real space representations as the doubled Nambu space is explicitly treating left and right movers separately. To recombine them properly we should return to first principles so that, for example:

$$g_{11}(x) = \langle c_\uparrow^\dagger(x) c_\uparrow(x) \rangle = \int_{-\infty}^{\infty} e^{ik_x x} g_{1,1}(k_x) \tag{3.38}$$

where matrix indices i, j correspond to spin and Nambu degrees of freedom according to the real space Nambu spinors $(c_\uparrow^\dagger(x), c_\downarrow^\dagger(x), c_\downarrow(x), c_\uparrow(x))$ or momentum space Nambu spinors $(c_\uparrow^\dagger(k_x), c_\downarrow^\dagger(k_x), c_\downarrow(-k_x), c_\uparrow(-k_x))$ where the doubling of the Nambu space has not yet been performed. This can be written:

$$\begin{aligned} g_{11}(x) &= \int_0^\infty dk_x e^{ik_x x} \langle c_{k_x,\uparrow}^\dagger c_{k_x,\uparrow} \rangle + \int_{-\infty}^0 dk_x e^{ik_x x} \langle c_{k_x,\uparrow}^\dagger c_{k_x,\uparrow} \rangle \\ &= \int_0^\infty dk_x \left(e^{ik_x x} \langle c_{k_x,\uparrow}^\dagger c_{k_x,\uparrow} \rangle + e^{-ik_x x} \langle c_{-k_x,\uparrow}^\dagger c_{-k_x,\uparrow} \rangle \right) \\ &= \int_0^\infty dk_x \left(e^{ik_x x} g_{11}(k_x) - e^{-ik_x x} g_{44}(k_x) \right). \end{aligned}$$

In this way, the real space, particle like Green's function takes into account both left and right moving wave packets travelling through a given x as required. This procedure is readily generalisable to a matrix transformation.

In figure 15 we plot $\det \mathcal{G}_A$ calculated numerically against magnetic interactions strength V_m, for a range of spiral wave-vectors k_m.

In these plots of $\det \mathcal{G}_A$ there is clearly a discontinuous drop to 0 [22] at a critical C_m (the unitless version of V_m, related by $C_m = \pi \rho_0 V_m$) which is precisely $\left((1 - (k_m/k_F)^2)^2 + \Delta^2/E_F^2\right)^{1/2}$. This critical value of V_m is the same as the condition at which the energies of bound states in the bulk of the chain present in region A reach zero at $k_x = 0$. In this entirely one dimensional

[22] Even for small $k_m \approx 0.1 k_F$ it is clear there is a discontinuous drop of several orders of magnitude which scales with the small $i\epsilon$ in the retarded Green's function as expected.

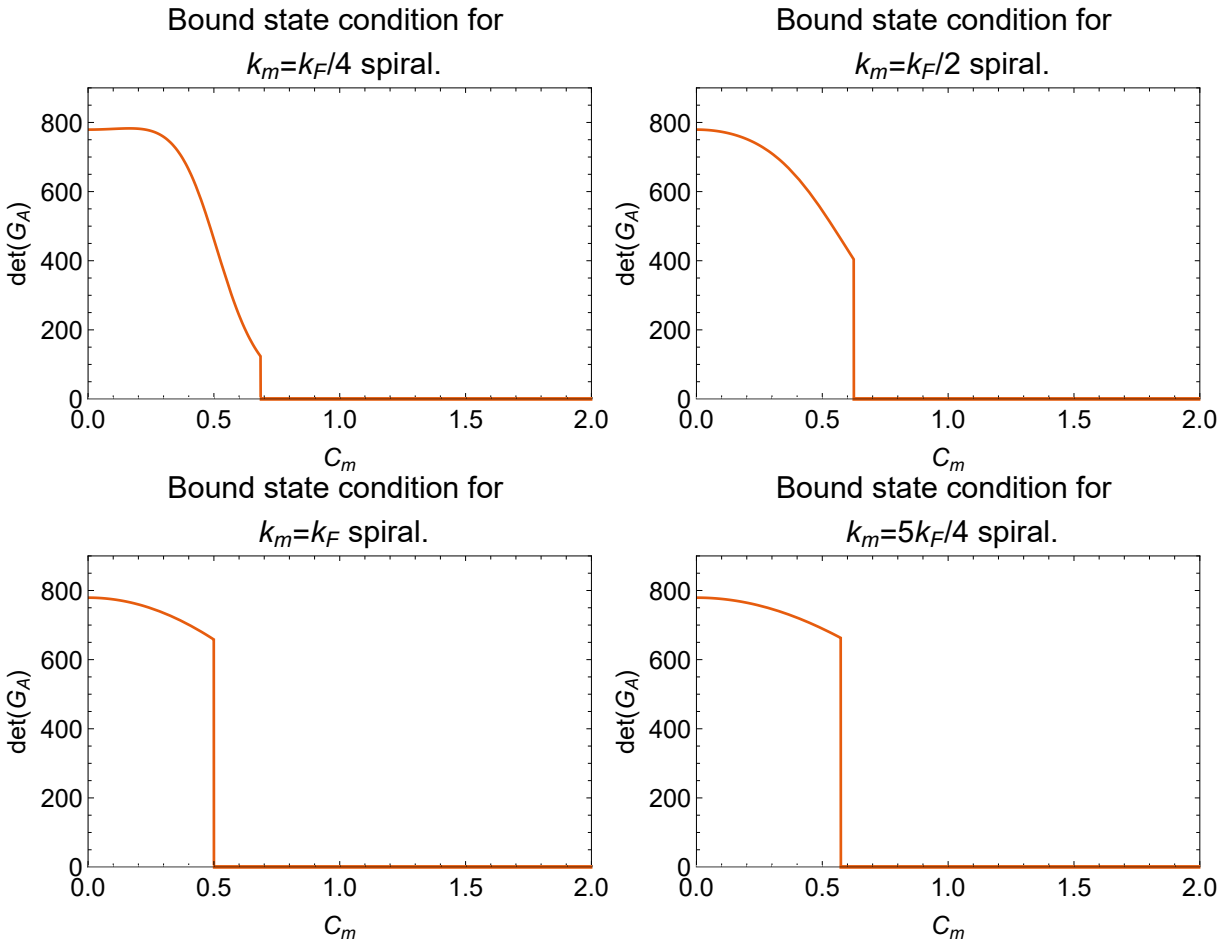

Figure 15: Plots of $\det \mathcal{G}_A$ for a purely 1D system as a function of unitless magnetic interaction strength C_m for the labelled k_m. In all plots the gap $\Delta = 0.5$. At a critical $C_m = \left((1 - k_m^2/k_F^2)^2 + \Delta^2\right)^{1/2}$ exactly coincident with that expected from consideration of time reversal invariant momenta in the sub-gap bands there is a discontinuous drop to zero, fulfilling the derived condition for bound states to form at the boundary of the system. For smaller k_m note that the scale of the discontinuity is reduced. This continues to smoothly decrease until it is absent for the ferromagnet ($k_m = 0$) so that we show without addition assumptions that ferromagnetic chains are always topologically trivial.

example this fact is a verification that the condition $\det \mathcal{G}_A = 0$ is the same as the more well known condition of there being an odd number of bands crossing the Fermi surface or the gap closing at time reversal invariant momenta such as $k_x = 0$.

Though the condition to have what we are identifying as bound states of a topological origin [23] requires only that the determinant fall to zero it is nonetheless interesting to note the way in which it changes as a function of V_m in figure 15. As k_m is reduced from k_F towards $k_m = 0$ the size of the discontinuity to zero reduces smoothly until, for the ferromagnet, there is no discontinuity. This is noteworthy as it seems our potential topological invariant is able to single out the ferromagnet as *not* being topologically non-trivial in the sense we are investigating without any extra input. It would seem that this method, because it is searching for the presence or absence of bound states, is sensitive to whether the symmetries necessary are present at all without any need to create a mathematical object that takes this into account. This can be compared to methods relying on the Pfaffian which in principle requires a check before calculation to be sure the correct symmetry transforms have been applied to the Hamiltonian and that the resulting matrix is antisymmetric.

In this manner, we have derived a condition equivalent to known measures of entry into the topological phase in the purely one-dimensional system. Having arrived at this condition, it is worthwhile to attempt to interpret what physical meaning it has. As previously noted, the condition $\det(\mathcal{G}_A) = 0$ refers to *zeroes* of the Green's function at the interface $x = 0$ between regions A and B. Based on this fact, it would seem that the condition for there to be a pole (and hence topological state) at the boundary in the composite Green's function G is equivalent to finding when there are zeroes of the Green's function G_A for an infinite chain, at $x = 0$. Interestingly, this fact seems to suggest something about the mechanism by which the edge state is formed beyond certain critical physical parameters: as an interference effect.

To better understand how it is that the zeroes of the bulk Green's function G_A seem to completely govern the entry into the topological phase it is helpful to study a quantity that directly image the effects of both the zeroes and poles of the Green's function through the transition. To do so, we will divert briefly to discuss the full Green's function for this 1D model in more depth.

[23] Though it is certainly worth investigating the nature of these states further due to the well known possibility of boundary states of non topological character (e.g. Shockley states).

3.3.2 Full Green's function towards boundary in one dimension

If we refer back to equation (3.33), specialised to an entirely one dimensional system we arrive at:

$$\begin{aligned}
&\mathbf{G}(x'', x') \\
&= \mathbf{G}_A(x'', x') - \mathbf{G}_A(x'', x=0)\mathcal{D}_B \left[\mathcal{G}_A\mathcal{D}_B + \mathcal{D}_A\mathcal{G}_B\right]^{-1} \mathbf{G}_A(x=0, x') \\
&+ \mathbf{G}'_A(x'', x=0)\mathcal{D}_A^{-1} \left(1 - \mathcal{G}_A\mathcal{D}_B \left[\mathcal{G}_A\mathcal{D}_B + \mathcal{D}_A\mathcal{G}_B\right]^{-1}\right) \mathbf{G}_A(x=0, x')
\end{aligned} \tag{3.39}$$

so that if we take the limit $\mathcal{G}_B \approx 0$ we see that

$$\left(1 - \mathcal{G}_A\mathcal{D}_B \left[\mathcal{G}_A\mathcal{D}_B + \mathcal{D}_A\mathcal{G}_B\right]^{-1}\right) \approx 0 \tag{3.40}$$

$$\mathcal{D}_B \left[\mathcal{G}_A\mathcal{D}_B + \mathcal{D}_A\mathcal{G}_B\right]^{-1} \approx \mathcal{G}_A^{-1} \tag{3.41}$$

so that the composite Green's function with $x'', x' \in A$ stitched to the vacuum can be written:

$$\mathbf{G}(x'', x') = \mathbf{G}_A(x'', x') - \mathbf{G}_A(x'', x=0)\mathcal{G}_A^{-1}\mathbf{G}_A(x=0, x'). \tag{3.42}$$

This is pleasingly similar to what one would expect from taking the Green's function for a system with a line of scalar impurities localised at $x = 0$ in the limit of incredibly strong interaction:

$$\begin{aligned}
\mathbf{G}(x'', x') &= \mathbf{G}_A(x'', x') + \mathbf{G}_A(x'', x=0) \left[V_s^{-1} - \mathcal{G}_A\right]^{-1} \mathbf{G}_A(x=0, x')|_{V_s \to \infty} \\
\mathbf{G}(x'', x') &= \mathbf{G}_A(x'', x') - \mathbf{G}_A(x'', x=0)\mathcal{G}_A^{-1}\mathbf{G}_A(x=0, x')
\end{aligned} \tag{3.43}$$

but here we have taken the appropriate care about approaching from the left and right of $x = 0$ so that we know this result is only valid for $x'', x' \in A$ which is otherwise an involved process to disentangle from this result [119].

Though we are searching for the presence of a pole at the boundary, which would manifest as a peak in the density of states, observe that as $x'', x' \to 0$ we are left with only $\mathcal{G} = 0$ so that the Green's function can match with the vacuum Green's function in region B. Even beyond this limit, in the vicinity of a zero of $\mathcal{G}_A$ so that $\det \mathcal{G}_A \to 0$ the effect of $\mathcal{G}_B$ on the full Green's function will be essentially negligible. This highlights the possibility that one should explicitly *not* be searching for topological bound states on the edge of systems, but searching for the 'tail' from the pole they generate a short distance to either side of the edge.

We will return to the full Green's function for the pure 1D model when generalising in the next section to the fully 2D model as it aids in clarifying that $\mathcal{G}_A$ essentially takes the form of a T matrix and thus must start and end at the same co-ordinates.

3.4 Stitching 2D superconductor (containing magnetic impurities) onto bare 2D superconductor

As with other methods outlined in this section, our goal is to ascertain whether it makes sense to claim that a one dimensional topological transition has occurred when the one dimensional region is only a sub-system of the physical two dimensional system. Concretely, in a purely one

dimensional model we have seen above that we can derive a condition that says whether bound states form at the interface of two phases on tuning a continuous parameter, hence allowing us to identify the presence of a topological phase. In order to establish whether this can be achieved for a fully two dimensional system we return to the sets of equations for the composite Green's function G where $x'', x' \in A$:

$$\begin{aligned}\mathbf{G}(\mathbf{x}'', \mathbf{x}') = \mathbf{G}_A(\mathbf{x}'', \mathbf{x}') \\ - \frac{1}{2m} \int dy \, [\mathbf{G}_A(x'', x=0; y'', y) \, \partial_x \mathbf{G}(x=0, x'; y, y') \\ - (\partial_x \mathbf{G}_A(x'', x=0; y'', y)) \mathbf{G}(x=0, x'; y, y')] \end{aligned} \tag{3.44}$$

and for $x'' \in A$, $x' \in B$:

$$\begin{aligned}\mathbf{G}(\mathbf{x}'', \mathbf{x}') = \frac{1}{2m} \int dy \, [\mathbf{G}_B(x'', x=0; y'', y) \, \partial_x \mathbf{G}(x=0, x'; y, y') \\ - (\partial_x \mathbf{G}_B(x'', x=0; y'', y)) \mathbf{G}(x=0, x'; y, y')] \, . \end{aligned} \tag{3.45}$$

Previously we proceeded formally from here to derive the condition for bound states at a zero dimensional interface between two, one dimensional sub-systems. For higher dimensional examples, of which two dimensions is archetypical, the need to integrate over the one dimensional boundary means that one must, in principle, perform an operator inverse or invert an infinite matrix in order to find the conditions one is searching for. We will proceed instead by discretising this integral and will see that the conditions so derived are, as necessary, similar to those from the previous, purely formal derivation.

Focusing on the appropriate limits of $x'', x' \to 0^{\pm}$ we can rearrange the above equations as:

$$\begin{aligned}\int dy \left(\delta(y - y'') - \frac{1}{2m} \mathcal{G}'_A(y'', y) \right) \mathcal{G}(y, y') \\ = \int dy \, \delta(y - y'') \mathcal{G}_A(y, y') - \frac{1}{2m} \left[\mathcal{G}_A(y'', y) \, \backprime \mathcal{G}(y, y') \right] \end{aligned} \tag{3.46}$$

and

$$\begin{aligned}\int dy \left(\delta(y - y'') + \frac{1}{2m} \mathcal{G}'_B(y'', y) \right) \mathcal{G}(y, y') \\ = \int dy \, \frac{1}{2m} \left[\mathcal{G}_B(y'', y) \, \backprime \mathcal{G}(y, y') \right] . \end{aligned} \tag{3.47}$$

where it is clear that, if we could invert the operator $\int dy \left(\delta(y - y'') \pm \frac{1}{2m} \mathcal{G}_{A/B} \right)$ the derivation would proceed as previously. For clarity, rather than bringing such mathematical apparatus to bear, we will instead discretise these equations and simply deal with matrix equations:

$$\left(\delta_{i,k'} - \frac{1}{2m} (\mathcal{G}'_A)_{i,k'} \right) \mathcal{G}_{k',j} = \delta_{i,k} (G_A)_{k,j} - \frac{1}{2m} \left[(\mathcal{G}_A)_{i,k} \, \backprime \mathcal{G}_{k,j} \right] \tag{3.48}$$

and

$$\left(\delta_{i,k'} - \frac{1}{2m} (\mathcal{G}'_B)_{i,k'} \right) \mathcal{G}_{k',j} = \frac{1}{2m} \left[(\mathcal{G}_B)_{i,k} \, \backprime \mathcal{G}_{k,j} \right] \tag{3.49}$$

so that the derivation proceeds as formerly but with the additional matrix indices corresponding to y'', y', y which are necessary as, in principle, there could be bound states at any particular location along the interface. Following the discretised version of the derivation we will return to the continuum description of the results derived.

The resulting matrix equation on assuming continuity of the compound region Green's function G at some y location labelled by k', j is that:

$$(\mathcal{D}_A^{-1})_{k',i}\left(\delta_{i,k}(G_A)_{k,j} - \frac{1}{2m}\left[(\mathcal{G}_A)_{i,k}\,`\mathcal{G}_{k,j}\right]\right) = (\mathcal{D}_B^{-1})_{k',i}\frac{1}{2m}\left[(\mathcal{G}_B)_{i,k}\,`\mathcal{G}_{k,j}\right] \tag{3.50}$$

where $\mathcal{G}_A$ and $\mathcal{G}_B$ are defined in equation (3.34). For clarity during matrix manipulations we will for the moment suppress the discretised y indices and work with a full matrix notation. In this way we essentially repeat steps in our earlier derivation to find an expression for $`\mathcal{G}$ in terms of $\mathcal{G}_A$ and $\mathcal{G}_B$.

In this way, we rearrange for $`\mathcal{G}$ as before:

$$\mathcal{D}_A^{-1}G_A = \left(\mathcal{D}_A^{-1}\mathcal{G}_A + \mathcal{D}_B^{-1}\mathcal{G}_B\right)\frac{1}{2m}`\mathcal{G} \tag{3.51}$$

$$\frac{1}{2m}`\mathcal{G} = \left(\mathcal{D}_A^{-1}\mathcal{G}_A + \mathcal{D}_B^{-1}\mathcal{G}_B\right)^{-1}\mathcal{D}_A^{-1}G_A \tag{3.52}$$

so that the condition for a bound state labelled by at some location y is that

$$\left(\mathcal{D}_A^{-1}\mathcal{G}_A + \mathcal{D}_B^{-1}\mathcal{G}_B\right)^{-1}\mathcal{D}_A^{-1} \tag{3.53}$$

more simply written as

$$\left(\mathcal{G}_A + \mathcal{D}_A\mathcal{D}_B^{-1}\mathcal{G}_B\right)^{-1} \tag{3.54}$$

is divergent. We can rewrite this using the same reordering of derivatives as previously to arrive at a result that does not require the calculation of D_A^{-1} or D_B^{-1}:

$$\left(\mathcal{G}_A + \mathcal{D}_A\mathcal{G}_B\bar{\mathcal{D}}_B^{-1}\right)^{-1} = \bar{\mathcal{D}}_B\left(\mathcal{G}_A\bar{\mathcal{D}}_B + \mathcal{D}_A\mathcal{G}_B\right)^{-1} \tag{3.55}$$

by using different directional derivatives to define:

$$\bar{\mathcal{D}}_B \equiv 1 + \frac{1}{2m}`\mathcal{G}_B \tag{3.56}$$

compared to the original definition:

$$D_B \equiv 1 + \frac{1}{2m}\mathcal{G}'_B. \tag{3.57}$$

At this point we can return the discretised y indices. In order to do this correctly we note that this expression must begin and end at the same y label. One can see this by writing out the

full Green's function as for the 1D example previously whence we arrive at:

$$\begin{aligned}
&\mathbf{G}(\mathbf{x}'', \mathbf{x}') \\
&= \mathbf{G}_A(\mathbf{x}'', \mathbf{x}') - \int dy \mathbf{G}_A(\mathbf{x}''; x = 0, y) \left[\bar{\mathcal{D}}_B \left[\mathcal{G}_A \bar{\mathcal{D}}_B + \mathcal{D}_A \mathcal{G}_B\right]^{-1}\right](y, y) \mathbf{G}_A(x = 0, y; \mathbf{x}') \\
&+ \int dy \mathbf{G}'_A(\mathbf{x}''; x = 0, y) \left[\mathcal{D}_A^{-1} - \mathcal{D}_A^{-1} \mathcal{G}_A \bar{\mathcal{D}}_B \left[\mathcal{G}_A \bar{\mathcal{D}}_B + \mathcal{D}_A \mathcal{G}_B\right]^{-1}\right](y, y) \mathbf{G}_A(x = 0, y; \mathbf{x}') \quad (3.58)
\end{aligned}$$

where we know there must only be a single y integral[24] to take into account all possible intermediate points on the boundary as the boundary is a one dimensional line. As a result, the combination of operators which identifies poles at a particular y is, when fully labelled with discrete indices:

$$(\bar{\mathcal{D}}_B)_{i,j} \left(\mathcal{G}_A \bar{\mathcal{D}}_B + \mathcal{D}_A \mathcal{G}_B\right)^{-1}_{j,i}. \quad (3.59)$$

It should be noted that this general form makes it clear that, though the end points are the same, due to the inverted operator this expression takes into account all possible excursions to *all* y along the interface. In this way, the expression for the full Green's function in equation (3.58) accounts for all Feynman paths at arbitrary locations in region A, travelling to the interface and including all possible corrections due to excursions along the length of the interface and from leakage due to possible 'hops' into region B.

Based on this understanding it is satisfying to see that, if we take $\mathcal{G}_B \to 0$ to simulate stitching of region A onto the vacuum the expression for the presence of bound states reduces to whether

$$\begin{aligned}
(\bar{\mathcal{D}}_B)_{i,j} \left(\mathcal{G}_A \bar{\mathcal{D}}_B\right)^{-1}_{j,i} &= (\bar{\mathcal{D}}_B)_{i,j} (\bar{\mathcal{D}}_B)^{-1}_{j,m} (\mathcal{G}_A)^{-1}_{m,i} = \delta_{i,m} (\mathcal{G}_A)^{-1}_{m,i} \quad (3.60) \\
&= (\mathcal{G}_A)^{-1}_{i,i} \quad (3.61)
\end{aligned}$$

is singular. This is a deceptively simple result as clearly the matrix $(\mathcal{G}_A)_{m,k}$ is not diagonal but only the diagonal elements of its inverse are relevant when stitching onto the vacuum. Thus, for some particular y, one could write $(\mathcal{G}_A)^{-1}_{i',i'}$ out in terms of all elements of the matrix $(\mathcal{G}_A)_{m,k}$. However, in this particular system we have an expectation that if any bound states are present, they will be restricted to the vicinity of the magnetic chain at $y = 0$. We can thus consider the possibility that the matrix $(\mathcal{G}_A)^{-1}$ is divergent due to one of it's sub-blocks (describing only local behaviour) rather than the entire structure. This would mean that particular elements in the lengthy expression for $(\mathcal{G}_A)^{-1}_{i',i'}$ would dominate and we should focus our attention there.

One can put this argument more mathematically by considering that the condition for $(\mathcal{G}_A)^{-1}$ to diverge requires that:

$$\det\left((\mathcal{G}_A)_{m,k}\right) = 0 \quad (3.62)$$

where the determinant is taken over the y degrees of freedom in addition to the spin and Nambu indices. However, we can split off a sub-block at a particular chosen i', i' via a Schur

[24] By single integral we refer to integrals external to any additional integrals required to formally take the integral inverse if we had not proceeded with a discretised derivation.

decomposition[25] so that:

$$\det\left((\mathcal{G}_A)_{m,k}\right) = \det\left[(\mathcal{G}_A)_{i',i'}\right]\det\left[\mathcal{S}\right] \tag{3.63}$$

where $\mathcal{S}$ is a combination of the remaining block matrices for other y labels given by the decomposition. We thus arrive at the condition for a bound state not present in the bulk to exist at a given y:

$$\det\left((\mathcal{G}_A)_{i',i'}\right) = 0 \tag{3.64}$$

from which we can safely return to the continuum picture and instead consider the condition:

$$\det\left(\mathcal{G}_A(y_i = y_f = y)\right) = 0 \tag{3.65}$$

where now the determinant is over only the Nambu and spin degrees of freedom. Hence, there are two distinct possibilities: entirely localised bound states at a given y or a pole at all y and thus an extended state along the boundary. We do not expect this to be relevant here but it is certainly a positive characteristic as such a thing is possible in general if for example region A were a non-trivial topological insulator.

This formulation also highlights in the full Green's function in equation (3.58) that, even if there is a bound state at a certain y, for example $y = 0$, there are a multitude of possible paths which bypass it. Naturally, this does not occur in the 1D formulation due to dimensional restrictions.

In figure 16 we plot $\det(\mathcal{G}_A(y_i = y_f = y))$ for a selection of fixed y as a function of the unitless magnetic interaction strength C_m. Unlike for the 1D stitching example in figure 15 the condition $\det(\mathcal{G}_A) = 0$ is not fulfilled but there is a notable discontinuity at $C_m = \left((1 - k_m^2/k_F^2)^2 + \Delta^2/E_F^2\right)^{1/4}$. As the scale of this discontinuity depends heavily upon the upper limit of the (strictly speaking divergent) k_x integral required to calculate the real space Green's function we strongly suspect that proper application of a cutoff or accounting for the background will clarify whether there is a true bound state present.

For the most part, as this discontinuity seems to track $C_m = \left(\left(1 - k_m^2/k_F^2\right)^2 + \Delta^2/E_F^2\right)^{1/4}$, this condition seems to suggest that the localised description, ignoring the background effects (condition I above) is a reasonable description of the topological phases. However, even here we see this issue is not settled as figure 16 (right) for $y = 0$ shows that the function smoothly tends towards a value close to zero following the discontinuity. An understanding of this larger value and the non-trivial manner in which the system returns to being topologically trivial at large y may require conditions like II or III which take into account the long distance behaviour.

Though still not conclusive due to the aforementioned divergence, this method does provide a tool which is unambiguous: either there is a state present which is absent in the bulk, or there is not.

We find that, as physically expected, if one calculates the condition for large y, far away from the chain, there is no discontinuity and hence no possibility of bound states. The manner in which the discontinuity smoothly vanishes for larger y is non-trivial as one can see by comparing

[25] In fact this requires that the matrix $(\mathcal{G}_A)_{i',i'}$ be invertible but this issue can be resolved by considering how the matrix behaves for $\omega = 0 + i\eta$ as $\eta \to 0$ as usual.

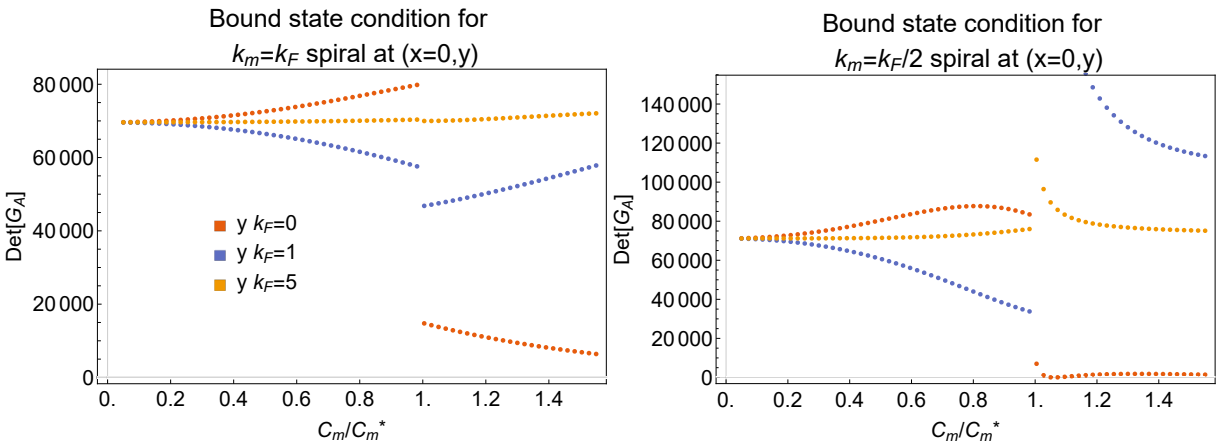

Figure 16: Condition for presence of bound states at $x = (0, y)$ by plotting $\det \mathcal{G}_A(y_i = y_f = y)$ evaluated at the location of the chain $y = 0$ and two remote locations from the chain $k_F y = 1$ and $k_F y = 5$ for spiral ordered chains with (left): $k_m = k_F$; (right): $k_m = k_F/2$ as a function of unitless magnetic interaction strength C_m, normalised to $C_m^\star = \left(\left(1 - k_m^2/k_F^2\right)^2 + \Delta^2/E_F^2\right)^{1/4}$. Though the condition $\det \mathcal{G}_A = 0$ is not fulfilled, there is a discontinuous change at $C_m/C_m^\star = 1$ (the condition for bulk bound states to cross zero energy at $k_x = 0$). This is seemingly not a complete picture of the physics present as can be seen for $y = 0$, $k_m = k_F/2$ where, following the discontinuity the function appears very close to zero at a larger C_m. This discontinuity is reduced at large y (excepting possibly at the critical C_m as in (right)). The lack of a true zero may be solvable by improved handling of large momentum states (the offset is currently highly cutoff dependent) or could be interpreted as the bound state becoming a resonance. $\tilde{\Delta} = 0.5$ here.

both its scale and *direction* between the left and right figures but is nonetheless necessarily smooth thus suggesting that whatever state is suddenly formed at a critical C_m, it spreads out along the interface with the vacuum until it is not distinguishable from the background.

It is worth noting that (though the results would not constitute a true pole) one would see a discontinuous and persistent change in the density of states as one tunes C_m through this discontinuity. This suggests that this method is a promising step towards a less ad hoc way to understand the presence of topological phases.

4 Coupled arrays of spiral ordered chains

Though isolated spiral ordered chains have the possibility of hosting already rather exotic states at boundaries, it is well worth considering how this picture may be extended. Rather than Majorana fermions is it possible to isolate more complicated anyonic states? It is entirely possible [8] to write down parafermionic (a type of anyon) extensions of the Kitaev chain toy model [6]. However, there is a caveat: strong interactions seem to be essential. Unlike for the special case of splitting each fermionic excitation into two Majoranas, the process of splitting states into three or more components maps to a strongly interacting model. This fact has complicated the process of finding physically realisable and theoretically treatable models which could host such states at the boundaries.

Fortunately, some progress has been made in this direction. In particular work by Klinovaja, Loss and Yacoby [45, 46, 120] explore the possibility that 1D proximitised, spin orbit coupled nanowires (individually expected to host Majorana end modes by analogy with the Kitaev chain toy model) can [26] produce $\mathbb{Z}_3$[27] parafermionic end states in the presence of electron-electron interactions. Though there is a requirement for fine tuning and the methods used are reliant on one dimensionality (bosonisation), this is plainly an interesting proof of concept.

The heuristic approach largely comes down to a search for methods which can split individual electrons into multiple parts. The most natural solution to this seems to be the phenomenon of fractionalisation observed in the presence of strong electron-electron interactions. As a result, when applied to states that are *already* split into pairs of Majorana fermions, the further splitting allows for one to move up the heirarchy of parafermionic states.

Further, this work has been extended [121] in related systems indicating the possibility that the states present in networks of 1D wires may be used to create anyonic states.

Similarly to the state of play with a single magnetic chain of adatoms, approaches to extending to these arrays tend to rely upon finding effective 1D models where the theoretical toolkit is arguably strongest. As we have seen in chapter 2 and 3, there are however highly nontrivial effects from the dimensional mismatch between the substrate and the 1D chains. In light of the fact that the mechanisms proposed to create higher order parafermions from the interaction of individual Majorana end states heavily relies upon communication via the substrate (largely Andreev scattering) one must properly take such effects into account.

Another benefit of the approach of building up networks of chains is the potential for self stabilisation. In the above approach careful fine tuning of the chemical potential is required. This is reminiscent of the comparison of 1D nanowire models to 1D models of proximitised magnetic chains where it was shown that the latter self stabilises without fine tuning due to the RKKY interaction. Though the RKKY interaction is weaker in 2D, it could be that relatively well separated chains, interacting with effectively 1D RKKY interactions along their lengths could still be stabilised. Though the substrate superconductor is two dimensional, the lower dimensionality of the impurity lines could be expected to generate an effectively 1D RKKY

[26] When paired together with either aligned or anti-aligned spin orbit coupling and the chemical potential is tuned.

[27] In this notation Majoranas are $\mathbb{Z}_2$, so this is the next most complicated and splits each Dirac fermion into three components.

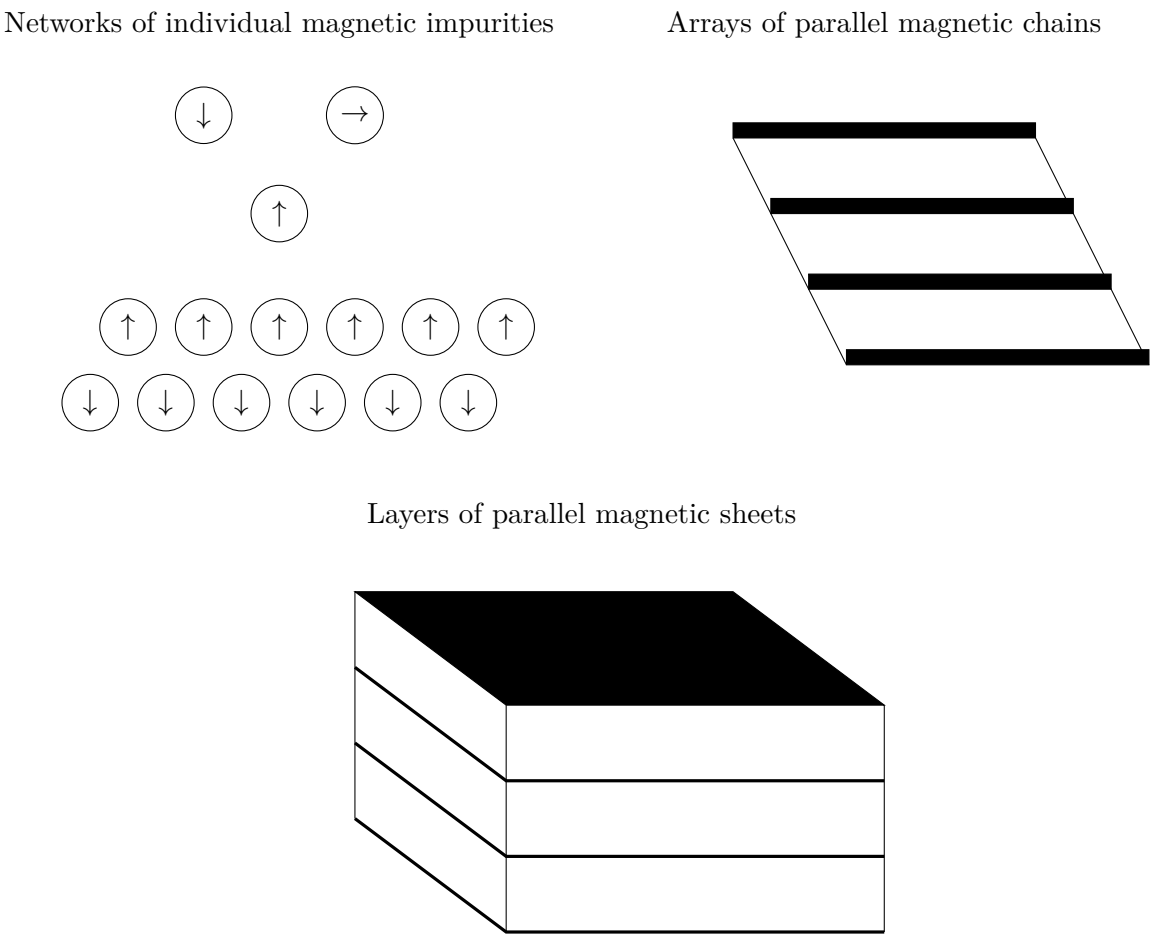

Figure 17: Diagrams depicting example scenarios that can be approached using the exact solution built up in this chapter. (top, left): arbitrarily located networks of magnetic moments with arbitrary orientation embedded in two or three dimensional substrates; (top, right): Arrays of parallel chains of dense spiral ordered magnetic moments embedded in two dimensional substrates (which we focus on in this work) or three dimensional substrates; (bottom): layered heterostructures of thin films of magnetic material stacked throughout a three dimensional bulk material.

interaction along their length (as this direction is the only one which can allow for the non-local spin flipping required for the RKKY interaction). This picture has thus has the potential for all of the benefits of 1D whilst also allowing for extension into 2D and engineering of anyonic states.

Interestingly, we will see that the Green's function formalism for multiple chains can equally well be applied to: arbitrarily placed individual magnetic impurities, parallel networks of chains or parallel sheets of magnetic material embedded in higher dimensional substrates as given as examples in figure 17. Though we will focus exclusively upon the embedding of chains of magnetic adatoms we note that the ability to place arbitrary networks of individual magnetic impurities is of further intrinsic interest. Such a formalism applied to this example allows for study of adatom chains with finite spacing, with zig-zag patterns or even glassy or disordered arrangements, all taking into account *every* possible interaction in a relatively straightforward

way, without restrictive assumptions.

Quite aside from the above considerations of engineering more complicated states, due to the potentially long range influence of the bound states around each chain, we should also investigate whether the band structures are modified substantially by the presence of even relatively distant chains of impurities. This is potentially of great experimental relevance as some methods for growing magnetic adatom chains rely upon effectively melting a central block and allowing multiple chains to form as strands from there [40].

In what follows we will devote great effort to writing the N chain Green's function in terms of the T matrices found in the solutions of the $N-1$, $N-2$, etc. solutions. Aside from the insight this provides there is, however, an additional benefit: computationally, one is required only to invert and multiply 4×4 matrices to calculate the full Green's function of a system with numerous impurity chains. If the procedure could be continued properly to three chains and beyond, this could lead to computational scaling to solve an N impurity problem in linear time and memory rather than exponential memory as a brute force numerical approach requires. This also compares favourably to direct numerical diagonalisation of the Dyson equation as all of the heavy lifting required to diagonalise $4N \times 4N$ matrices would instead be performed by the repeated, formal resummation encoding all possible Feynman paths.

We will proceed to develop an exact, analytical treatment for two, spiral ordered magnetic chains and decouple the solution so that it is written entirely in terms of the solution to each individual chain. A similar, though necessarily more involved, treatment is applied for three chains where the decoupling is incomplete but still illustrative for a potential solution for N such chains.

We explore the modifications made to the band structures derived in chapter 2 due to coupling to a second and third chain for the case where all chains are ferromagnetic [28]. The changes made can be traced to their physical origin due to the decoupling described above.

4.1 Two chains by resummation

We can generalise our approach of exact resummation to cases where there are multiple impurities, or chains depending on geometry, in a surprisingly simple manner. There are two ways of approaching this calculation, both of which make different features clear. As a result, we will display both.

We will proceed initially with a formal resummation, which is seemingly the quickest and least ambiguous way to arrive at the solution, and follow by literally enumerating all possible diagrammatic terms and grouping them for summation. The latter has minimal benefit in this case, except to show precisely what happens in the second level of resummation which will occur during the calculation. This second method is essential to understand cases with 3 or more impurities so must be discussed here before moving on to those, significantly more complicated, cases.

[28] The formalism is not restricted ferromagnetic chains; we explore them first to build up an understanding as in chapter 2 for a single chain.

The Dyson equation we must solve in this case is:

$$G_{if} = g_{if} + g_{iA}V_A G_{Af} + g_{iB}V_B G_{Bf} \tag{4.1}$$

where i, f refer to the real space dependence of the Green's function, so that in the case of two localised impurities the problem would be entirely in real space; for two chains would be in mixed real and momentum space and so on to higher dimensions. Writing the equation in this form allows us the freedom to solve all such problems simultaneously. The positions A and B are the positions of impurity scatters which have strengths V_A and V_B which could be magnetic or scalar though naturally we will intend to view them as magnetic and spiral ordered in some fashion.

Let us re-write this equation in a matrix notation:

$$G_{if} = g_{if} + \begin{pmatrix} g_{iA}V_A & 0 \\ 0 & g_{iB}V_B \end{pmatrix} \begin{pmatrix} G_{Af} \\ G_{Bf} \end{pmatrix} \tag{4.2}$$

$$= g_{if} + \begin{pmatrix} g_{iA}V_A & 0 \\ 0 & g_{iB}V_B \end{pmatrix} \mathbf{G}_F \tag{4.3}$$

such that we can solve the problem by calculating $\mathbf{G}_F$. By substitution of A and B for i into this equation, we are left with a set of equations:

$$\begin{pmatrix} G_{Af} \\ G_{Bf} \end{pmatrix} = \begin{pmatrix} g_{Af} \\ g_{Bf} \end{pmatrix} + \begin{pmatrix} g_{AA}V_A & g_{AB}V_B \\ g_{BA}V_A & g_{BB}V_B \end{pmatrix} \begin{pmatrix} G_{Af} \\ G_{Bf} \end{pmatrix} \tag{4.4}$$

or

$$\mathbf{G}_f = \mathbf{g}_f + \begin{pmatrix} g_{AA}V_A & g_{AB}V_B \\ g_{BA}V_A & g_{BB}V_B \end{pmatrix} \mathbf{G}_f. \tag{4.5}$$

This equation can be written to give us an expression for $\mathbf{G}_F$

$$\mathbf{G}_f = \Gamma^{(2)}\mathbf{g}_f \tag{4.6}$$

$$= \begin{pmatrix} 1 - g_{AA}V_A & -g_{AB}V_B \\ -g_{BA}V_A & 1 - g_{BB}V_B \end{pmatrix}^{-1} \mathbf{g}_f \tag{4.7}$$

which, if one can invert this block matrix, allows an exact solution of the problem.

Fortunately, one can invert *any* block matrix

$$\begin{aligned} \begin{pmatrix} A & B \\ C & D \end{pmatrix}^{-1} &= \begin{pmatrix} A^{-1}\left(1 + B(D - CA^{-1}B)^{-1}CA^{-1}\right) & -A^{-1}B(D - CA^{-1}B)^{-1} \\ -(D - CA^{-1}B)^{-1}CA^{-1} & (D - CA^{-1}B)^{-1} \end{pmatrix} \\ &= \begin{pmatrix} (A - BD^{-1}C)^{-1} & -(A - BD^{-1}C)^{-1}BD^{-1} \\ -D^{-1}C(A - BD^{-1}C)^{-1} & D^{-1}\left(1 + C(A - BD^{-1}C)^{-1}BD^{-1}\right) \end{pmatrix} \end{aligned} \tag{4.8}$$

so long as A and D are square and invertible, and the combination $D - CA^{-1}B$ is invertible (which guarantees that $A - BD^{-1}C$ is invertible) and that all matrices are of commensurate size

such that the entire block matrix is square [122, 123]. Though the proof that the off diagonal elements are equivalent is trivial, the proof for on diagonal ones is slightly more involved. The decomposition in this manner is what will allow us to extract single chain/impurity terms and thus write the solution in an elegant, physically relevant form. To achieve this form, we will use the most expanded forms for on diagonal elements of α in the above equations.

To illustrate how the second level of resummation occurs in this calculation we will focus on $\Gamma^{(2)}_{AB}$ for now. The resultant definition allows great simplification in all other terms and is most clear in the off diagonal components of $\Gamma^{(2)}$. Using the above definitions we can write $\Gamma^{(2)}_{AB}$ as:

$$(1 - g_{AA}V_A)^{-1} g_{AB} V_B \left[1 - g_{BB}V_B - g_{BA}V_A(1 - g_{AA}V_A)^{-1} g_{AB}V_B\right]^{-1} \tag{4.9}$$

which we can manipulate and group together any instances of $T_A = V_A \left[1 - g_{AA}V_A\right]^{-1}$ or $T_B = V_B \left[1 - g_{BB}V_B\right]^{-1}$, the one chain T matrices:

$$\begin{aligned} \Gamma^{(2)}_{AB} &= V_A^{-1} T_A \left[(1 - g_{BB}V_B)V_B^{-1} g_{AB}^{-1} - g_{BA}T_A\right]^{-1} \\ &= V_A^{-1} T_A \left[(g_{AB}T_B)^{-1} - g_{BA}T_A\right]^{-1} \end{aligned} \tag{4.10}$$

We can then write this in a form of a string of single chain/impurity operators followed by a term of the form $(1 - O)^{-1}$ (which we will interpret as a T matrix) for some string of operators O:

$$\Gamma^{(2)}_{AB} = V_A^{-1} T_A g_{AB} T_B \left[1 - g_{BA}T_A g_{AB} T_B\right]^{-1} \equiv V_A^{-1} T_{AB}. \tag{4.11}$$

In the final line we have defined the *two* chain T matrix T_{AB}. In this way we can interpret T_{AB} as all possible interaction events which begin at the first chain, interact an arbitrary number of times, travels to the second chain, interacts an arbitrary number of times, but then moves back and forth between the chains themselves, repeating this entire process an arbitrary number of times. This is what is meant by "second level of resummation": the already resummed single impurity T matrices T_A and T_B are the resummed again into new, two chain operators T_{AB} and T_{BA}. We will see that using just these four operators one can write the solution in a very elegant manner.

Proceeding to calculate $\Gamma^{(2)}_{BB}$ the solution is readily split into two parts: $(1 - g_{BB}V_B)^{-1} = V_B^{-1} T_B$ (the single chain contribution due to chain/impurity B) and:

$$\begin{aligned} (1 - g_{BB}V_B)^{-1} g_{BA} V_A \left[1 - g_{AA}V_A - g_{AB}V_B(1 - g_{B}BV_B)^{-1} g_{BA}V_A\right]^{-1} \\ \times g_{AB}V_B(1 - g_{BB}V_B)^{-1}. \end{aligned} \tag{4.12}$$

As for the $\Gamma^{(2)}_{AB}$ terms we write this in terms of single chain T matrices T_A and T_B:

$$\begin{aligned}
&V_B^{-1}T_B g_{BA}V_A\left[1-g_{AA}V_A-g_{AB}T_B g_{BA}V_A\right]^{-1}g_{AB}T_B\\
&=V_B^{-1}T_B\left[(1-g_{AA}V_A)V_A^{-1}g_{BA}^{-1}-g_{AB}T_B g_{BA}V_A\right]^{-1}g_{AB}T_B\\
&=V_B^{-1}T_B\left[T_A^{-1}g_{BA}^{-1}-g_{AB}T_B g_{BA}V_A\right]^{-1}g_{AB}T_B\\
&=V_B^{-1}T_B g_{BA}T_A g_{AB}T_B\left[1-g_{BA}T_A g_{AB}T_B\right]^{-1}
\end{aligned} \tag{4.13}$$

but now can take the additional step of writing this in terms of the two chain T matrix T_{AB} so that we are left with:

$$V_B^{-1}T_B g_{BA}T_{AB} \tag{4.14}$$

which, from our previous definition of T_{AB}, is all possible combinations of bounces back and forth between chains A and B, given that the contribution must begin and end at chain B.

The calculation proceeds in much the same way for the remaining components of $\Gamma^{(2)}$, so that we are finally left with:

$$\Gamma^{(2)}=\begin{pmatrix}V_A^{-1}T_A(1+g_{AB}T_{BA}) & V_A^{-1}T_{AB}\\ V_B^{-1}T_{BA} & V_B^{-1}T_B(1+g_{BA}T_{AB})\end{pmatrix} \tag{4.15}$$

where it is worth noting that we could also have known the second row of $\Gamma^{(2)}$ in advance by permuting indices in the upper row, as the solution must be symmetric with respect to the transformation $A\leftrightarrow B$.

Hence, the full Green's function can be written:

$$G^{(2)}_{if}=g_{if}+\begin{pmatrix}g_{iA}\\ g_{iB}\end{pmatrix}\begin{pmatrix}T_A(1+g_{AB}T_{BA}) & T_{AB}\\ T_{BA} & T_B(1+g_{BA}T_{AB})\end{pmatrix}\begin{pmatrix}g_{Af}\\ g_{Bf}\end{pmatrix}. \tag{4.16}$$

where:

$$T_\alpha=\left[V_\alpha^{-1}-g_{\alpha\alpha}\right]^{-1}=V_\alpha\left[1-g_{\alpha\alpha}V_\alpha\right]^{-1} \tag{4.17}$$

$$T_{\alpha\beta}=T_\alpha g_{\alpha\beta}T_\beta\left[1-g_{\beta\alpha}T_\alpha g_{\alpha\beta}T_\beta\right]^{-1} \tag{4.18}$$

where α, β refer to the location of the chain in question (A or B in this case). As shorthand it can be helpful to define a term which takes into account all on-site corrections due to the second chain:

$$T^\beta_{\alpha\alpha}=T_\alpha\left(1+g_{\alpha\beta}T_{\beta\alpha}\right)=T_\alpha\left[1-g_{\alpha\beta}T_\beta g_{\beta\alpha}T_\alpha\right]^{-1} \tag{4.19}$$

where the second equality can be proven using Woodbury matrix identities.

4.1.1 Subgap bands - two ferromagnetic chains with parallel magnetisation

Though the above formalism can be applied quite generally to pairs of spiral ordered magnetic chains, we will proceed to add each ingredient individually to thoroughly investigate differences from independent chains and to ascertain novel features and their precise origins. Even with the simplest case of two ferromagnetic chains there is the possibility of a non perturbatively accessible feature from this treatment as a sort of "non local" version of the same mechanism that forms Shiba states around single impurities [124–126]. If one were to imagine constructing dense arrays of chains, such that many such chains would be within the coherence length of the underlying superconductor then the emergence of such states could not be neglected. To be more concrete, coherence lengths in superconductors are typically $10 - 10^3$nm in bulk [127], where 2D films tend to be at the lower end of this range [84, 85]. This can be compared to k_F^{-1} which is typically of the order 1nm [127]. It thus seems that arrays in the dense limit should, aside from other experimental obstacles, be constructible. In the limit of well separated chains such states dissapear in some manner as the two chains become essentially uncoupled. We will investigate the manner in which they dissapear and thus seek to understand at what range we can consider multiple chains as well separated. We will investigate whether such states are possible and what effect they have on the bands known to be present due to the interactions of bands of Shiba states and the background superconductor as discussed in previous sections. From the point of view of engineering novel topological states, it is desirable to understand the mechanisms for lines of impurities to communicate via the background superconductor and hence, even in the absence of ends on which topological bound states could form, we can see precisely how they would be able to interact through the interplay of the interactions present.

In addition to initially focusing on ferromagnetic chains with parallel magnetisations, we will initially restrict our attention to the spectral properties directly beneath chain A or chain B rather than locations between them. This is entirely reasonable as, even if we were to imagine the situation with bound states forming from interactions between the chains, we would still need to understand what is happening on each chain individually to be able to disentangle the origin of states. Additionally, we can make the magnetic interaction strength V_m equal on both chains for now, i.e. assume that the adatom chains are of the same type.

In figure 18 we plot the momentum resolved density of states beneath chain A from terms in the full Green's function that begin and end at chain A ($T^B_{AA} = T_A\left(1 + g_{AB}T_{BA}\right)$ where $T_{BA} = T_B g_{BA} T_A \left[1 - g_{AB}T_B g_{BA} T_A\right]^{-1}$) and terms that link chains A and B ($T_{AB} = T_A g_{AB} T_B \times$ $\left[1 - g_{BA}T_A g_{AB} T_B\right]^{-1}$). The latter allow for spectral weight to move towards or away from chain A as defined in equations (4.18) and (4.19). Splitting in this way is convenient as these are the terms which will actually contribute at the chain in question. The same is true at chain B. Even for small separation l, terms such as T_{BB} do not meaningfully contribute to sub gap band structures beneath chain A and vice versa.

Figures 18(b-g) display such contributions where the chains are separated by $1, 10, 20, 30, 40, 50$ and 100 times k_F^{-1}. Pleasingly, some expected features are observable such as, for small separation, states beneath each chain act as though in the presence of a single chain with $V_m \to 2V_m$ as in figure 18(a), conversely, for $l \gg k_F^{-1}$ both chains decouple and we see sub gap bands approaching those from a single chain as shown in figure 18(i) for reference.

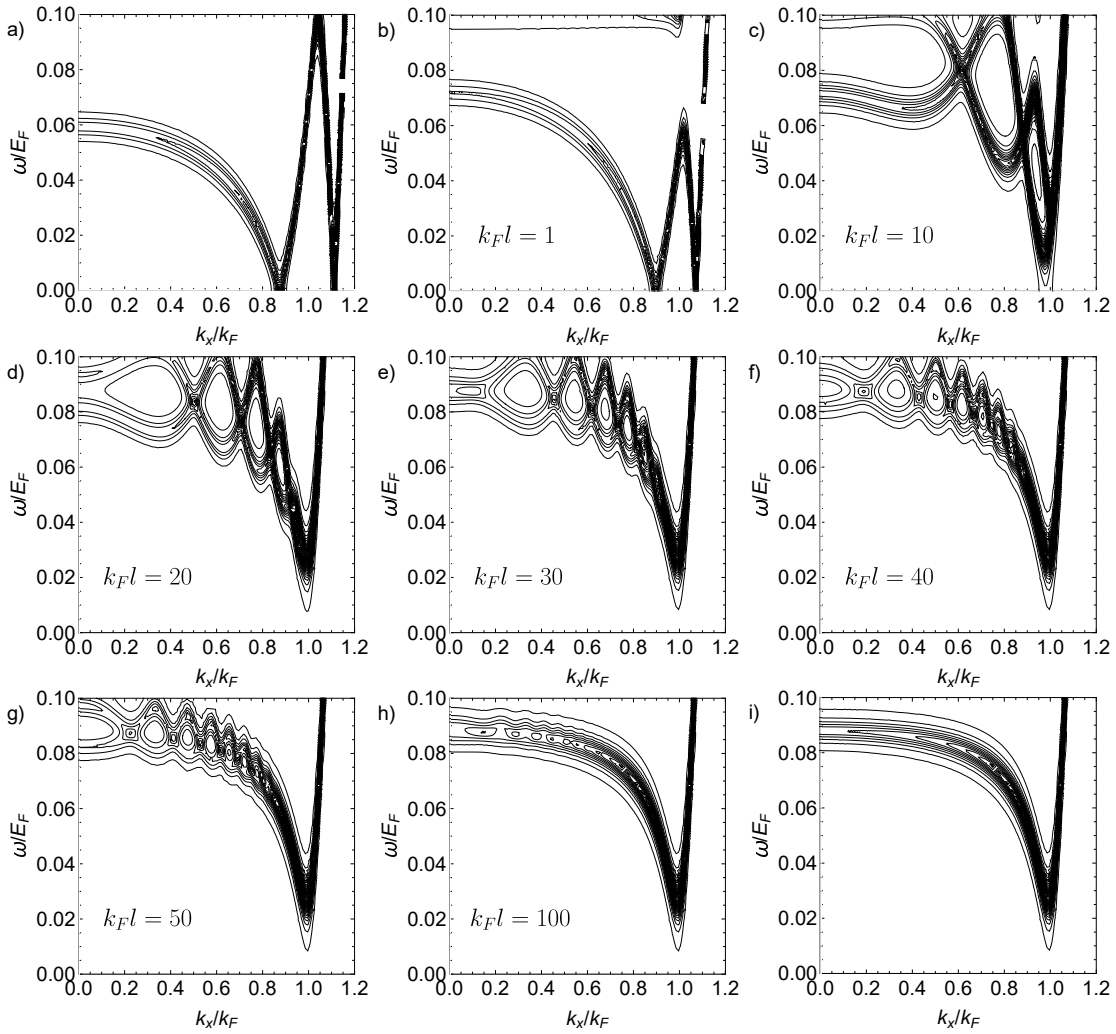

Figure 18: Momentum resolved density of states beneath: (a) a single chain with $V_m = 2V_m^*$ where $V_m^* = 0.8\tilde{\Delta}^{1/2}$ is chosen simply to display the transition from sub-gap bands which close near $k_x = k_F$ to those which close at $k_x = 0$ as l is tuned. In (b-h) the momentum resolved density of states beneath chain A with two chains present separated by l increasing through from left to right as $1, 10, 20, 30, 40, 50, 100$ times k_F and figure (i) a single chain with $V_m = V_m^*$. Comparing figures (a) and (i) to (b-h) it is clear this formalism can smoothly describe all situations from essentially uncoupled chains up to and including the case where they are close enough to be essentially atop one another. For the particular V_m chosen this also describes a smooth transition from a case before any gap closures in figure (i) to one beyond the gap closure at $k_x = 0$ in (a). In all figures $\Delta = 0.1E_F$.

More interesting are the oscillations which arise at intermediate separation l. These appear identically beneath chain A and B and, due to the way in which this formalism decouples the origin of particular terms, it is possible to see precisely why they form. Figure 19 displays the contributions to the momentum resolved density of states beneath chain A due to the on site correction to chain A due to chain B: $T_{AA}^{B} = T_A g_{AB} T_{BA}$ (middle row) and T_{AB} (bottom row). The combined result summing all terms contributing at chain A is reproduced in the top row. Note that, due to this not being the full density of states, some regions are negative (displayed in blue shades). These negative regions in T_{AA} always exactly coincide with the location of the subgap band from T_A, hence cancelling out these bands for most, if not all, $k_x < k_F$. For large l it is clear that $T_{AB} \to 0$ and $T_{BA} \to 0$ as the factors $g_{AB} = g_{BA} \to 0$ so that one returns to single, independent chains described by T_A and T_B. Similarly, for very small l one must approach a description in terms of a single chain T matrix with $V_m \to 2V_m$ so that it is clear there must be an exact cancellation of the T matrix for a single chain. For intermediate l, it is less clear how the cancellation comes about. The single chain poles are clearly absent for a wide range of k_x in figures 19 (a-c) where the momentum resolved density of states for the full Green's function beneath chain A is plotted. One can see that there are negative regions in figures 19 (d-i) where we plot only the contributions to the full Green's function containing either T_{BA} or T_{AB}. It seems that these negative regions exactly cancel the single chain poles for a broad range of k_x. This is particularly striking in figure 19 (d) where $k_F l = 1$ so that the effect of the second chain's presence is to completely cancel the poles present and replace them with those for $C_m \to 2C_m$. Simultaneous to this cancellation, two bands, oscillating around the original band with increasing frequency for larger l are formed, presumably to lift the increasingly possible degeneracy as the two chains are brought into proximity.

In this manner, the effect of T_{AA} terms is to completely destroy the original T_A terms and replace them with an oscillating version.

It is unfortunately not clear how to extract this destructive result, but it seems to suggest that $T_{AA} \to -T_A$ and $T_{BA} \to T_A$ with doubled V_m if $l \to 0$. It is seems that a proof of this requires calculation of the location of the poles themselves as it does not obviously follow from the matrix structure alone.

These oscillations are reminiscent of the finite size effects which one sees in numerical studies of such systems. This is reasonable as we have introduced a new length scale l, but crucially the 'boundaries' for the standing waves which cause such effects are here not at featureless system edges but necessarily cause spin flips. Though not precisely analogous, one can see what sort of effect this has using the numerical model described in chapter 2 by comparing hard wall against periodic boundary conditions in the direction perpendicular to the magnetic adatom chain. In figure 9 there are clearly oscillations to the band structure for both periodic (red dots) and open (black dots) boundary conditions. By using periodic boundary conditions the boundaries are effectively two chains of magnetic impurities separated in this plot by 70 lattice sites, compared to hard wall boundary conditions which are effectively two infinitely strong lines of *scalar* impurities separated by the same distance. We do not observe the more rich, double helix like structure seen in our analytic solution in the periodic condition, merely what could be either a phase shift due to different boundary conditions. A more comprehensive

numerical attempt to reproduce these results, especially to investigate stability with respect to self consistency, is necessary.

Further still, one can see that T_{BA} terms modify the resulting bands from the T_{AA} terms. Even for $l \gg k_F^{-1}$ ($l = 50k_F^{-1}$ as plotted in figure 19(i)) this roughly has the effect of moving some spectral weight from the upper edge of the novel oscillating band to the lower energy side. In the limit of $l \approx k_F^{-1}$ we see that this is the mechanism by which the bands are transformed into those with $V_m \to 2V_m$ as would be expected for $l \to 0$ in this case. It seems clear that something quite drastic is happening between $l = k_F^{-1}$ and $l = 10k_F^{-1}$ as at some point the bands must twist or 'break' to undergo the change they do.

Hence, it would appear that T_{BA} terms have the effect of modifying not the original band structure, but the modified band structure due to the presence of a second chain, in such a way that when the second chain is brought into close proximity the system is essentially indistinguishable from a single chain with a larger V_m.

The particular nature and ability to separate out the origin of these mechanisms within this formalism seems particularly interesting as, unlike when considering only a single chain, here it is necessary to understand not just the poles of the various T matrices but also at least some of what is happening in the spectral function as clearly sometimes poles exactly coincide, but cancel due to a difference in sign. It seems clear that the only place this sign change can come from is the spectral function or, equivalently, zeros in the wave function.

Continuing the systematic study of this system, we tune V_m through the locations at which gap closures should happen: V_{m,k_1} (figure 20) where the gap would close at $k_x = k_F$ for a single, isolated chain and V_{m,k_0} (figure 21) for where the gap would close at $k_x = 0$. In the plots shown, a quite large separation $l = 40k_F^{-1}$ is chosen to illustrate that the effects of the oscillations in the bands are robust for relatively well separated chains. As described previously, bands beneath both chains A and B both continue to now oscillate around the band structure expected of single, well isolated chains. This does however, have a rather severe consequence for gap closures. For well isolated chains it was found that the only locations where the gap could close were $k_x = 0$ or $k_x = k_F$. Here, however, it seems clear that one can close the gap at essentially arbitrary k_x. Though conventionally not expected to have an effect topologically due to these points not necessarily being at time reversal invariant momenta, it does raise the question of how the phase diagram must be changed. In particular, looking at figure 21 one can see that the single state at $k_x = 0$ has been split. Hence, on tuning V_m, recalling that states at negative k_x must also be counted, the number of crossings seems to go from an even (figure 21(a)) to odd (figure 21(b)), *back* to even in (figure 21(c)) and back to odd again in (figure 21(d)). If similar behaviour is observed for $k_m \neq 0$ this could lead to an additional transition to a trivial state before settling in a non-trivial state for larger V_m and thus potential access to richer topological phases.

The period and dependence of the oscillations with Δ and with closeness to the gap centre bears further study as one can see in figure 20 where the amplitude of the oscillations grow as the gap centre is approached. This could be due to the changing effective coherence length. As l is tuned, it seems as though new 'nodes' develop from around $k_x = k_F$ but, as the amplitude of the oscillations reduce massively in this region it is not clear how to tell what is happening.

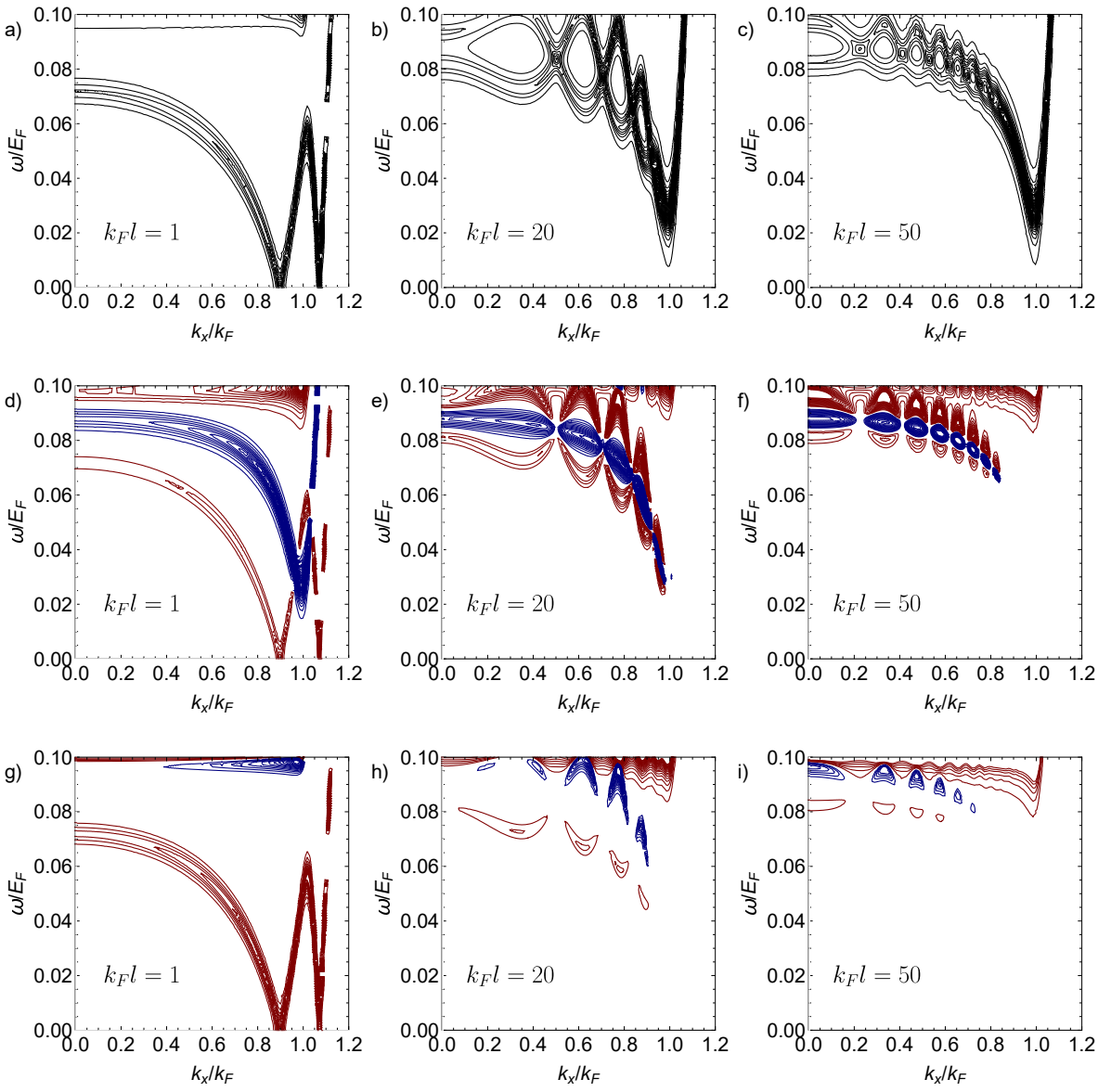

Figure 19: Momentum resolved density of states beneath A chain due to (a-c): all terms combined; (d-f): due to terms like $T_A g_{AB} T_{BA}$ (the new two chain terms which return to site A) and (g-i): terms like T_{AB} (new two chain terms that do not end at A). Separation l increases through figures from left to right in each row as $1, 20$ and 50 times k_F. Blue curves are negative regions in the contour plots, red regions are positive. The spread is due to the quite large imaginary offset used in the retarded Green's function to make features clear. Note in particular that summing the two bottom plots in each row (plus the contribution due to the single chain alone) produces the top plots. This demonstrates the exact cancellation of the single chain band structure for a wide range of k_x.

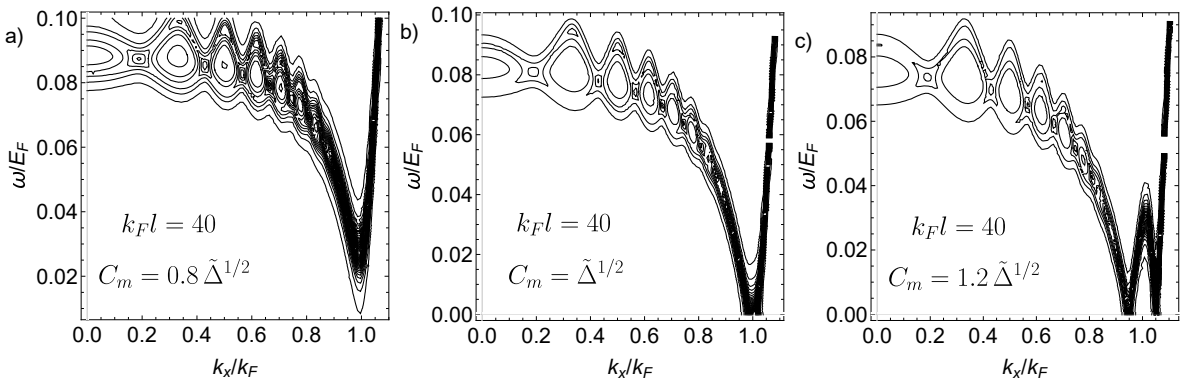

Figure 20: Momentum resolved density of states beneath A chain, magnetic interaction strength V_m increasing through figures tuning through k_1 closing point $C_m = \tilde{\Delta}^{1/2}$ observed in separated chains. Chain separation is fixed at $k_F l = 40$ in all figures. With increasing magnetic interaction strength bands are moved rigidly with little qualitative change and k_1 closing point seems essentially unchanged. Here $\tilde{\Delta} = 0.1$.

4.1.2 Two identical chains, with non parallel magnetisation

To investigate the origin of the oscillations which arise when two chains are brought into proximity, I decided to include the possibility of a phase shift into one of the chains so that their magnetisation is no longer parallel. For spiral textures this has the effect of applying a phase shift to the spiral of one chain relative to the other. There are multiple ways to do this, including modifying the unitary transform used to unwind the spirals, but the simplest way can be seen by looking at the magnetic interaction term after the regular unitary transform described in equation (2.18) which for two chains would look like:

$$H_{int} = V_A \int dk_x \left(\tilde{c}^\dagger_{k_x,y_A,\uparrow} \tilde{c}_{k_x,y_A,\downarrow} + \tilde{c}^\dagger_{k_x,y_A,\downarrow} \tilde{c}_{k_x,y_A,\uparrow} \right) \tag{4.20}$$

$$+ V_B \int dk_x \left(e^{i\phi} \tilde{c}^\dagger_{k_x,y_B,\uparrow} \tilde{c}_{k_x,y_B,\downarrow} + e^{-i\phi} \tilde{c}^\dagger_{k_x,y_B,\downarrow} \tilde{c}_{k_x,y_B,\uparrow} \right) \tag{4.21}$$

where V_A and V_B are the magnetic interactions strengths for chains A and B respectively, ϕ is the phase shift given to chain B relative to chain A and the spiral order has been simultaneously removed from both chains by unitary transform as it was assumed to have the same wave vector k_m. [29] Here we can simply redefine $V_B \to V_B \exp^{i\phi}$ such that V_B is allowed to become complex but not change in size. With this modification we are able to investigate whether introducing a phase shift between the chains causes the oscillations present due to chain proximity to move. This would prove interesting as a potential pumping mechanism for topological charge if the phase in one chain were controllable by external field for example.

Additionally, the freedom to tune the phase shift of the second chain allows exploration of a situation which, in our continuum model, is otherwise very difficult: antiferromagnetically aligned chains. This is particularly of interest as, if one can tune the phase shift in one chain, and the chains are in close proximity, one would be able to freely tune into and out of proposed topological phases. This can be understood simply as, when the phase shift $\phi = 0$, we have

[29] If the chains have *different* k_m then we must unwind a two dimensional magnetisation structure which is significantly more involved.

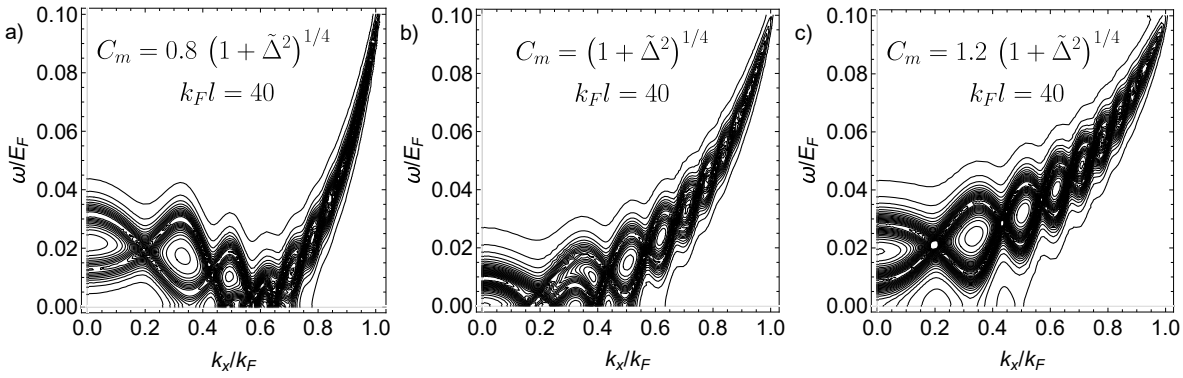

Figure 21: Momentum resolved density of states beneath A chain, magnetic interaction strength V_m increasing through figures tuning through k_0 closing point observed in separated chains. Chain separation is fixed at $k_F l = 40$ in all figures. In contrast to figure 20 there are qualitative differences despite bands still moving rigidly with increasing magnetic interaction strength. Due to the oscillations for small k_x induced by the second chain there are multiple gap closures at different k_x. In (b) in particular one can observe a feature around $k_x/k_F = 0.3$ which seems to be due to oscillations at negative ω crossing over into positive ω. Here $\tilde{\Delta} = 0.1$.

seen the system behaved as though there were a single chain with $V_m \to 2V_m$, however, for $\phi = \pi$, antiferromagnetically aligned chains, they must behave as though $V_m \to 0$ and hence have no sub gap bands. Hence, if V_m is such that the system is in a topological phase, there must be some ϕ such that the system can be tuned out of it, controllably. In figures 22 and 23 one can see the momentum resolved density of states beneath chains A and B respectively. Note in particular that, despite the introduction of a relative phase shift between the chains, both chains have identical sub gap band structure. This is unsurprising as, when essentially decoupled, the chains are identical up to a choice of spin-(x, y) axis and are thus the same up to a global phase. It is then quite interesting to see how the sub-gap bands evolve as the separation is reduced and this global phase can no longer be trivially removed.

Figure 24 displays the results for a phase shift of $\phi = \pi/2$, both to explore the transition between ferromagnetism and antiferromagnetism and to see what effect having an effectively imaginary V_m has on the system. In this case one is in a situation where V_A points consistently in the x direction whereas V_B is entirely in the y direction, hence the interactions are in some sense "orthogonal". One can see that, for small $l \approx 1$ both chains behave as though they are a single chain with $V_m \to \sqrt{2}V_m$ as one might expect from a direct superposition of the two chains of magnetic moments.

This superposition harks back to our expectation for chains with non-parallel magnetisations: if they are far apart then the phase makes no difference, acting as a choice of spin basis but as the chains are brought into proximity there are interesting mixing effects as the spin projections combine. We might also expect that mixing of bands depending on spin projections would mean hybridisation is most effective when spins are all parallel which is indeed the case: for small l, parallel spins look like a single chain with $2V_m$, antiparallel completely cancel out so $V_m = 0$ and orthogonal spins give somewhere smoothly between ($V_m = \sqrt{2}V_m$) if both original chains had a magnetic interaction strength of V_m.

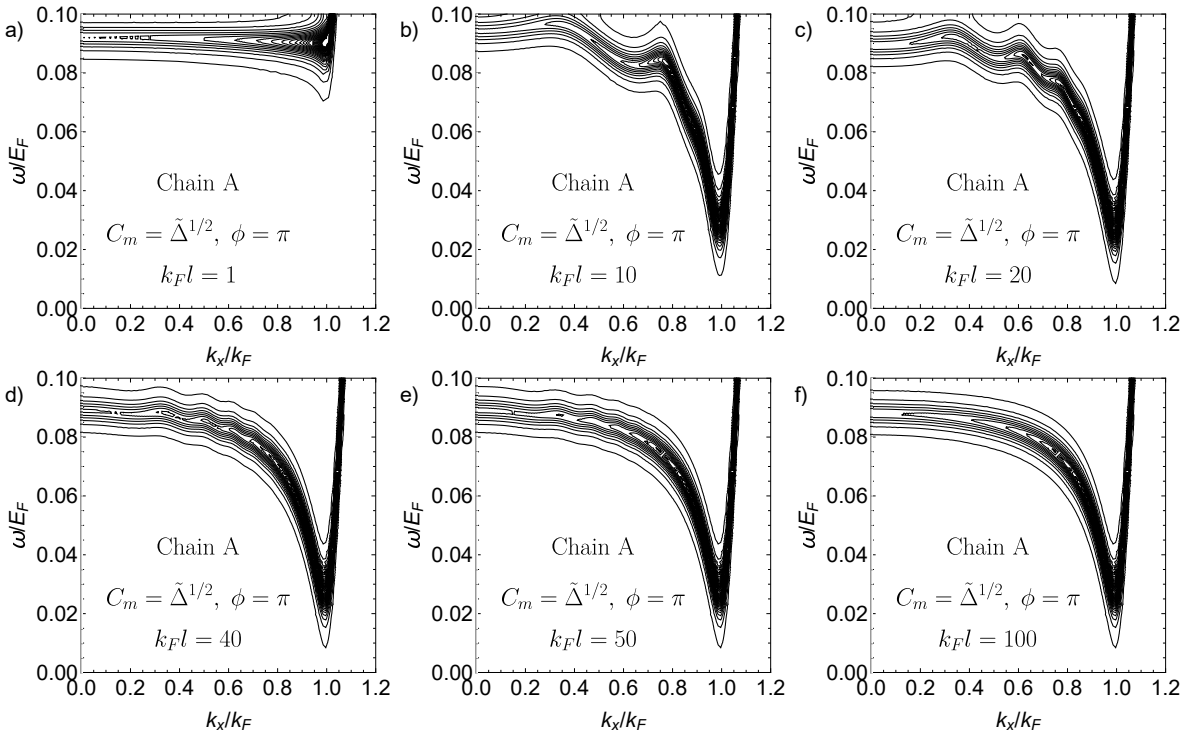

Figure 22: Momentum resolved density of states beneath A chain for antiferromagnetically aligned pairs of chains ($\phi = \pi$) at fixed $C_m = 0.8\tilde{\Delta}^{1/2}$ from all terms contributing there. Separation l increases through figures (a-f) as $1, 10, 20, 40, 50, 100$ times k_F^{-1}. $\tilde{\Delta} = 0.5$ here.

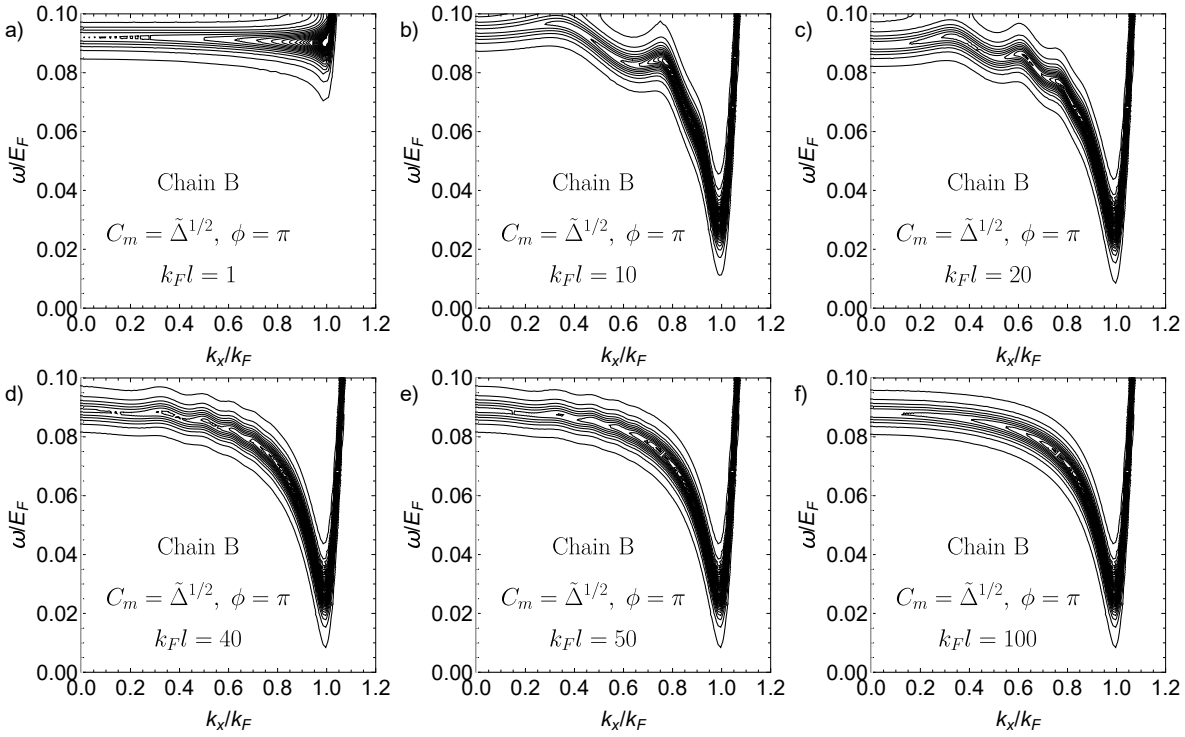

Figure 23: Momentum resolved density of states beneath B chain for antiferromagnetically aligned pairs of chains ($\phi = \pi$) at fixed $C_m = 0.8\tilde{\Delta}^{1/2}$ from all terms contributing there. Separation l increases through figures (a-f) as $1, 10, 20, 40, 50, 100$ times k_F^{-1}. Comparing to figure 23, all cases appear identical despite the antiferromagnetic alignment of magnetic moments. $\tilde{\Delta} = 0.5$ here.

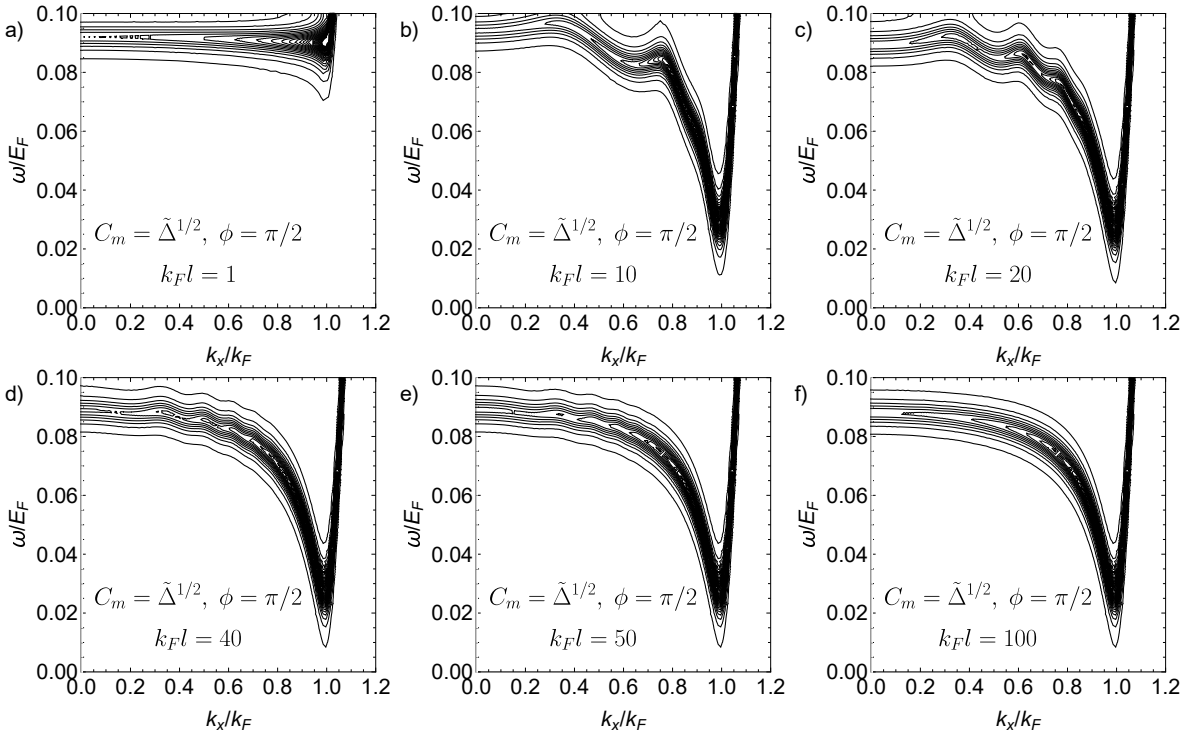

Figure 24: Momentum resolved density of states beneath A chain for phase shifted chains with $\phi = \pi/2$ at fixed $C_m = 0.8\tilde{\Delta}^{1/2}$ from all terms contributing there. Separation l increases through figures (a-f) as $1, 10, 20, 40, 50, 100$ times k_F^{-1}. $\tilde{\Delta} = 0.5$ here.

With this in mind further investigation into the spin components of these structures seems warranted.

Though this solution allows for a great deal of further investigation (including coupled spiral ordered chains which are potential analogues of systems with parafermionic edge states [45, 46]) we will move on to develop the formalism further. In doing so we are able to provide further outlook for future calculations.

4.2 Three chains by nested resummation

As a stepping stone to understanding networks of potentially strongly interacting chains of magnetic adatoms, an understanding of the case of three chains can be considered something of a milestone. With three chains one can, for the first time, construct a nearest neighbour hopping model (chains $i-1$, i and $i+1$) and enclose two dimensional regions (and hence have multiple points of chain intersection). Unfortunately, unlike with two chains, we will see that it is significantly more involved to understand classes of interactions involving three chains in terms of interactions involving two or one chain.

To best illustrate the latter point, consider how one would go about enumerating all possible interaction terms. To begin, we will consider the case of two chains labelled by their locations A and B. We will see in this case that it is possible to enumerate all possible diagrams and hence write down the same solution as found in the previous chapter.

If we define the one chain T matrices for chains A and B as T_A and T_B:

$$\text{(A)} \equiv T_A = V_A \left(1 - g_{AA} V_A\right)^{-1} \tag{4.22}$$

$$\text{(B)} \equiv T_B = V_B \left(1 - g_{BB} V_B\right)^{-1} \tag{4.23}$$

which take into account all possible couplings [30] which can occur at each of the chains A and B individually. We can then begin to enumerate the possible interchain couplings using these as building blocks. There are four possible classes of diagram as the interaction terms can 1) begin at A, end at A, 2) begin at A, end at B, 3) begin at B, end at A or finally 4) begin at B and end at B. We will begin looking at case 2 and will see that all other cases follow from this.

The smallest possible unit which begins at A, taking into account all couplings there, then takes an excursion to B, similarly taking into account couplings there, is

$$\text{(A)}\!-\!\text{(B)} = T_A g_{AB} T_B \tag{4.24}$$

from which the only possible way to add further corrections and satisfy the boundary conditions of returning to B is by duplicating the same pattern:

$$\begin{aligned}
&\text{(A)}\!-\!\text{(B)} + \text{(A)}\!-\!\text{(B)}\!-\!\text{(A)}\!-\!\text{(B)} + \ldots \\
&= \text{(A)}\!-\!\text{(B)} \sum_{n=0}^{\infty} \left(-\text{(A)}\!-\!\text{(B)} \right)^n \\
&= T_A g_{AB} T_B \left(1 - g_{BA} T_A g_{AB} T_B\right)^{-1} \\
&\equiv T_{AB} \equiv \text{(AB)}
\end{aligned} \tag{4.25}$$

where we have resummed the repeating motif in the usual way. In this way we define a new T matrix T_{AB} which describes all possible two chain interactions, starting at A and ending at B.

For clarity, we can see this operator takes into account all possible couplings by trying to add further combinations of single or double chain operators from our growing dictionary: T_A, T_B and now T_{AB}. We cannot append a T_A because this would not obey our boundary conditions, we cannot append a T_B as all diagrams end with a T_B anyway which would lead to overcounting and similarly, we cannot append T_{AB} to T_{AB} as this clearly doesn't lead to any new diagrams.

We can naturally proceed to case 3), terms beginning at B and ending at A by permuting labels $A \to B$ so that:

[30] Unlike for the single impurity/chain case where the interaction V_m appears directly in the Hamiltonian, here we are directly considering corrections to the self energy that couple the different chains by considering all the possible Feynman paths scattering for example on chain A, travelling to chain B, scattering there and then returning. By finding a way to package all such corrections for all such paths into a T matrix structure we can formally solve the equations of motion and study the poles to identify novel bound states.

$$T_B g_{BA} T_A \left(1 - g_{AB} T_B g_{BA} T_A\right)^{-1} \equiv T_{BA} \equiv \text{(BA)} \tag{4.26}$$

so that it remains only to establish cases 1) and 4) where the initial and final positions are either at A or B. We can construct the possible diagrams for these cases using only the dictionary of operators we have already developed. Prepending T_{AB} with T_B gives:

$$\begin{aligned} &\text{(B)–(A)–(B)} + \text{(B)–(A)–(B)–(A)–(B)} + \ldots \\ &= T_B g_{BA} T_A g_{AB} T_B \left(1 - g_{BA} T_A g_{AB} T_B\right)^{-1} \\ &\equiv T_B g_{BA} T_{AB} \equiv \text{(B)–(AB)} \end{aligned} \tag{4.27}$$

where once again we cannot form any new types of diagram due to boundary conditions or repetitions of operators leading to overcounting. It is worth noting that appending T_A may seem like a new class of diagram, but this can just be re written as $T_{BA} - T_B g_{BA} T_A$.

As with case 3) we can find the final boundary condition case by permuting indices $A \to B$ to give:

$$T_A g_{AB} T_B g_{BA} T_A \left(1 - g_{AB} T_B g_{BA} T_A\right)^{-1} \equiv T_A g_{AB} T_{BA} \equiv \text{(A)–(BA)} \tag{4.28}$$

so that we can separate any one or two chain couplings out when writing the full Green's function.

However, if we attempt to do this for three chain couplings, between chains A, B and C, and try to follow the same enumeration scheme we encounter a new problem. Having built up a dictionary from all one and two chain interaction terms, we would like to construct three chain coupling terms. Our dictionary as it stands is:

$$\begin{aligned} &\text{(A)} \quad \text{(B)} \quad \text{(C)} \\ &\text{(AB)} \quad \text{(AC)} \quad \text{(BA)} \quad \text{(BC)} \quad \text{(CA)} \quad \text{(CB)} \end{aligned} \tag{4.29}$$

from which we can try to construct for example T_{ABC}, the three chain operator that starts at A, ends at C but takes into account all possible couplings with B as well as A and C. We would like to identify repeating motifs in order to resum operators into this new type of operator. For two chain operators, we found that motifs of length two were all that was required. Here we

start with motifs of length three of which there are six:

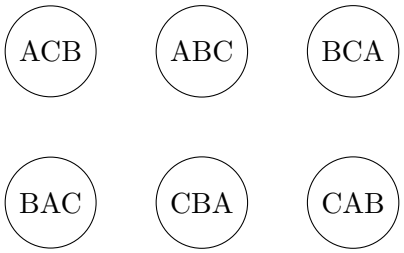

(4.30)

which, unlike for two chain operators, does not close off our ability to define new operators. If we append T_C then we define a new motif of length four which can repeat. We could also append T_C followed by any of the now 9 out of 15 elements of our dictionary of operators which do not begin C or BC and define a new operator of length four or five which could then repeat arbitrarily. This will be restricted slightly further by not allowing repetitions which would lead to reducible diagrams but not enough to allow the same "closure" observed for one or two chain interactions.

This issue can perhaps be illustrated best by considering a slightly different method for enumerating classes of diagrams. In trying to move from chain A to C we could clearly go:

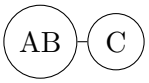

(4.31)

but now, being at chain C, we are unconstrained by boundary conditions from addition of further interactions with chains A and B so that we can build up patterns like:

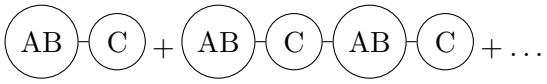

(4.32)

which contains motifs of arbitrary length due to the already resummed two chain T_{AB}. These strings can themselves then be resummed into new classes of operator which *do* take into account three chain interactions properly but which are of a fundamentally different class than one and two chain operator strings due to this additional level of resummation required.

This same process can be repeated for any insertion of operators that does not lead to reducible diagrams, leaving us with, for interactions starting and ending at chain A:

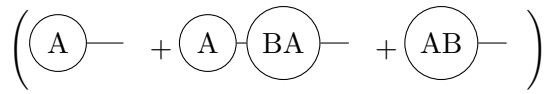

(4.33)

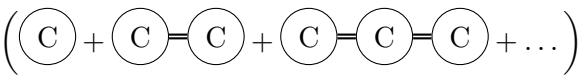

(4.34)

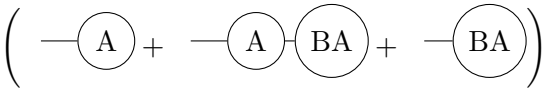

(4.35)

where renormalised double line propagators are defined as:

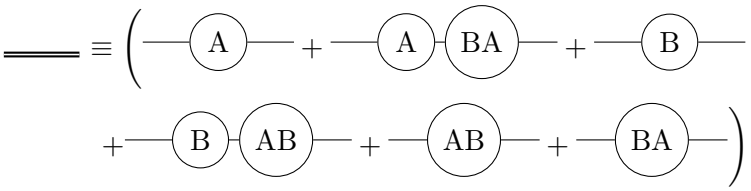

(4.36)

(4.37)

which contains any possible one or two chain coupling with chains A or B. We can thus formally resum the strings containing chain C to define:

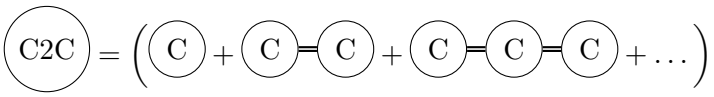

(4.38)

which contains all one, two and three chain coupling terms, starting and ending at C.

This process of enumerating possible couplings illustrates that three chain coupling terms are of a different nature than those of lower chain terms. Hence, at this point we demonstrate what seems to be a hierarchy of resummation required on adding additional coupling locations. Where the single chain requires one to consider any number of individual local magnetic interactions, the two chain case requires one to consider infinite strings of the potentially infinite numbers of couplings at each of the two interaction sites. Now we see that on addition of a third chain even this is not sufficient and we require infinite strings build from any number of interactions between already twice resummed interaction locations.

It is not clear whether, on adding further chains, this pattern of increasingly recursive resummation continues or if the level of complexity stops at this point due to the fact that we are already considering arbitrary length strings of interactions of any kind. We will argue in what follows that the solution to the three chain case in terms of cycles suggests the latter is sufficiently general.

With the generality of the formalism as presented (where the various Green's functions could describe individual impurities, chains or sheets and how they must interact) it is noteworthy that this quite drastic increase in complexity occurs first when one has three impurities. In that case, for the first time, one can easily imagine structures forming vertices of two dimensional shapes. The simple example of three magnetic impurities at vertices of an equilateral triangle make the necessity of the above additional resummation clear: if the impurities are close enough to interact with each other at the two chain level then one also needs to consider *cycles* of interaction and the resulting feedback this would have on each of the individual vertex locations. Such arrangements should be considered carefully when considering the physics of chains of adatoms in close proximity. In all of our considerations we have built up continuum models of chains of magnetic impurities. Though these do take into account arbitrary ranged interactions along each chain, the loss of a finite adatom separation may mean that there is some additional physics possible beyond that we observe if the two chains are staggered in real space. As a particular example to illustrate this issue consider two chains separated by a distance l, both with the same finite adatom spacing a_h but offset by half a lattice spacing. As the distance $l \to 0$ this should smoothly correspond to a chain with lattice spacing $a_h/2$, a phenomenon the continuum

approach is not equipped to deal with as implemented here (as a_h and $a_h/2$ are both zero in this limit).

Though the above calculation illustrates the crucial additional step required to solve this problem, it is manifestly not symmetric with respect to which chains are initially present and which is 'added'. As a result, it is not obvious how to decouple the novel physics due to the addition of a third interaction term and that which is just a relabelled copy of the one or two chain results derived previously. It is possible to proceed using the same formalism as applied to solve the two chain case (and is in fact numerically advisable to do so as we will see the expressions become quite lengthy) but again, it is awkward to decouple all of the two chain terms by symmetrising the result.

Instead, we approach the problem in a manner constructed entirely to provide a solution which treats each of the three interaction locations in the same fashion and is thus manifestly symmetric. We will, in three separate steps, firstly isolate the background superconducting term, then the one chain terms T_A, T_B, T_C, then finally isolate all possible two chain terms: T_{AB}, T_{AC}, T_{BA}, T_{BC}, T_{CA}, T_{CB} so that everything which remains must be due to "three chain" terms. As previously noted in using matrix notation to solve the two chain model, having solved any given row in the matrix notation, all others must follow from permuting indices if the final solution is expected to be symmetric. In that case this was not of major concern, here we will see that it is essential to avoid treating the new impurity at C as special. Unfortunately, due to the fact that all possible interactions are not of the same form up to permutations (unlike for the two chain case) we will see that this method does not completely decouple all two chain terms. Nonetheless, it is illustrative as it is possible to see the suggestive form which the nearly decoupled three chain terms take.

Starting from the Dyson equation for three interaction locations, written in matrix notation:

$$G^{(3)}_{if} = g_{if} + \begin{pmatrix} g_{iA}V_A & 0 & 0 \\ 0 & g_{iB}V_B & 0 \\ 0 & 0 & g_{iC}V_C \end{pmatrix} \begin{pmatrix} G^{(3)}_{Af} \\ G^{(3)}_{Bf} \\ G^{(3)}_{Cf} \end{pmatrix} \tag{4.39}$$

which can be solved by solving the set of incidental equations:

$$\begin{pmatrix} G^{(3)}_{Af} \\ G^{(3)}_{Bf} \\ G^{(3)}_{Cf} \end{pmatrix} = \begin{pmatrix} g_{Af} \\ g_{Bf} \\ g_{Cf} \end{pmatrix} + \begin{pmatrix} g_{AA}V_A & g_{AB}V_B & g_{AC}V_C \\ g_{BA}V_A & g_{BB}V_B & g_{BC}V_C \\ g_{CA}V_A & g_{CB}V_B & g_{CC}V_C \end{pmatrix} \begin{pmatrix} G^{(3)}_{Af} \\ G^{(3)}_{Bf} \\ G^{(3)}_{Cf} \end{pmatrix}. \tag{4.40}$$

Note that in writing this set of three equations out, we have separated out the background term. This can be thought of as a "zeroth" level to the process which follows which is straightforward here as the background is considered to be essentially fixed.

Each of the three equations so defined can be solved formally so that each line now depends

exclusively on the terms in the other two. This defines a new set of three equations:

$$G^{(3)}_{Af} = V_A^{-1} T_A \left(g_{Af} + g_{AB} V_B G^{(3)}_{Bf} + g_{AC} V_C G^{(3)}_{Cf} \right) \tag{4.41}$$

$$G^{(3)}_{Bf} = V_B^{-1} T_B \left(g_{Bf} + g_{BA} V_A G^{(3)}_{Af} + g_{BC} V_C G^{(3)}_{Cf} \right) \tag{4.42}$$

$$G^{(3)}_{Cf} = V_C^{-1} T_C \left(g_{Cf} + g_{CA} V_A G^{(3)}_{Af} + g_{CB} V_B G^{(3)}_{Bf} \right) \tag{4.43}$$

which explicitly has the "one chain" terms T_α isolated. Notice that the manifest relation by permutation of indices is still present: two of these equations can be related to the first by permuting indices. None of the interaction locations are treated differently. To maintain this property in a manner that will lead to a useful solution, we would like to generate a new set of three equations from these so that each equation now depends on *one* other function.

Unfortunately, there are two ways to achieve this, up to permutation of indices: one generates a set of equations so that G_{Af} depends only on G_{Bf}, G_{Bf} on G_{Cf} and G_{Cf} on G_{Af} so that our solution clearly does not treat any site differently to any other and the other by swapping the order of any pair of sites. The former is achieved by substituting equation (4.43) into (4.41), (4.41) into (4.42) and (4.42) into (4.43) and solving for G_{Af}, G_{Bf}, G_{Cf} formally respectively, the latter by the same method but swapping any single pair of substitutions.

The result of the first is a new set of three equations:

$$\begin{pmatrix} V_A G^{(3)}_{Af} \\ V_B G^{(3)}_{Bf} \\ V_C G^{(3)}_{Cf} \end{pmatrix} = \begin{pmatrix} T_A \left(1 + g_{AC} T_{CA}\right) & 0 & T_{AC} \\ T_{BA} & T_B \left(1 + g_{BA} T_{AB}\right) & 0 \\ 0 & T_{CB} & T_C \left(1 + g_{CB} T_{BC}\right) \end{pmatrix} \begin{pmatrix} g_{Af} \\ g_{Bf} \\ g_{Cf} \end{pmatrix} + \\ \begin{pmatrix} 0 & T^C_{AA} \left(g_{AB} + g_{AC} T_C g_{CB}\right) V_B & 0 \\ 0 & 0 & T^A_{BB} \left(g_{BC} + g_{BA} T_A g_{AC}\right) V_C \\ T^B_{CC} \left(g_{CA} + g_{CB} T_C g_{BA}\right) V_A & 0 & 0 \end{pmatrix} \begin{pmatrix} G^{(3)}_{Af} \\ G^{(3)}_{Bf} \\ G^{(3)}_{Cf} \end{pmatrix} \tag{4.44}$$

where we have used the shorthand notation $T^\beta_{\alpha\alpha} = T_\alpha \left[1 - g_{\alpha\beta} T_\beta g_{\beta\alpha} T_\alpha\right]^{-1} = T_\alpha \left(1 + g_{\alpha\beta} T_{\beta\alpha}\right)$. Note that this final equality follows from either the Woodbury matrix identities used in the solution to the two chain model or by noting that they account for different ways of counting up available Feynman paths: in the former case one adds up all interactions at a given site including those present already at that location, in the latter one explicitly splits off the on site (single chain) and off site (two chain) couplings. We have explicitly used this relationship to split off the two chain couplings above from which it is clear that we are have accounted for all one chain terms but are missing half of the two chain terms.

These are accounted for by the second set of three equations which can be generated from equations (4.41), (4.42) and (4.43), resulting instead in:

$$\begin{pmatrix} V_A G^{(3)}_{Af} \\ V_B G^{(3)}_{Bf} \\ V_C G^{(3)}_{Cf} \end{pmatrix} = \begin{pmatrix} T_A\left(1+g_{AB}T_{BA}\right) & T_{AB} & 0 \\ 0 & T_B\left(1+g_{BC}T_{CB}\right) & T_{BC} \\ T_{CA} & 0 & T_C\left(1+g_{CA}T_{AC}\right) \end{pmatrix} \begin{pmatrix} g_{Af} \\ g_{Bf} \\ g_{Cf} \end{pmatrix} + \\ \begin{pmatrix} 0 & 0 & T^B_{AA}\left(g_{AC}+g_{AB}T_B g_{BC}\right)V_C \\ T^C_{BB}\left(g_{BA}+g_{BC}T_C g_{CA}\right)V_A & 0 & 0 \\ 0 & T^A_{CC}\left(g_{CB}+g_{CA}T_C g_{AB}\right)V_B & 0 \end{pmatrix} \begin{pmatrix} G^{(3)}_{Af} \\ G^{(3)}_{Bf} \\ G^{(3)}_{Cf} \end{pmatrix} \tag{4.45}$$

which contains the other half of the two chain terms, an additional copy of the one chain terms and encodes another set of what will become three chain terms γ in what follows.

It is unclear how to combine this set of six equations in a useful manner so in what follows we content ourselves with disentangling only half of the two chain terms and hence only defining half of the possible three chain 'paths'. As the two sets of equations are related by swapping any single pair of indices it is then clear what their solution would provide, even if it is not so obvious how to combine them to fully disentangle the results.

Moving forward with the solution of the first set of three equations note that, by construction, each row is related to the others by permutation of indices so that we solve the G_{Af} equation in terms of the others:

$$\begin{aligned} V_A G_{Af} = &\left[1 - T^C_{AA}\left(g_{AB}+g_{AC}T_C g_{CB}\right)T^A_{BB}\left(g_{BC}+g_{BA}T_A g_{AC}\right)T^B_{CC}\left(g_{CA}+g_{CB}T_B g_{BA}\right)\right]^{-1} \\ &\times \Big[\left(T^C_{AA}+\left(T^C_{AA}g_{AB}+T_{AC}g_{CB}\right)T_{BA}\right)g_{Af} \\ &\quad + \left(T^C_{AA}g_{AB}+T_{AC}g_{CB}\right)\left(T^A_{BB}+\left(T^A_{BB}g_{BC}+T_{BA}g_{AC}\right)T_{CB}\right)g_{Bf} \\ &\quad + \left(T_{AC}+\left(T^C_{AA}g_{AB}+T_{AC}g_{CB}\right)\left(T^A_{BB}g_{BC}+T_{BA}g_{AC}\right)T^B_{CC}\right)g_{Cf}\Big]. \end{aligned} \tag{4.46}$$

Though lengthy, there is clearly a pattern present in this expression. This is made even more clear on noting that, for example, $T^C_{AA}\left(g_{AB}+g_{AC}T_C g_{CB}\right) = \left(T^C_{AA}g_{AB}+T_{AC}g_{CB}\right)$. Though unfortunately not the same as defining a new set of T matrices we can define operators γ to identify repeating motifs which make the pattern more transparent and re write as:

$$\begin{aligned} V_A G_{Af} = &\left[1-\gamma_{ACB}\gamma_{BAC}\gamma_{CBA}\right]^{-1}\Big[\left(T^C_{AA}+\left(T^C_{AA}g_{AB}+T_{AC}g_{CB}\right)T_{BA}\right)g_{Af} + \\ &+\left(\gamma_{ACB}\left(T^A_{BB}+\left(T^A_{BB}g_{BC}+T_{BA}g_{AC}\right)T_{CB}\right)\right)g_{Bf}+\left(T_{AC}+\gamma_{ACB}\gamma_{BAC}T^B_{CC}\right)g_{Cf}\Big]. \end{aligned} \tag{4.47}$$

The operators $\gamma_{\alpha\beta\delta}$ describe all possible paths from a points where interactions can occur α to δ travelling via β taking into account all possible one or two chain couplings.

By construction, the equations for G_{Bf} and G_{Cf} are related to the one for G_{Af} by permutation of indices.

$$V_A G_{Af} = \left[1 - \gamma_{ACB}\gamma_{BAC}\gamma_{CBA}\right]^{-1} \Big(\left(T^C_{AA} + \gamma_{ACB} T_{BA}\right) g_{Af} + \gamma_{ACB} \left(T^A_{BB} + \gamma_{BAC} T_{CB}\right) g_{Bf} + \left(\gamma_{ACB}\gamma_{BAC} T^B_{CC} + T_{AC}\right) g_{Cf} \Big) \tag{4.48}$$

$$G^{(3)}_{if} = g_{if} + \begin{pmatrix} g_{iA} \\ g_{iB} \\ g_{iC} \end{pmatrix} \left\{ \begin{pmatrix} T_A & 0 & 0 \\ 0 & T_B & 0 \\ 0 & 0 & T_C \end{pmatrix} + \begin{pmatrix} T_A g_{AC} T_{CA} & 0 & T_{AC} \\ T_{BA} & T_B g_{BA} T_{AB} & 0 \\ 0 & T_{CB} & T_C g_{CB} T_{BC} \end{pmatrix} + \begin{pmatrix} AA & AB & AC \\ BA & BB & BC \\ CA & CB & CC \end{pmatrix} \right\} \begin{pmatrix} g_{Af} \\ g_{Bf} \\ g_{Cf} \end{pmatrix} \tag{4.49}$$

where the terms in the final matrix are related by permuting indices from the following instances:

$$AA = \gamma_{ACB} \left(\gamma_{BAC}\gamma_{CBA} \left[1 - \gamma_{ACB}\gamma_{BAC}\gamma_{CBA}\right]^{-1} T^C_{AA} + \left[1 - \gamma_{BAC}\gamma_{CBA}\gamma_{ACB}\right]^{-1} T_{BA} \right) \tag{4.50}$$

$$BA = \gamma_{BAC}\gamma_{CBA} \left(\left[1 - \gamma_{ACB}\gamma_{BAC}\gamma_{CBA}\right]^{-1} T^C_{AA} + \gamma_{ACB} \left[1 - \gamma_{BAC}\gamma_{CBA}\gamma_{ACB}\right]^{-1} T_{BA} \right) \tag{4.51}$$

$$CA = \gamma_{CBA} \left(\left[1 - \gamma_{ACB}\gamma_{BAC}\gamma_{CBA}\right]^{-1} T^C_{AA} + \gamma_{ACB} \left[1 - \gamma_{BAC}\gamma_{CBA}\gamma_{ACB}\right]^{-1} T_{BA} \right). \tag{4.52}$$

Though a great deal of progress has been made in separating out terms, this is still not the complete picture. All of the single chain operators T_α have been successfully extracted but, though all of the possible $T_{\alpha\beta}$ are present, some of the two chain terms are still bound up inside the complicated recursive structure capturing the three chain couplings.

This has occurred as there are terms which our treatment thus far was completely unable to produce.

However, despite not being a complete decomposition, the form of this solution does suggest how one should think about the Feynman paths in order to resum them: add up all closed loop paths as repeating motifs. With this interpretation the single impurity solution requires no excursions, a two impurity solution requires consideration of lines connecting all points and three impurities requires consideration of arbitrary repeating cycles around all possible triangular paths (which in turn are constructed from edges (two impurity solutions) and vertices (one impurity solutions)). Though it is not clear if this holds generally, this suggests the rather pleasing ansatz for N impurities that one must consider all paths consisting of all shapes up to and including N-gons. Such a solution is unfortunately beyond our grasp at this stage.

5 Conclusions and outlook

We have developed a robust and readily extendible Green's function formalism with the scope to describe arrays of impurity chains. Additionally, we are able to stitch together solutions and thus investigate the interface between heterostructures of such arrays, here shown with the example of stitching onto the vacuum.

More specifically, in chapter two, we investigated dense chains of spiral ordered magnetic adatoms atop 2D superconducting substrates and found the mismatched dimensionality plays a crucial role in understanding the physics. We are able to write down an exact, analytic solution for the case of a ferromagnetic chain and thus trace the novel sub-gap structure to a combination of influence of the background superconductor and hybridised bands of YSR states. One finds that physical quantities governing gap closures of potential topological relevance are renormalised and found strong suggestions that there is a fundamental difference between the physics of sparse and dense chains. We find remarkable agreement with numerical models and show that our conclusions are unchanged by consideration of a self consistent gap, so long as the bulk gap (far from the chain) is comparable.

In chapter three, we outlined the ambiguity in defining a topological index due to the dimensional mismatch of the substrate and effective band structure. Though in sparse chain models one can clearly separate an effective 1D model we show that there are at least two such models one can sensibly write down which give contradictory topological phase diagrams over a wide range of parameters. In an attempt to address this issue we develop a formalism to write down the Green's function with a boundary from the Green's function without boundaries and are able to find simple conditions which decide whether there will be topological bound states at the system edge. We find excellent agreement when this formalism is applied to purely 1D systems and an inconclusive but certainly discontinuous change in behaviour at the expected transition point using the 2D model developed in chapter 2.

In chapter four we extend our solution of a single magnetic spiral to that of pairs and triplets of magnetic spirals exactly, taking into account all possible interactions from the (classical) magnetic moments. The same solution is noted to be usable to investigate networks of individual magnetic adatoms or sheets of magnetic material though we here use it only to study parallel chains. We investigate the sub gap bands beneath each chain from the solution to the two chain model for parallel and non parallel ferromagnetic chains. For parallel magnetisation, one finds a cancellation of the solution to the one chain model and development of an oscillating band structure which is visible even for chains very well separated compared to system length scales such as $1/k_F$. By writing the solution to the two chain model in terms of the T matrices for the one chain model, resummed a second time, we are able to ascertain which terms cause this cancellation. For non parallel magnetisation we look at anti-ferromagnetically coupled chains and chains with orthogonal magnetisation and find that coupled chain's magnetisations add in a vectorial fashion when in close proximity compared to $1/k_F$. The solution for triplets of chains is provided, though not completely decoupled into terms consisting entirely of all two and one chain interactions as would be desirable for computational and interpretational benefit. The difficulty is noted to stem from this being the first example where all terms in the Dyson equation are not equivalent under permutation, one is required to allow for swapping any pair

of terms also. Nonetheless, the form of the solution suggests the possibility of an ansatz to solve the N chain system by resummation of all possible networks of Feynman paths on all 1-gons, 2-gons, ... up to N-gons (or up to the range at which the coherence length makes further terms unnecessary).

The generality of the formalism so developed has opened a great deal of promising avenues for further study. Aside from an in depth study of the two and three chain solutions (of which one can have spiral ordered, non identical or non-parallel magnetisations in addition to studying the effect of their separation) we suggest a few avenues of particular interest.

5.0.1 Networks of individual magnetic impurities

The Kitaev chain toy model is capable of entering a topological phase with as few as two sites. As noted, the solutions found in chapter 4 can be readily applied not just to chains but to arbitrarily placed impurities. This suggests a number of interesting avenues of investigation. Can one engineer a topologically non-trivial phase using only *two* magnetic impurities, separated by a critical distance (perhaps relating to $1/k_F$)? Even if this is not possible, consider that there is really nothing to say that the Kitaev chain toy model needs to be in a perfect straight line. Could one more easily study disordered magnetic adatoms on a superconductor? Using the exact solution to the two impurity Green's function one could average over the location of the second impurity (and its magnetic orientation relative to the first) and study *glassy* phases as are beginning to be studied in the literature [116]. Through such a system one might imagine instead of a single Kitaev chain toy model that one ends up with networks following the shortest path between magnetic impurities, but notably such paths may not be unique and it is far from clear what effect this could have on potential topological edge states.

5.0.2 Continuum model for semi-infinite chain

A potentially interesting avenue for further work is to study the Dyson equation

$$G(x_f - x_i) = g(x_f - x_i) + \int_{-\infty}^{0} dx' g(x_f - x_\prime) V G(x' - x_i) \tag{5.1}$$

which describes a dense chain of magnetic impurities which is only *semi* infinite in extent, ending at $x = 0$. This links to a number of matters highlighted throughout this thesis. Though not included explicitly, the methods in chapter 4 can be used to construct finite length chains. Though necessarily increasingly complicated, it should in principle continue to be possible to resum the diagrams present as they will only ever be ladder diagrams. As a result, though probably prohibitively complicated, this approach should be able to describe arbitrary length chains. This method however, would essentially jump straight to the final step of this iterative procedure and provide direct access to what the end of a dense chain would look like, and how it would influence the surrounding substrate.

Similarly, the methods developed in chapter 3 to stitch together solutions would provide an interesting comparison to the solution of this Dyson equation as they should describe exactly the same situation. Interestingly, this suggests that the conditions derived in chapter 3 for the existence of topological bound states should also be relevant to this model.

Finally, and far from least, the method to approach this model seems fairly straightforward. Though one does not have translation symmetry in the x direction, it seems clear that one could instead perform a Laplace transform and then solve via a T matrix approach in Laplace space. Though this highlights the slight difficulty of interpreting bound states in Laplace space rather than the more familiar Fourier space, it remains fairly clear how to calculate real space quantities and hence view the nature of any novel excitations forming at the boundary.

5.0.3 Stitching applied to two chain model

As noted, there has been some work to find physically realisable models which have parafermionic edge states [45, 46]. Here we have now developed the ingredients (exact solution to the two chain model and stitching so that the ends can communicate) to potentially allow investigation of such a phenomenon. As a first step, one would need to investigate whether Kramers doublets of Majorana end states can be induced in pairs of chains before electron-electron interactions are included. As previous approaches rely heavily on purely 1D theoretical tools such as bosonisation, it would be interesting to see whether the same features are observable in a more realistic model.

A Formalism

A.1 Calculation of Nambu space retarded Green's function from first principles

We will focus here upon calculating the 2×2 Nambu, retarded Green's function [31]:

$$\mathbf{G}_{\mathbf{k}}(\omega) = \begin{pmatrix} G_{\mathbf{k}\uparrow}(\omega) & F_{\mathbf{k}}(\omega) \\ \tilde{F}_{\mathbf{k}}(\omega) & -G_{-\mathbf{k}\downarrow}(-\omega) \end{pmatrix} \tag{A.1}$$

from which it is clear how to construct the full 4×4 Nambu space. The Nambu Green's function $\mathbf{G}$ is defined in terms of scalar Green's functions as:

$$\begin{aligned} G_{\mathbf{k}\sigma}(t) &= -i\,\theta(t)\langle\{c_{\mathbf{k}\sigma}(t), c^{\dagger}_{\mathbf{k}\sigma}(0)\}\rangle \\ F_{\mathbf{k}}(t) &= -i\,\theta(t)\langle\{c_{\mathbf{k}\uparrow}(t), c_{\mathbf{k}\downarrow}(0)\}\rangle \\ \tilde{F}_{\mathbf{k}}(t) &= -i\,\theta(t)\langle\{c^{\dagger}_{\mathbf{k}\uparrow}(t), c^{\dagger}_{\mathbf{k}\downarrow}(0)\}\rangle \end{aligned} \tag{A.2}$$

from which we can calculate the necessary ω space Green's functions. One can write these Green's functions in terms of Bogoliubov-de Gennes wave functions $u_{\mathbf{k}}$ and $v_{\mathbf{k}}$ defined through the transformation:

$$\alpha^{\dagger}_{\mathbf{k}} = u_{\mathbf{k}} c^{\dagger}_{\mathbf{k}\uparrow} - v_{\mathbf{k}} c_{-\mathbf{k},\downarrow} \tag{A.3}$$

$$\beta^{\dagger}_{\mathbf{k}} = u_{\mathbf{k}} c^{\dagger}_{-\mathbf{k}\downarrow} + v_{\mathbf{k}} c_{\mathbf{k},\uparrow} \tag{A.4}$$

which diagonalises the BCS Hamiltonian:

$$H = \sum_{\mathbf{k}} E_{\mathbf{k}} \left(\alpha^{\dagger}_{\mathbf{k}} \alpha_{\mathbf{k}} + \beta^{\dagger}_{\mathbf{k}} \beta_{\mathbf{k}} \right) \tag{A.5}$$

in terms of operators $\alpha_{\mathbf{k}}$, $\beta_{\mathbf{k}}$ where $E_{\mathbf{k}} = \sqrt{\epsilon_{\mathbf{k}} + |\Delta_{\mathbf{k}}|^2}$ and in turn $\epsilon_{\mathbf{k}}$ is the dispersion of electrons in the normal state and $\Delta_{\mathbf{k}}$ is the two particle gap function which we have allowed to have momentum dependence for generality.

Up to a choice of overall phase we can hence define:

$$u_{\mathbf{k}} = \frac{1}{\sqrt{2}} \sqrt{1 + \frac{\epsilon_{\mathbf{k}}}{E_{\mathbf{k}}}} \tag{A.6}$$

$$v_{\mathbf{k}} = \frac{e^{i\phi_{\mathbf{k}}}}{\sqrt{2}} \sqrt{1 - \frac{\epsilon_{\mathbf{k}}}{E_{\mathbf{k}}}} \tag{A.7}$$

where $e^{i\phi_{\mathbf{k}}} = \Delta_{\mathbf{k}}/|\Delta_{\mathbf{k}}|$ defines the phase of the two particle gap function. In this way we can write:

$$G_{\mathbf{k}\uparrow}(\omega) = \int_{-\infty}^{\infty} dt e^{i\omega t} G_{\mathbf{k}\uparrow}(t) = -i \int_{0}^{\infty} dt e^{i\omega t} \langle\{c_{\mathbf{k}\uparrow}(t), c^{\dagger}_{\mathbf{k}\uparrow}(0)\}\rangle \tag{A.8}$$

[31] Though in general one should use time ordered functions for diagrammatics, if the only interaction to be considered is an external potential then there are no complications in using the retarded function instead. This follows as a result of Langreth's rules [128] and allows us to avoid concerns about Wick rotations or analytic continuation which are otherwise required.

in terms of $\alpha_{\mathbf{k}}$, $\beta_{\mathbf{k}}$, extracting any t dependence by acting with the Hamiltonian in the usual way this can be written:

$$G_{\mathbf{k}\uparrow}(\omega) = -i\int_0^\infty dt e^{i\omega t}\langle \left(u_{\mathbf{k}}\alpha_{\mathbf{k}}e^{-iE_{\mathbf{k}}t} + v_{\mathbf{k}}^\star\beta_{\mathbf{k}}^\dagger e^{iE_{\mathbf{k}}t}\right)\left(u_{\mathbf{k}}^\star\alpha_{\mathbf{k}}^\dagger + v_{\mathbf{k}}\beta_{\mathbf{k}}\right)\rangle + \langle \left(u_{\mathbf{k}}^\star\alpha_{\mathbf{k}}^\dagger + v_{\mathbf{k}}\beta_{\mathbf{k}}\right)\left(u_{\mathbf{k}}\alpha_{\mathbf{k}}e^{-iE_{\mathbf{k}}t} + v_{\mathbf{k}}^\star\beta_{\mathbf{k}}^\dagger e^{iE_{\mathbf{k}}t}\right)\rangle \tag{A.9}$$

where all remaining operators α, β are evaluated at $t = 0$. At zero temperature, the only non-zero expectation values are $\left\langle \alpha_{\mathbf{k}}\alpha_{\mathbf{k}}^\dagger\right\rangle = \left\langle \beta_{\mathbf{k}}\beta_{\mathbf{k}}^\dagger\right\rangle = 1$ so that:

$$G_{\mathbf{k}\uparrow}(\omega) = -i\int_0^\infty dt\left[|v_{\mathbf{k}}|^2 e^{i(\omega+E_{\mathbf{k}})t} + |u_{\mathbf{k}}|^2 e^{i(\omega-E_{\mathbf{k}})t}\right] \tag{A.10}$$

so that the integral can be performed if $\omega \to \omega + i\epsilon = \omega_+$ for some small ϵ in such a way that the upper half complex plane is analytic, as should be the case for the retarded function:

$$\begin{aligned} G_{\mathbf{k}\uparrow}(\omega) &= -\left(\frac{|u_{\mathbf{k}}|^2}{\omega - E_{\mathbf{k}} + i\epsilon} + \frac{|v_{\mathbf{k}}|^2}{\omega + E_{\mathbf{k}} + i\epsilon}\right) \\ &= \frac{1}{2}\left[\frac{(1+\epsilon_{\mathbf{k}}/E_{\mathbf{k}})(\omega_+ + E_{\mathbf{k}}) + (1-\epsilon_{\mathbf{k}}/E_{\mathbf{k}})(\omega_+ - E_{\mathbf{k}})}{(\omega_+ - E_{\mathbf{k}})(\omega_+ + E_{\mathbf{k}})}\right] \\ &= \frac{\omega_+ + \epsilon_{\mathbf{k}}}{\omega_+^2 - E_{\mathbf{k}}^2}. \end{aligned} \tag{A.11}$$

The Green's function in the hole sector $G_{\mathbf{k}}^h(\omega) = -G_{-\mathbf{k}}(-\omega)$ can thus be written:

$$-G_{-\mathbf{k}}(-\omega) = -\frac{-\omega - i\epsilon + \epsilon_{-\mathbf{k}}}{\omega_+^2 - E_{-\mathbf{k}}^2} \tag{A.12}$$

so that the Green's function in the hole sector is also analytic in the upper half ω plane. If we restrict ourselves to dispersions $\epsilon_{\mathbf{k}} = \epsilon_{-\mathbf{k}}$ and gap functions $|\Delta_{\mathbf{k}}| = |\Delta_{-\mathbf{k}}|$ then we can write:

$$-G_{-\mathbf{k}}(-\omega) = \frac{\omega_+ - \epsilon_{\mathbf{k}}}{\omega_+^2 - E_{\mathbf{k}}^2}. \tag{A.13}$$

The derivation for the anomalous Green's functions F and $\tilde{F}$ follow in much the same fashion so that we finally arrive at the Nambu Green's function:

$$\mathbf{G}_{\mathbf{k}}(\omega) = \frac{1}{\omega_+^2 - E_{\mathbf{k}}^2}\begin{pmatrix} \omega_+ + \epsilon_{\mathbf{k}} & \Delta_k \\ \Delta_{\mathbf{k}}^* & \omega_+ - \epsilon_{\mathbf{k}} \end{pmatrix} \tag{A.14}$$

A.2 Required integrals

A.2.1 Partial Fourier transform of 2D superconducting Green's function

In the process of calculating the full Green's function for systems with lines of magnetic impurities embedded in 2D superconductors with quadratic dispersion (which naturally also describes metallic backgrounds if the gap $\Delta = 0$ and has a fairly natural extension to 3D substrates) one

encounters integrals of the form:

$$I_1 = \int_{-\infty}^{\infty} dk_y e^{iyk_y} \frac{1}{k_y^4 + \alpha_2 k_y^2 + \alpha_0}, \tag{A.15}$$

$$I_2 = \int_{-\infty}^{\infty} dk_y e^{iyk_y} \frac{k_y^2}{k_y^4 + \alpha_2 k_y^2 + \alpha_0}, \tag{A.16}$$

where the constants α_1, α_0 are functions of $k_x/k_F, k_m/k_F, \tilde{\Delta}, \tilde{\omega}$. Unlike for the case of a linearised spectrum, or a complete Fourier transform (over both k_x and k_y) these integrals are convergent without need for a cutoff and may be solved exactly via the Cauchy residue theorem. Both integrals are convergent with a choice of semi-circular contour closing in the upper half complex plane for $y \geq 0$ and the lower half complex plane if $y < 0$. Thus the problem reduces to identifying which of the four of the integrand's poles lie within these regions.

For the particular example of a 2D superconductor with quadratic dispersion the four poles can be written as $\pm p_+$ and $\pm p_-$ where:

$$p_+ = k_F \sqrt{1 - \left(\frac{k_x + \sigma k_m}{k_F}\right)^2 + \sqrt{-\tilde{\Delta}^2 + \tilde{\omega}^2 + i\eta}} \tag{A.17}$$

$$p_- = k_F \sqrt{1 - \left(\frac{k_x + \sigma k_m}{k_F}\right)^2 - \sqrt{-\tilde{\Delta}^2 + \tilde{\omega}^2 + i\eta}} \tag{A.18}$$

which can be written in the form $a \pm ib$ by repeated use of the identity

$$\sqrt{A \pm iB} = \frac{1}{\sqrt{2}} \left[\sqrt{A + \sqrt{A^2 + B^2}} \pm i \sqrt{-A + \sqrt{A^2 + B^2}} \right] \tag{A.19}$$

for $B > 0$. In this way we find that the poles $+p_+$ and $-p_-$ always lay in the upper half complex plane, and the other two always in the lower half plane.

With this classification we find that the integrals I_1 and I_2 are given by:

$$I_1 = -2\pi i \frac{1}{p_+^2 - p_-^2} \left(\frac{e^{ip_+|y|}}{p_+} + \frac{e^{-ip_-|y|}}{p_-} \right), \tag{A.20}$$

$$I_2 = -2\pi i \frac{1}{p_+^2 - p_-^2} \left(e^{ip_+|y|} p_+ + e^{-ip_-|y|} p_- \right), \tag{A.21}$$

for any y, without any approximations or cutoff required.

References

[1] I. Gil-Botella, CERN Yellow Report CERN-2013-003, pp. 157.

[2] E. Majorana, Il Nuovo Cimento **14**, 171 (1937).

[3] C. Nayak, S. H. Simon, A. Stern, M. Freedman, S. Das Sarma, Rev. Mod. Phys. **80**, 1083 (2008).

[4] S. Weinberg, *The quantum theory of fields. Vol. 1, Foundations.* (Cambridge University Press, 1995).

[5] F. Wilczek, Phys. Rev. Lett. **49**, 957 (1982).

[6] A. Y. Kitaev, Phys. Usp. **44**, 131 (2001).

[7] N. Read, D. Green, Phys. Rev. B **61**, 10267 (2000).

[8] P. Fendley, J. Stat. Mech. **2012**, 11020 (2012).

[9] L. Fu, C. L. Kane, Phys. Rev. Lett. **100**, 096407 (2008).

[10] M. Z. Hasan, C. L. Kane, Rev. Mod. Phys. **82**, 3045 (2010).

[11] J. Alicea, Phys. Rev. B **81**, 125318 (2010).

[12] R. M. Lutchyn, J. D. Sau, S. Das Sarma, Phys. Rev. Lett. **105**, 077001 (2010).

[13] Y. Oreg, G. Refael, F. von Oppen, Phys. Rev. Lett. **105**, 177002 (2010).

[14] J. D. Sau, R. M. Lutchyn, S. Tewari, S. Das Sarma, Phys. Rev. Lett. **104**, 040502 (2010).

[15] M. Sato, S. Fujimoto, Phys. Rev. B **79**, 094504 (2009).

[16] B. Braunecker, P. Simon, Phys. Rev. Lett. **111**, 147202 (2013).

[17] J. Klinovaja, P. Stano, A. Yazdani, D. Loss, Phys. Rev. Lett. **111**, 186805 (2013).

[18] M. M. Vazifeh, M. Franz, Phys. Rev. Lett. **111**, 206802 (2013).

[19] M. Schecter, M. S. Rudner, K. Flensberg, Phys. Rev. Lett. **114**, 247205 (2015).

[20] W. Hu, R. T. Scalettar, R. R. P. Singh, Phys. Rev. B **92**, 115133 (2015).

[21] B. Braunecker, P. Simon, Phys. Rev. B **92**, 241410(R) (2015).

[22] T. P. Choy, J. M. Edge, A. R. Akhmerov, C. W. J. Beenakker, Phys. Rev. B **84**, 195442 (2011).

[23] M. Kjaergaard, K. Wölms, K. Flensberg, Phys. Rev. B **85**, 020503(R) (2012).

[24] F. Pientka, L. I. Glazman, F. von Oppen, Phys. Rev. B **88**, 155420 (2013).

[25] F. Pientka, L. I. Glazman, F. von Oppen, Phys. Rev. B **89**, 180505(R) (2014).

[26] K. Pöyhönen, A. Weststrom, J. Röntynen, T. Ojanen, Phys. Rev. B **89**, 115109 (2014).

[27] J. Röntynen, T. Ojanen, Phys. Rev. B **90**, 180503 (2014).

[28] A. Heimes, P. Kotetes, G. Schön, Phys. Rev. B **90**, 060507(R) (2014).

[29] P. M. R. Brydon, S. Das Sarma, Hoi-Yin Hui, Jay D. Sau, Phys. Rev. B **91**, 064505 (2015).

[30] K. Pöyhönen, A Weststrom, T. Ojanen, Phys. Rev. B **93**, 014517 (2016).

[31] S. Hoffman, J. Klinovaja, D. Loss, Phys. Rev. B **93**, 165418 (2016).

[32] J. Li, H. Chen, I. K. Drozdov, A. Yazdani, B. A. Bernevig, A. H. MacDonald, Phys. Rev. B **90**, 235433 (2014).

[33] H. O. H. Churchill, V. Fatemi, K. Grove-Rasmussen, M. T. Deng, P. Caroff, H. Q. Xu, C. M. Marcus, Phys. Rev. B **87**, 241401 (2013).

[34] S. M. Albrecht, A. P. Higginbotham, M. Madsen, F. Kuemmeth, T. S. Jespersen, J. Nygård, P. Krogstrup, C. M. Marcus, Nature (London) **531**, 206 (2016).

[35] A. D. K. Finck, D. J. Van Harlingen, P. K. Mohseni, K. Jung, X. Li, Phys. Rev. Lett. **110**, 126406 (2013).

[36] L. P. Rokhinson, X. Liu, J. K. Furdyna, Nat. Phys. **8**, 795 (2012).

[37] A. Das, Y. Ronen, Y. Most, Y. Oreg, M. Heiblum, H. Shtrikman, Nano Lett. **8**, 887 (2012).

[38] M. T. Deng, C. L. Yu, G. Y. Huang. M. Larsson, P. Caroff, H. Q. Xu, Nano Lett. **12**, 6414 (2012).

[39] V. Mourik, K. Zuo, S. M. Frolov, S. R. Plissard, E. P. A. M. Bakkers, L. P. Kouwenhoven, Science **336**, 1003 (2012).

[40] S. Nadj-Perge, I. K. Drozdov, J. Li, H. Chen, S. Jeon, J. Seo, A. H. MacDonald, B. A. Bernevig, A. Yazdani, Science **346**, 6209 (2014).

[41] M. Ruby, F. Pientka, Y. Peng, F. von Oppen, B. W. Heinrich, K. J. Franke, Phys Rev. Lett. **115**, 197204 (2015).

[42] R. Pawlak, M. Kisiel, J. Klinovaja, T. Meier, S. Kawai, T. Glatzel, D. Loss, R. Meyer, Quant. Inf. **2**, 16035 (2016).

[43] A. Kamlapure, L. Cornils, J. Wiebe, R. Wiesendanger, Nat. Comms. **9**, 3253 (2018).

[44] M.-T. Deng, S. Vaitekénas, E. Prada, P. San-Jose, J. Nygård, P. Krogstrup, R. Aguado, C. M. Marcus, Phys. Rev. B **98**, 085125 (2018).

[45] J. Klinovaja, D. Loss, Phys. Rev. B **90**, 045118 (2014).

[46] J. Klinovaja, D. Loss, Phys. Rev. Lett. **112**, 246403 (2014).

[47] B. I. Halperin, Y. Oreg, A. Stern, G. Rafael, J. Alicea, F. von Oppen, Phys. Rev. B **85**, 144501 (2012).

[48] D. J. Clarke, J. D. Sau, S. Tewari, Phys. Rev. B **84**, 035120 (2011).

[49] J. Alicea, Y. Oreg, G. Rafael, F. von Oppen, M. P. A. Fisher, Nat. Phys. **7**, 412 (2011).

[50] A. Altland, M. R. Zirnbauer, Phys. Rev. B **55**, 1142 (1997).

[51] M. R. Zirnbauer, Journal of Mathematical Physics **37**, 1986 (1996).

[52] J. K. Pachos, *Introduction to Topological Quantum Computation* (Cambridge University Press, 2012).

[53] F. Garcia-Moliner, J. Rubio, J. Phys. C: Solid State Phys. **2**, 1789 (1969).

[54] F. Garcia-Moliner, J. Rubio, Proc. R. Soc. Lond. A. **324**, 257 (1971).

[55] J. E. Inglesfield, J. Phys. C: Solid State Phys. **4**, L14 (1971).

[56] N. J. Morgenstern Horing, *Quantum Statistical Field Theory: An Introduction to Schwinger's Variational Method with Green's Function Nanoapplications, Graphene and Superconductivity* (Oxford University Press, 2017).

[57] E. Lieb, T. Schultz, D. Mattis, Ann. Phys. **16**, 407 (1961).

[58] B. van Heck, F. Hassler, A. R. Akhmerov, C. W. J. Beenakker, Phys. Rev B **84**, 180502 (2011).

[59] B. van Heck, A. R. Akhmerov, F. Hassler, M. Burrello, C. W. J. Beenakker, New J. Phys. **14**, 035019 (2012).

[60] F. Hassler, D. Schuricht, New J. Phys. **14**, 125018 (2012).

[61] I. Martin, A. F. Morpurgo, Phys. Rev. B **85**, 144505 (2012).

[62] S. Nadj-Perge, I. K. Drozdov, B. A. Bernevig, A. Yazdani, Phys. Rev. B **88**, 020407 (2013).

[63] N. Y. Yao, L. I. Glazman, E. A. Demler, M. D. Lukin, J. D. Sau, Phys. Rev. Lett. **113**, 087202 (2014).

[64] Y. Kim, M. Cheng, B. Bauer, R. M. Lutchyn, S. Das Sarma, Phys. Rev. B **90**, 060401(R) (2014).

[65] I. Reis, D. J. J. Marchand, M. Franz, Phys. Rev. B **90**, 085124 (2014).

[66] M. H. Christensen, M. Schecter, K. Flensberg, B. M. Andersen, J. Paaske, Phys. Rev. B **94**, 144509 (2016).

[67] M. Schecter, K. Flensberg, M. H. Christensen, B. M. Andersen, J. Paaske, Phys. Rev. B **93**, 140503(R) (2016).

[68] B. Braunecker, P. Simon, D. Loss, Phys. Rev. Lett. **102**, 116403 (2009).

[69] B. Braunecker, P. Simon, D. Loss, Phys. Rev. B **80**, 165119 (2009).

[70] B. Braunecker, G. I. Japaridze, J. Klinovaja, D. Loss, Phys. Rev. B **82**, 045127 (2010).

[71] N. D. Mermin, H. Wagner, Phys. Rev. Lett. **17**, 1133 (1966).

[72] P. Bruno, Phys. Rev. Lett. **87**, 137203 (2001).

[73] P. Simon, B. Braunecker, D. Loss, Phys. Rev. B **77**, 045108 (2008).

[74] D. Loss, F. L. Pedrocchi, A. J. Leggett, Phys. Rev. Lett. **107**, 107201 (2011).

[75] L. Yu, Acta Phys. Sin. **21**, 75 (1965).

[76] H. Shiba, Prog. Theor. Phys. **40**, 435 (1968).

[77] A. I. Rusinov, JETP Lett. **9**, 85 (1969).

[78] G. D. Mahan, *Many-particle physics* (Springer, 2000).

[79] R. D. Mattuck, *A guide to Feynman diagrams in the many-body problem* (McGraw-Hill Inc., 1976)

[80] A. L. Fetter, J. D. Walecka, *Quantum theory of many-particle systems* (McGraw-Hill, 1971).

[81] A. A. Abrikosov, L. P. Gor'kov, I. E. Dzyaloshinkski, *Methods of quantum field theory in statistical physics* (Dover Publications, 1975).

[82] P. W. Anderson, J. Phys. Chem. Solids **11**, 26 (1959).

[83] A. Weststrom, K. Pöyhönen, T. Ojanen, Phys. Rev. B **91**, 064502 (2015).

[84] G. C. Ménard, S. Guissart, C. Brun, S. Pons, V. S. Stolyarov, F. Debontridder, M. V. Leclerc, E. Janod, L. Cario, D. Roditchev, P. Simon, T. Cren, Nat. Phys. **11**, 1013 (2015).

[85] T. Uchihasi, Supercond. Sci. Technol. **30**, 013002 (2017).

[86] B. Feldman, M. T. Randeria. J. Li, S. Jeon, Y. Xie, Z. Wang, I. K. Drozdov, B. A. Bernevig, A. Yazdani, Nat. Phys. **13**, 286 (2017).

[87] J. Li, S. Jeon, Y. Xie, A. Yazdani, B. A. Bernevig, Phys. Rev. B **97**, 125119 (2018)

[88] S. Jeon, Y. Xie, J. Li, Z. Wang, B. A. Bernevig, A. Yazdani, Science **358**, 6364 (2017).

[89] J. Alicea, Rep. Prog. Phys. **75**, 076501 (2012)

[90] F. J. Dyson, Journal of Mathematical Physics **3**, 1199 (1962).

[91] Q. H. Wang, Z. D. Wang, Phys. Rev. B **69**, 092502 (2004).

[92] F. Pientka, L. I. Glazman, F. von Oppen, Phys. Rev. B **89**, 180505(R) (2014).

[93] Y. Peng, F. Pientka, L. I. Glazman, F. von Oppen, Phys. Rev. Lett. **114**, 106801 (2015).

[94] A. Heimes, D. Mendler, P. Kotetes, New J. Phys. **17**, 023051 (2015).

[95] D. Asahi, N. Nagaosa, Phys. Rev. B **86**, 100504(R) (2012).

[96] V. Gurarie, Phys. Rev. B **83**, 085426 (2011).

[97] G. Volovik, *The Universe in a Helium Droplet* (Clarendon Press, 2003).

[98] Y. Peng, Y. Bao, F. von Oppen, Phys. Rev. B **95**, 235143 (2017).

[99] T. D. Stanescu, G. Kotliar, Phys. Rev. B **74**, 125110 (2006).

[100] W. Ding, Q. Si, arXiv:1810.03309.

[101] R. M. Konik, T. M. Rice, A. M. Tsvelik, Phys. Rev. Lett. **96**, 086407 (2006).

[102] M. R. Norman, M. Randeria, H. Ding, J. C. Campuzano, Phys. Rev. B **57**, R11093 (1998).

[103] J. Alsup, E. Papantonopoulos, G. Siopsis, K. Yeter, Phys. Rev. D **90**, 126013 (2014).

[104] G. 't Hooft, Nucl. Phys. B **75**, 461 (1974).

[105] I. Dzyaloshinskii, Phys. Rev. B **68**, 085113 (2003).

[106] T. D. Stanescu, P. W. Phillips, T. Choy, Phys. Rev. B **75**, 104503 (2007).

[107] S. Sakai, Y. Motome, M. Imada, Physica B **404**, 3183 (2009).

[108] K. Y. Yang, T. M. Rice, F. C. Zhang, Phys. Rev. B **73**, 174501 (2006).

[109] K. Y. Yang, H. B. Yang, P. D. Johnson, T. M. Rice, F. C. Zhang, Europhys. Lett. **86**, 37001 (2009).

[110] K. Le Hur, T. M. Rice, Ann. Phys. **324**, 1452 (2009).

[111] E. Z. Kuchinskii, M. V. Sadovskii, JETP **103**, 415 (2006).

[112] F. H. L. Essler, A. M. Tsvelik, Phys. Rev. B **65**, 115117 (2002).

[113] C. Berthod, T. Giamarchi, S. Biermann, A. Georges, Phys. Rev. Lett. **97**, 136401 (2006).

[114] S. Sakai, Y. Motome, M. Imada, Phys. Rev. Lett **102**, 056404 (2009).

[115] S. Sakai, Y. Motome, M. Imada, Phys. Rev. B **82**, 134505 (2010).

[116] K. Pöyhönen, I. Sahlberg, A. Weststrom, T. Ojanen, Nat. Comms. **9**, 2103 (2018).

[117] Y-F Zhang et al, Chin. Phys. B **22**, 11 (2013).

[118] X. Wen, Z. Wang, arXiv:1801.09938.

[119] B. Braunecker, P. A. Lee, Z. Wang, Phys. Rev. Lett. **95**, 017004 (2005).

[120] J. Klinovaja, A. Yacoby, D. Loss, Phys. Rev. B **90**, 155447 (2014).

[121] J. Klinovaja, Y. Tserkovnyak, Phys. Rev. B **90**, 115426 (2014).

[122] I. Schur, Math. Ann. **66**, 488 (1909).

[123] G. H. Golub, C. F. Van Loan, *Matrix Computations*, pp. 312 (John Hopkins University Press, 1996).

[124] V. Kaladzhyan, J Röntynen, P. Simon, T. Ojanen, Phys. Rev. B **94**, 060505 (2016).

[125] J. Röntynen, T. Ojanen, Phys. Rev. B **93**, 094521 (2016).

[126] G. C. Ménard, S. Guissart, C. Brun, M. Trif, F. Debontridder, R. T. Leriche, D. Demaille, D. Roditchev, P. Simon, T. Cren, Nat. Comms. **8**, 2040 (2017).

[127] C. Kittel, *Introduction to Solid State Physics 7th Ed.* (Wiley, 1996).

[128] H. Haug, A. Jauho, *Quantum Kinetics in Transport and Optics of Semiconductors* (Springer, 2008).